POLITECNICO DI TORINO

COLLEGIO DI INGEGNERIA MECCANICA, AEROSPAZIALE,
DELL'AUTOVEICOLO E DELLA PRODUZIONE

Corso di Laurea in Ingegneria Meccanica

Tesi di Laurea Magistrale

Design of a wavemaker for the water tank at the Politecnico di Torino

Relatore

prof. Giovanni Bracco

Correlatore

prof. Giuliana Mattiazzo

Laureando

Mario Beneduce

matricola: 244380

ANNO ACCADEMICO 2018 – 2019

Ai miei genitori

Abstract

Wavemakers are devices used in test tanks to generate waves. In these tanks are usually tested models of ships, offshore and onshore structures and wave energy converter: in this way, it is possible to evaluate the resistance offered by the hull of a ship during the motion and then define the power to install on board of the real ship or studying its seakeeping, evaluating the consequences of the action of waves on coastal facility and the energy conversion capabilities of a wave energy converter. Testing models in tank is fundamental in these sectors because it make possible to avoid critical and expensive mistakes in the early phases of the project and to study the behavior of prototypes.

This thesis aims to analyze the wave generation capabilities of the tank presents in the laboratory of the department of Mechanical and Aerospace engineering of Politecnico di Torino and to make a first dimensioning of the actuation system to use. The final goal is to understand if this testing environment could be interesting for our needs, mainly focused on tests on wave energy converter devices.

The first chapter gives an overview on test tanks. It is reported a historical introduction in which is summarized the evolution of these tests and a description of the main features of wave tanks; a collection of the most important facilities of the world, Europe and Italy closes this chapter. The second one reports the mean features of the linear water waves theory and the third one the first order wavemaker problem including the oblique wave generation. The fourth chapter reports the study made in the present work for our test tank. First, it is made an analysis of the ideal wave generation capabilities: in this phase in fact, it is considered an ideal wave generator that means that all the problems due to the physical realization of the actuation system are not considered. Then we analyzed the forces acting on the paddle and the velocities during our working cycles: this is important to obtain the F-v characteristic that we need to realize to generate our waves. With this input data, we searched a suitable actuator for our application; the choice made introduces cuts in the wave generation capabilities that is it is not possible to generate all the waves reported in the first ideal analysis. This constrain yields to a new F-v characteristic that it is used like input data for the motor choice. This last analysis, made without and with a speed reducer, and its results closes the chapter. In the last chapter there is a summary of the work made and the main results are pointed out. The recommendations for further and in proceeding works, that is the CFD analysis in which I collaborate, close this last chapter.

Contents

Chapter 1

Test tanks

Nel trattar con l'acque
consulta pria l'esperienza e
poi la ragione

Leonardo da Vinci

The aim of this chapter is to introduce the tests in tank. In the first part, there is a historical introduction to better understand the significant changes that this approach introduced not only in the naval engineering; for this part, the main reference is [10]. After this, there is a description of the main features of a test tank and a summary of the main types. The chapter is closed by a collection of the most important facilities.

1.1 Origins and develop of test tanks

Birth and use of test tanks are strictly linked to the naval engineering. It seems that towing tests on ship models were made in Venice in '500; the aim of this tests was to determine the resistance offered by the hull to the motion. It is proven that ships models were used to study the interaction between water and hull since XVII century. In fact, it is known that in England Samuel Fortray (1622-1681) used test tanks in which the vertical motion of a falling weight was used, with a simple pulley system, to drag the ship models. However there still was not the classical mechanic theory, so tests were qualitative.

Emanuel Swedenborg (1688-1772)

In 1687 the publication of *Philosophiae naturalis principia matematica* by Isaac Newton (1642-1726) and the following diffusion of the law of mechanical similarity, gave a scientific background to the tests. The first evidence of scientific rigor is dated back to 1720 in the studies of Emanuel Swedenborg (1688-1772), a theologian, philosopher and scientist follower of the Newton's theory. Like Fortray, he used a tank in which the ship model was dragged by the action of falling down weights. The general principle of these tests was to compare the resistance offered by different hulls during the entrainment; in this way, the motion of different models with the same length were compared in order to find the hull with less resistance absolute.

Pierre Bouguer (1698-1758)

In France Pierre Bouguer (1698-1758), author of *Traité du Navire (1746)*, made similar tests with the same goal. He still used the so called *gravity tank* and models in which the maximum width was set to one third of the length. More

attention was payed to get a straight path for the models: the towing cables crossed all the tank and models had hooks on the top in order to maintain the correct trim.

These tests stated that the best hull was the one with the biggest prow. However, these experiments had an important limit. In fact, it was quite impossible to obtain a drag with a constant velocity because the dragging weight is subject to the gravity acceleration and this yields to an accelerated motion. To overcome this problem one should use very long tanks or very small models, but in this way several and important experimental mistakes take over.

Frederik Henrik af Chapman (1721-1808)

Between 1750 and 1760, Frederik Henrik af Chapman (1721-1808), designer of the Royal swedish Navy, made his experimental campaign; he recorded his tests in Architectura Navalis Mercatoria (1768) and in Traité de la construction des vaisseaux (1781). He still used gravity tanks but the poles from which the weights came down were 30 m high, the ship models were in weighted wood and they reached the record length of 8.5 m. The dragging cable was linked both forward and aft for maintaining a straight path along the tank. From these experiments he stated that the longitudinal position of the master section to obtain the minimum resistance varies with the testing velocity and, for that time, this was a very important conclusion. The Chapman's studies established that the absolute best hull doesn't exist; however there are various possible geometries each one of these with its best efficiency point in certain working condition. The consequence of these studies was the introduction of more hydrodynamic hulls: the bow and the stern were sharpened and the length started to be five or six times the width instead three times.

In the same period progress were made in hydraulics and fluid mechanics. Henri de Pitot (1695-1771), Daniel Bernoulli (1700-1782), Leonard Euler (1707-1783) and others gave the first instruments to understand the physics behind the motion of an object on the separation surface between air and water. Others important studies were made by Jean de Rond d'Alambert (1717-1783), Joseph Louis Lagrange (1736-1813) and Giovanni Battista Venturi (1746-1822). All these studies influenced the geometries of the hulls.

Meanwhile also the testing modalities were improving. In 1775 d'Alambert, Condorcet (1743-1794) and Bossut (1730-1814) built a gravity tank on request of the academy of Paris: it was 32.5 m long, 17.2 m wide and 2 m depth. Even if the dragging method was the same of the other tanks, the speed was measured timing the passage of the model through some doors positioned at known distance one from the other.

Scottish Maid Prototype Half Model by James And William Hall, 1839

An evidence of the growing importance of test tanks in ship designing is given by the studies made by the Scottish brothers James and William Hall around 1830. Sons of Alexandre Hall, an important shipbuilder of Aberdeen, they used a tank 3 m long, 40 cm width and 25 cm depth for testing several ships models; the walls of the tank were transparent and they also used tracer liquid to better observe the interaction between water and hull. These studies led to the invention of the raked bow of ships, the so called *Aberdeen bow*; in fact, from the tests it emerged that the raked bow created smoother waves around the hull, a symptom of better interaction between water and ship. This was confirmed by the construction of the schooner *Scottish Maid* in 1839 by Alexander Hall and Company, in which speed and sailing performances were improved.

However, even if the first good results of models testing were arriving, still there was not a complete and solid theory to use; also there was the wrong belief that the model that offered less resistance in the test, would have been the best also in real scale. For these reason, designers did not trust too much in these experiments but times were ready for a decisive change.

John Scott Russel (1808-1882)

Around the half of XIX century, John Scott Russel (1808-1882), a Scottish naval engineer, made his studies on waves generation due to ship motion. In 1860 he formalized his research in which he connected the hull length and the goal velocity with the waves generated by the ship. In particular, he stated that for each hull there is a critical velocity after which the resistance grows rapidly; this phenomenon can be reduced by hull geometries that help the interaction with the water. After this, there were all the basis for discover the law of similarity which is one of the most important law of naval engineering.

In the same period, William Froude (1810-1879), a railway engineer, started to be interested in hydrodynamics and worked with Russel designing two important ships, the Great Western and the Great Eastern. At the beginning, he made his studies with a small gravity tank but he understood all the limitations, above mentioned, of this experiment. Froude made his studies between 1860 and 1870 and formulated his law of similarity based on Newton's theory.

William Froude (1810-1879)

The hypothesis of this law is that the resistance offered by water to the hull motion can be divided into two components: the friction one caused by the contact between water and hull and a general one, composed of many contributions, in which the most important is the waves generation due to the motion. Froude stated that only the general component follows the mechanical law of similarity of Newton. The friction component instead it is comparable to the one of a flat plate, of negligible width and with length and surface equal to the studied hull, immersed and longitudinally directed with respect to the motion direction. Steel now, these are the basis for tests in water tanks and Froude carried qualitative experiments to a superior level with an important scientific background.

In 1870 Froude convinced the British admiralty to build a water tank and in 1871 it was established in Torquay, in the south west of England. This testing facility it is considered the first modern water tank for the plant itself and for the innovative testing methods used. The tank was 85 m long, 11 m width and 3 m depth; over the tank in longitudinal direction there were rails on which a cart can run from one side of the tank to the other. The cart was moved at the desired velocity by a metal cable that winded around a rotating drum put in rotation by a steam engine; this was very important because before it wasn't possible to drag the model with a constant velocity with not negligible effects on the resistance

William Froude and the admiralty's first naval test tank at Torquay 1872

evaluation. The hull model was connected to the cart, it was between 3 m and 4 m and it was made with paraffin, much more workable than wood. Between cart and model there were the instruments for the resistance measure and on the top of the cart there were devices that took over the dynamic and trim variation of the model. The solution of the towing cart with instruments, used for the first time by Froude in Torquay, is steel now present in every water tank. The reliability of the Froude's method was ascertained by towing tests in real scale in Portsmouth: the results of tests in tank were compared with the resistance evaluated during the dragging of a small ship by a bigger one and this yielded very similar conclusions. The good results of these first tests led to the construction of a new test tank in 1894 in Porthsmouth, by Froude's soon: it was 110 m long, 6.1 m width and 2.8 m depth.

Meanwhile these experiments were spreading also out of UK. Tests, steel with gravity tank but using Froude's theory, were made in Holland, Italy and France; in particular, in the arsenal of Brest, were also made studies of naval propulsion studying the push gave to the models by helix.

Aleksey Nikolaevich Krylov

Very soon the importance of these testing facilities was clear in all Europe and in the rest of the world. In 1894 in the Russian Empire was established what it is now called the Krylov State Research Centre, that is now one of the most important institution of the world in ship research and design. In 1894 was the first facility in the Russian Empire and the sixth in the world for ship models tests. This institution takes the name of Aleksey Nikolaevich Krylov, a Russian naval engineer that developed the studies of Froude.

David Watson Taylor(1864-1940)

In 1898 was realized the first test tank of USA under the supervision of David Watson Taylor, naval architect and engineer of the United States Navy which still now detains the record of highest grade average in the history of U.S. Naval Academy; the facility in Carderock, Maryland, in which there is maybe the most important test tank of the world, the MASK, retains his name.

Military navy and shipbuilders firms played an important role in spreading this design method; they understood how much important would have been models testing for research and to avoid very expensive mistakes: it is clear that from this depend both the military power of a nation and the business success of a company. Like evidence of this fast spread, before WWI there were about twenty testing tanks all over the world. This fast diffusion was due to two technical reason mainly. First, the steam engine and the helix propulsion simplified the modeling and the hull optimization: in fact, the propulsion direction was now fixed respect to the longitudinal symmetry plane of the ship and not variable like in sail propulsion. Second, but not less important, it was now fundamental to know with a good accuracy the power required by propulsion to avoid critical and expensive mistakes.

After WWI, the number of water tanks all over the world increased. An evidence of the growing importance of these tests in these years is the meeting of the International Hydro-mechanical

Congress, held in Hamburg in 1932; this was the first step of the organization that we now call International Towing Tank Conference. The aim of ITTC is to gather the scientific institutions that operate tests in tanks, define standard testing methodology and link researcher. In this atmosphere of constant develop the number of test tanks increased, reaching about forty before WWII. In these years tests in tank developed and water tanks were used like alternative to wind tunnel and to test port and offshore structure.

During XX century important research center with several water tanks for different tests were built in the USA, URSS, China, Japan and lots of researcher daily work to improve scientific knowledge in fluid dynamic. Tests in water tanks developed both in theory and facilities: for example, wavemaking theory gave us the possibility to study the ship behavior in rough sea and we can now use iced tank to test ice breaker ship. In the last years the develop of CFD gave also an important boost in this sector, giving us the possibility to study fluid dynamics problems in all their complexity. Recently, the new develop of sea energy converters gave another impulse to tests in tank. By the way, it can be mentioned the EU MARINET project: its goal is to coordinate research and development of sea energy converters, starting from models until open sea tests, and to ease the use of testing facilities for researcher.

It is interesting to remember here the develop of tank testing in Italy. In 1886 the minister of the navy, admiral Benedetto Brin, decided to finance the construction of a water tank. In this way, Italy was the first nation, after UK, to build a modern test tank. The plant was built in the arsenal of La Spezia and became active between 1889 and 1890. The design was made following the Froude's facilities projects and it was directed by Giuseppe Rota (1860-1953), promising engineer of the military navy, whose life would have been braided with testing tanks. Concluded the construction, he was also the plant first director. The tank was 150 x 6 x 3 m, it had a wooden towing cart with dynamometer and it was moved by a steam engine, exactly like the one in Torqay tank, with a maximum velocity of 5 m/s. The activity of this plant led to important discoveries about water depth influence on the motion resistance and the propulsion with two helixes with the same axis but rotating in opposite directions. About this experience, Rota wrote *La vasca per le esperienze di architettura del R. Arsenale di Spezia (Genova 1898)*; this publication had a good success between naval engineers. After WWI, the facility of La Spezia proved to be not sufficient to meet new technical needs: there was the request of better experimental apparatus and bigger tanks. Moreover, was difficult to satisfy the increase of demands for tests by private shipbuilders companies: in fact, the tank was a military facility and military navy tests had the priority. In this situation, the action of Rota, in these years member of Senate, convinced the government of the *"necessity and urgency"* to give to the Italian industry the possibility of making naval tests in Italy.

Benedetto Brin (1833-1898)

For these reasons, in 1927 the Italian government established in Rome the *Vasca Nazionale per Studi ed Esperienze di Architettura Navale*. This new plant was created in Rome for testing the solution of the *Comitato progetti delle navi* and for its the central position, quite easy to reach from all Italy. The name of this institution would have been then INSEAN, *Istituto Nazionale per Studi ed Esperienze di Architettura Navale*. The tank was 275 x 12.5 x 6.3 m and the towing cart could reach 10 m/s. The institution started the activities in 1929; Rota, like in La Spezia, became the first director and in 1931 published *La vasca nazionale per le esperienze di architettura navale*

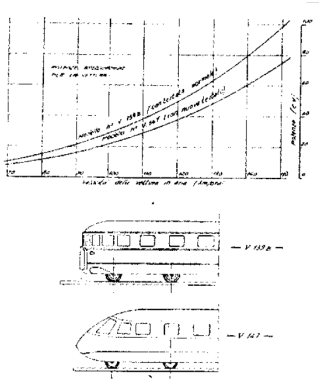

Test on locomotives in Rome

(Roma 1931). The facility was soon used intensively for many tests; classical experiments of naval engineering, like towing and propulsion tests, were put besides by aerodynamics studies for others engineering fields. In particular, FIAT Auto ordered aerodynamics tests on different car bodies, including the popular *"Balilla",* and Ferrovie dello Stato tested the shape of *"littorina"* railcar. These experiments were made dragging on a table the completely immersed model in the water; even if cars and trains don't move in water, tests are solids because air and water are both fluids and differences between them is corrected in calculations.

In 1935 another tank was built in Guidonia in the plant of Direzione Superiore Studi ed Esperienze (DSSE) by *Aeronautica Militare*. The tank was 475 x 6 x 3.5 m and had two measuring carts for high speed tests on airfoils and seaplanes models. The slowest cart could reach 20 m/s, the fastest 40 m/s; in particular, the fastest was carinate and towed the model at sufficient distance form it with a long horizontal arm for avoiding aerodynamics influences. The history of this research center is as important as forgotten. In Guidonia, under the boost of war development, was created an integrated environment in which Italian scientist could make researches and then tests in laboratory; in the same area there was also the possibility to build aircraft prototypes and to make them tested by pilots of *Aeronautica Militare*.
The activities ended in 1943 due to the war but in eight years of work remarkable results were obtained and worldwide
recognized: we can remember here the scientists Antonio Ferri and Luigi Crocco, after WWII both in the USA in prestigious research positions, and Luigi Broglio, the father of Italian astronautics; many others researcher took part to the activity of DSSE with important results but here are not cited.

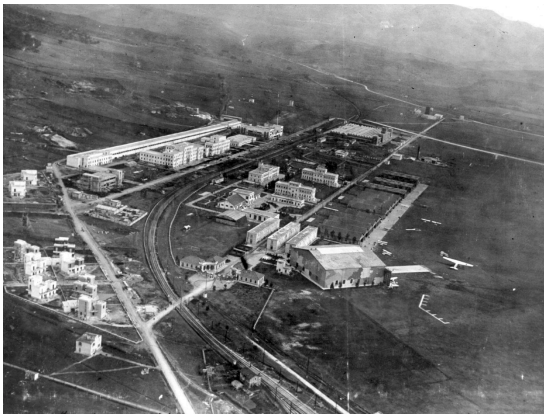

Direzione Superiore Studi ed Esperienze (DSSE)

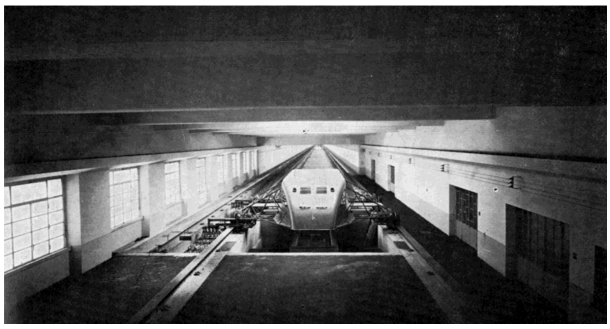

DSSE, slowest cart

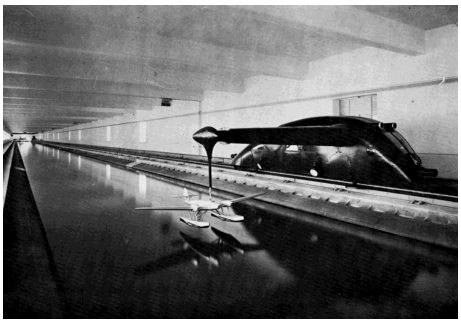

DSSE, fastest cart

For what has been said, before WWII Italy claimed three big water tanks but during the war lost the facilities of La Spezia and Guidonia; the only tank of Rome survived to this period. The reconstruction of Italy after war disasters, brought a lot of work for INSEAN. Already in 1956, the Italian merchant fleet was one of the first in the world, the transport fleet the second absolute and Italians shipbuilders received many orders from all over the world. If this was possible it was also for the activity of INSEAN; in fact, law stated that all the ships to build had to be preventively tested, with corresponding models, in the tank of Rome. For this reason we can say that, in that period, there was not any ships, flying Italian flag, that was not tested before at INSEAN. The data of 1955 are eloquent: 85 helix models, 55 hull models and 555 experimental campaign. Even if war spared this facility, structural problems occurred; in 1974 the actual INSEAN plant, endowed of two tanks, started his activity.

The bigger tank is 470 x 13.5 x 6.5 m with a maximum velocity test of 15 m/s; during construction, it was the longest tank of all western Europe. The smaller one is 220 x 9 x 3.5 m with a maximum velocity test of 10 m/s; in this tank there is also a flap type wavemaker. INSEAN has also others facilities like the circulating water channel, for cavitation and pressure field tests, and the maneuvering basin: this one is located on the shore of Nemi's lake where is possible to perform maneuvering outdoor tests.

In Italy there are also other plants.
Since 1980, is also active the test tank of Università di Napoli Federico II that, with the dimensions of 150 x 9 x 4 m, is the biggest university water tank of Europe; the maximum velocity is 10 m/s and it's also endowed of a flap type wavemaker.

Politecnico di Bari has an important facility: there are two tanks of dimensions $90\ m\ x\ 50\ m\ x\ 1.2\ m$ and $30\ m\ x\ 50\ m\ x\ 3\ m$ and two wave flumes, both of dimensions $40\ m\ x\ 2.4\ m\ x\ 1.2\ m$, active since 2001. The bigger tank is mainly used for studies on coastal dynamic and onshore structures defense while the smaller one is used for offshore model tests.

In the University of Genova there is a 60 x 2.5 x 3 m tank with a measuring cart that can reach 3 m/s but it is not equipped with wave generator.

University of Padova has a wave flume with dimensions of $35\ m\ x\ 1\ m\ x\ 1.3\ m$ and a marine tank of $20.6\ m\ x\ 17.8\ m\ x\ 0.8\ m$; research area is mainly focused on waves hydrodynamics, floating structures, wave energy converter and onshore structures.

The Laboratory of Maritime Engineering (LABIMA) of Università di Firenze has two tanks: one of $37\ m\ x\ 0.8\ m\ x\ 0.8\ m$, operative since 1980 and completely rebuilt in 2013, and another one of $52\ m\ x\ 1.5\ m\ x\ 2\ m$, recently built by researchers and completely operative from 2020. In both tanks, waves are generated by a piston type wavemaker and it is also possible to study currents actions.

Politecnico di Torino has a tank of 30 x 0.7 x 2.2 m with a towing cart that can run for 23 m with velocity included between 0.004 and 2.8 m/s. For the this facility it is in evaluation the insertion of a wavemaker device and the present work would like to be the first step of this project.

Despite the presence of the above mentioned facilities, new technologies challenges are imposing new plants. It is recent (July 2019) the construction announcement of the first ocean tank in Italy in the arsenal of La Spezia, there where all started with Brin and Rota at the end of XIX century.

As we saw, this sector of engineering, even if maybe a bit hidden, has its history and it is surely a dynamic environment made of researchers, new projects and discoveries. These tests give to designers the security that their project will satisfy all the requirement, allowing important resources saving

What at the beginning was considered an expensive play for the various intellectuals like Svedemborg, Chapman, the brothers Hall and steel the same Froude, is nowadays needful in every ship and sea facilities design, always with the same basic idea: studying a model to forecast the reality.

1.2 Wave tanks

As probably understood, wave tanks are particular test tanks in which it is possible to generate waves and then to study the model behavior in a more realistic sea state. From the historical introduction it is clear that testing models is fundamental to better understand eventual design mistakes, to correct them before it becomes impossible and then saving money.

There are three fundamentals zones in a wave tank: the wavemaker, the model and the beach zone.

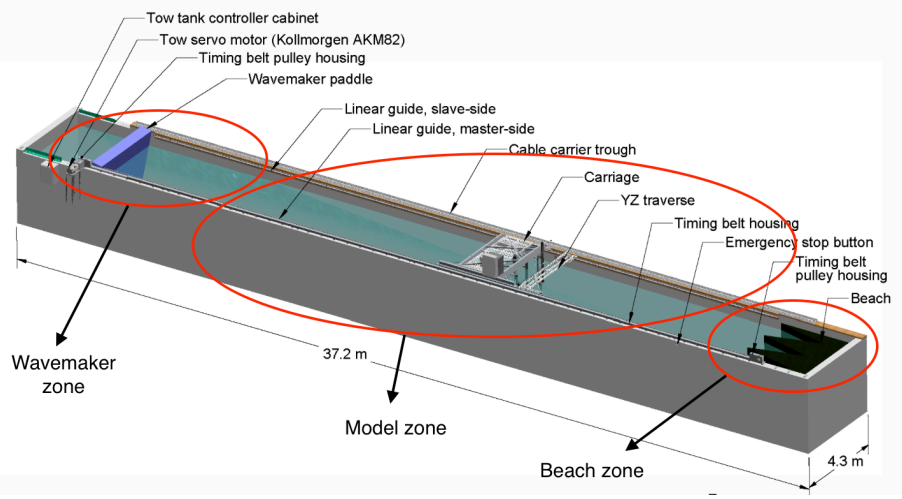

The first one contains the wavemaker and it's up to three times the water depth from the device to allow the extinction of the local disturbances; these, as we will see in the following chapters, are due to the mismatching between the paddles and the water motion. Though there are several types of wavemakers, the most common are the piston and the flap types; for this reason, in the present work we will focus on only these two devices.

The model zone has to host the model, to allow measures and it has to be enough to have the correct simulation environment; for example, referring to a towing tank, we need enough space to accelerate the model, to drag it at a constant velocity and then to slow down and stop.

The last zone hosts the beach, that is the element, usually on the opposite side of the wavemaker, that has to dissipate the wave energy avoiding wave reflection. This has to be avoided because waves can reach the model zone disturbing the measurements and making tests not repeatable. If the beach is a fixed structure, we can have the sloped or the mesh style beach; otherwise, it is possible to have a wavemaker that works like a wave absorber, generating waves in phase opposition respect to the incoming ones.

It is often possible to have a towing cart which allows to drag models in the wave tank exactly like in a towing tank; again, here we have the dynamometer and other measurements devices.

We have several types of wave tanks and here it is given a general overview.

The frontal wave tank is the most common; it usually has a rectangular shape, with the wavemaker that occupies one of the four sides and the beach opposite. If the width is so small to allow the presence of only one paddle, we call them wave flumes. Otherwise, if there is the possibility to host more paddles, we can create a so called *snake wavemaker* through which we can generate both straight and oblique waves. Since there aren't wavemakers on the others two sides, reflected waves could create testing problems.

Frontal wave tank

The corner wave tanks have wavemakers on adjacent sides of the tank; with this solutions it is possible to generate oblique waves with a good accuracy and we can avoid the rearrangement of the set up during tests. The basic solution is the dual face snake type wavemaker but there are also the C and the squared type in which we can both generate and absorb waves through wavemakers.

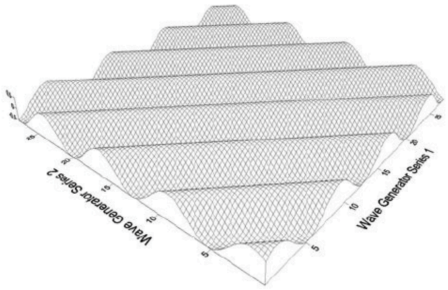

Dual face snake type wave maker

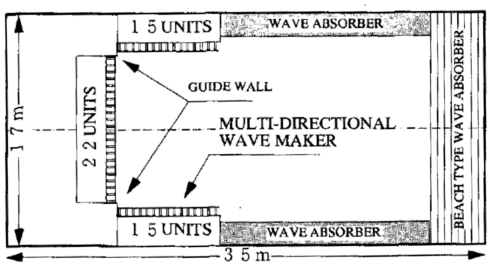

C type

Squared type

The last typologies are the curved and circular wave tank. If we drive all wavemaker with no phase delay between them, we generate a curved wave direct to the center of the wavemakers arc; otherwise, giving a phase lag between adjacent paddles, it's possible to generate a straight wave. In the curved tank we need a kind of beach on the opposite side of wavemakers while this is not required in the circular tank because we can use wavemakers to absorb waves.

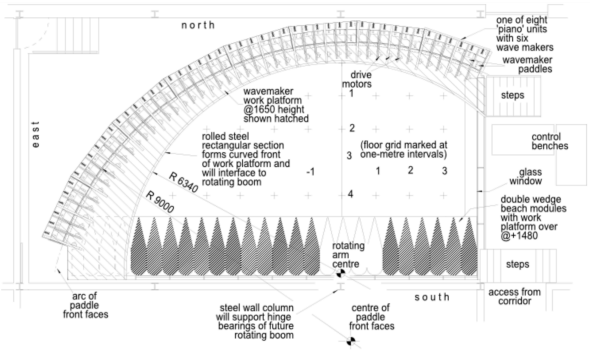

Curved Type

Circular Type

1.3 Collection of test tanks

1.3.1 Test tanks in the world

In this section we are going to present some of the most important facilities in the world to have a general overview about the state of art of these tests and some references.

One of the most important institutions of the world for test tanks is the **Naval Surface Warfare Center, Carderock Division "David Watson Taylor" (Maryland, USA)**. This institution is part of the Naval Sea Systems Command, the biggest system command of the United States Navy; the aim of this organization is the research, develop and maintenance for the fleet of United States. Though there are many testing facilities in this site, we mention the MASK basin (Maneuvering and Seakeeping Basin); this is the biggest tank in the world in which it is possible to generate waves. The basin dimensions are 106 x 76 x 6 m and it is equipped with 216 flap wavemakers. It is possible to generate waves with a maximum height of 0.6 m, a maximum wave length of 12.2 m and there is also a towing carriage that can reach the maximum velocity of 7.2 m/s. The maximum model length is 9 m.

The **Krylov State Research Centre** is the reference institution for the shipbuilding industry in **Russian Federation**; it was founded in 1894 in St. Petersburg with the creation of the first model tank of the Russian Empire. A. N. Krylov, a world famous Russian naval engineer and mathematician, became the person in charge of this institution in 1900. The construction of the actual facility, located in the south part of St. Petersburg, was started in 1936 and ended in 1960. The activities of this research centre cover the most important fields of shipbuilding in both civil and military sector. From all the facilities present in this institute, we focus on the Large Scale Seakeeping/maneuvering model basin. Its dimensions are 162 m x 37 m x 5 m and there are segmented flap type wave generators on two of the four sides of this rectangular tank. The maximum wave height reachable is 0.45 m with a period of 2 s and there is a carriage that can reach 6 m/s in the x direction and 4 m/s in the y one. The maximum model length is 12 m.

The most important institution in **China** is the **China Ship Scientific Research Center**. Closely linked to the China Shipbuilding Industry Corporation, CSSRC has a wide range of research activities in shipbuilding, offshore and underwater structure design. It was established in 1951 in the city of Wuxy, Jiangsu province, not far from Shanghai; from 1978 is part of ITTC. Also in this case, we focus on the Seakeeping basin. Its dimensions are 69 m x 46 m x 4 and it is equipped with 188 flap type wavemakers on the adjacent short and long side of the basin; on the opposite sides there are the beaches. It is possible to generate regular waves with a maximum wave height of 0.5 m and with a period between 0.5 – 5 s; there is also a carriage that can tow model with a maximum velocity of 4 m/s. The maximum model length is 5 m.

Still in the far East, we find the **National Maritime Research Institute of Japan**. The first unit of this institution was established in 1916 under the control of the Ministry of Telecommunication and Transport and it developed with continuous improvements along the last century. The Actual Sea Model Basin is 80 m x 40 m x 4.5 m and it has 382 flap type absorbing wavemakers. The maximum wave height reachable is 0.35 m and the wave periods are between 0.43 – 4 s; there is

also the possibility to realize towing tests with the main carriage that can reach a maximum velocity of 3.5 m/s. The model size range is comprised between 2 and 4.5 m.

In **South Korea** we find the **Korea Research Institute of Ships and Ocean Engineering**. It was established in 1973 and its main activities are shipping technology, marine traffic system technology, marine accident response and underwater robot. The towing tank is 221 m x 16 m x 7 m (various depth) and it has a single flap type wavemaker that covers all the width of the tank; on the opposite side there is the beach. It is possible to generate regular waves with a maximum height of 0.5 m; for irregular waves, the height limit is 0.3 m. Since it is a towing tank, there is a carriage to drag models that can reach a maximum velocity of 6 m/s. The model size range is between 6 – 12 m

A very important institution in **Australia** is the **Australian Maritime College**. It was established in 1978 in Launceston and it collaborates with international government and industrial organizations. Its towing tank is the only one active in Australia and it is 100 m (length) x 3.5 m (width) x 1.5 m (depth); there is a single flap type that covers all the width and through which it is possible to generate waves with a maximum height of 0.7 m. The towing carriage can reach the maximum velocity of 5 m/s and the model length range is 1-2.5 m.

The Naval Science and Technological Laboratory is part of the Defense Research and Development Organization of **India**. It was established in 1969 in Visahapatnam and its research activities are closely linked to military applications. The Seakeeping and Maneuvering basin is 135 m (length) x 37 m (width) x 5 m (depth) and it is equipped with 256 flap type wavemakers on two adjacent sides; the maximum wave height achievable is 0.5 m. The towing carriage can reach a maximum velocity of 6 m/s and the model length range is 3 – 5 m.

In **Iran** there is the **National Iranian Marine Laboratory (NIMALA)**. It was established in 2012 in Tehran and its researches are focused on offshore structures and resistance, maneuvering, seakeeping and propulsion of vessels and submarines. The towing tank is 400 m (length) x 6 m (width) x 4 m (depth) and it has a piston type wavemaker that can generate both regular and irregular waves; the maximum regular wave height reachable is 0.5 m. The maximum carriage speed is 19 m/s.

A very important institution in South America is the **Brazilian Ocean Technology Laboratory** with its Ocean Basin. Part of the Ocean Engineering Department of the Rio de Janeiro Federal University, it works since 2003 and it was created mainly for testing oil and gas offshore structures. With its record depth of 15 m, that becomes 25 m in a hole of 5 m of diameter in the bottom of the tank, the Ocean Basin is the deepest basin in the world. It has a rectangular shape with the dimension of 40 m (length) x 30 m (width) x 15 m (depth); the central hole has a diameter of 5 m and it reaches a depth of 25 m. On the shorter side there are 75 flap type wavemakers that can generate a maximum regular wave height of 0.5 m; the wave period range is between 0.5 – 5 s.

The following table sums up the main information about the above cited facilities:

State and Institution	Tank	Tank dimensions	Wave maker type	Wave Height		
				Wave Height (not specified)	**Maximum Regular Wave Height**	**Maximum Irregular Wave Height**
USA Naval Surface Warfare Center, Carderock Division	Maneuvering and Seakeeping Basin	106 m x 76 m x 6 m	Flap		0.6 m	
Russian Federation Krylov State Research Centre	Maneuvering and Seakeeping Basin	162 m x 37 m x 5 m	Flap	0.45 m		
Public Republic of China China Ship Scientific Research Center	Seakeeping Basin	69 m x 46 m x 4 m	Flap		0.5 m	
Japan National Maritime Research Institute	Actual Sea Model Basin	80 m x 40 m x 4.5 m	Flap	0.35 m		
South Korea Korea Research Institute of Ships and Ocean Engineering	Towing Tank	221 m x 16 m x 7 m	Flap		0.5 m	

Australia Australian Maritime College	Towing Tank	100 m x 3.5 m x 1.5 m	Flap		0.7 m	
India Naval Science and Technological Laboratory	Seakeeping and Maneuvering basin	135 m x 37 m x 5 m	Flap		0.5 m	
Iran National Iranian Marine Laboratory	Towing Tank	400 m x 6 m x 4 m	Piston	0.5 m		
Brazil Brazilian Ocean Technology Laboratory	Ocean Basin	40 m x 30 m x 15 m	Flap		0.5 m	

1.3.2 Test tanks in Europe

Now we are going to focus on European facilities. Informations are mainly taken from the website of Marinet2. This last one acronym stands for Marine Renewables Infrastructure Network, that is a European project that aims to develop wave energy converter devices covering the costs of accessing test facilities.

One of the best facility in Europe is the **FloWave Ocean Basin** of the **University of Edinburgh**. It was built in 2014 by the already mentioned Edinburgh Design and it is mainly used to test wave energy converter devices; thanks to its circular geometry, it is possible to simulate complex sea state combining wave and current generation capability. The FloWave is a circular basin with a diameter of $25\ m$ and $2\ m$ deep equipped with 168 active-absorbing flap type wavemakers. It is optimised for generating waves with a period of $2\ s$ and a wave height of $0.7\ m$ and the maximum current velocity is $1.6\ m/s$; the testing scales are approximately between $1{:}\,20 - 1{:}\,30$.

In **Ireland** we find the **Lir National Ocean Test Facility**, an excellence center for marine renewable energy research and marine engineering in general. One of the four test tanks present in this research center is the Ocean Emulator, a rectangular basin with dimensions $25\ m\ x\ 18\ m\ x\ 1\ m$; there is also a trench of $11.2\ m\ x\ 10\ m$ equipped with a movable floor plate that makes possible the depth regulation between $1\ m$ and $2.5\ m$. There are 80 flap type

wavemakers on two sides of the basin and this allows to generate waves with adjustable direction. The maximum regular wave height is $0.32\ m$ and the maximum irregular wave height is $0.16\ m$. This tank is used for testing devices in the early development phase and the models scale range is between $1{:}\,50 - 1{:}\,100$.

In **Germany**, **University of Hannover** has one of the biggest wave flume of the world. It is $300\ m\ x\ 5\ m\ x\ 7\ m$ and it is equipped with piston type wavemaker with a maximum stroke of $4\ m$. The maximum wave height reachable is more than $2\ m$.

The most important wave tank in **France** is the **Hydrodynamic and Ocean Engineering Tank** of the **École centrale de Nantes**; the activity of this facility is focused on naval, oil and gas and marine renewable energy sectors. The dimensions are $50\ m\ x\ 30\ m\ x\ 5\ m$ with a central square cavity of $5\ m\ x\ 5\ m\ x\ 5\ m$; on the $30\ m$ side there is a snake type wavemaker made of 48 flaps independently controlled that allows to simulate complex sea state. It is possible to generate regular waves with a maximum wave height of $1\ m$ and irregular waves with a maximum significant waves height of $0.65\ m$.

The **Wave and Current Basin** of the **Aalborg University**, **Denmark**, was built in 2017 and it is mainly used for testing coastal and offshore structure models and wave energy converter. It is $14.6\ m\ x\ 19.3\ m\ x\ 1.5\ m$ and there is also a pit of $6.5\ m\ x\ 2\ m$ in which it is possible to have ulterior $6\ m$ of depth. In this tank there are 30 piston type wavemakers that realize a snake type wavemaker. The maximum regular wave height is $0.45\ m$ and the maximum irregular one is between $0.25 - 0.30\ m$. The possibility to generate currents, allows tests with waves and current combination.

In **Spain** we find the **Cantabria Coastal and Ocean Basin**, a facility of the **University of Cantabria**; it is suitable for tests on coastal and offshore structures and on wave energy converter. The dimensions are $44\ m\ x\ 30\ m\ x\ 4\ m$ with the possibility to add $8\ m$ to the depth using a depth adjustable pit of $6\ m$ of diameter. There are 64 flap type wavemakers capable of generating waves with a maximum height of $1\ m$. There is also the possibility to generate current with a flow rate up to $18\ m^3/s$.

In **Portugal** the **University of Porto** has a wave tank with dimensions of $28\ m\ x\ 12\ m\ x\ 1.2\ m$; a central pit $(4.5\ m\ x\ 2\ m\ x\ 1.5\ m)$ makes possible the reproduction of deep water environment. It is equipped with a wavemaker composed by several pistons that allows the reproduction of regular and irregular waves.

The following table sums up the main information about the above cited facilities:

State and Institution	Tank	Tank dimensions	Wave maker type	Wave Height		
				Wave Height (not specified)	**Maximum Regular Wave Height**	**Maximum Irregular Wave Height**
UK FloWave Ocean Basin	Ocean Basin	diameter 25 m 2 m deep	Flap	0.7 m		
Ireland Lir National Ocean Test Facility	Ocean Emulator	25 m x 18 m x 1 m	Flap		0.32 m	0.16 m
Germany University of Hannover	Wave Flume	300 m x 5 m x 7 m	Piston	2 m		
France École centrale de Nantes	Hydrodynamic and Ocean Engineering Tank	50 m x 30 m x 5 m	Flap		1 m	0.65 m
Denmark Aalborg University	Wave and Current Basin	14.6 m x 19.3 m x 1.5 m	Piston		0.45 m	0.25 – 0.30 m
Spain University of Cantabria	Cantabria Coastal and Ocean Basin	44 m x 30 m x 4 m	Flap	1 m		
Portugal University of Porto	Wave tank	28 m x 12 m x 1.2 m	Piston	N.A.	N.A.	N.A.

1.3.3 Test tanks in Italy

Since we have already presented several facilities inside the historical introduction, here we only summarize the main features.

Institution	Tank	Tank dimensions	Wavemaker type	Wave Height		
				Wave Height (not specified)	**Maximum Regular Wave Height**	**Maximum Irregular Wave Height**
INSEAN	Towing Tank	220 m x 9 m x 3.5 m	Flap	N.A.	0.45 m	N.A.
Università Federico II Napoli	Towing Tank	140.2 m x 9 m x 4.25 m	Flap	N.A	N.A	N.A
Politecnico di Bari LIC	Coastal Dynamic Tank	90 m x 50 m x 1.2 m	N.A.	N.A	N.A	N.A
	Offshore Model Tank	30 m x 50 m x 3 m	N.A.	N.A	N.A	N.A
	Wave Flume	40 m x 2.4 m x 1.2 m	N.A.	N.A	N.A	N.A
	Wave Flume	40 m x 2.4 m x 1.2 m	N.A.	N.A	N.A	N.A
Università degli studi di Firenze LABIMA	Wave - Current Flume one	37 m x 0.8 m x 0.8 m	Piston	N.A.	0.35 m	N.A.
	Wave - Current Flume Two	52 m x 1.5 m x 2 m	Piston	N.A.	1.1 m	N.A.
Università degli studi di Padova	Wave Flume	35 m x 1 m x 1.3 m	Piston	N.A	N.A	N.A
	Marine Tank	20.6 m x 17.8 m x 0.8 m	Piston	N.A	N.A	N.A

Chapter 2

Linear water wave theory

This chapter introduces the linear water wave theory until the two dimensional solution for standing and progressive waves. The main reference for this chapter is [1].

2.1 Linear water wave theory

A volume of liquid without any force acting on it presents a flat interaction surface between air and liquid itself, exactly like the water in a basin after few seconds after filling; this is due to the action of gravity and surface tension. The opposite situation, an interaction surface crossed by waves, is an evidence of the action of forces acting on the liquid volume against gravity and surface tension; these forces can be caused by different reasons: the motion of an object inside the liquid volume, the wind, an earthquake and also the gravitational attraction of astronomical bodies. After the creation of the waves, the action of gravity and surface tension, that tend to recreate a flat interaction surface, causes the propagation of the waves.

Let observe now the following sketch:

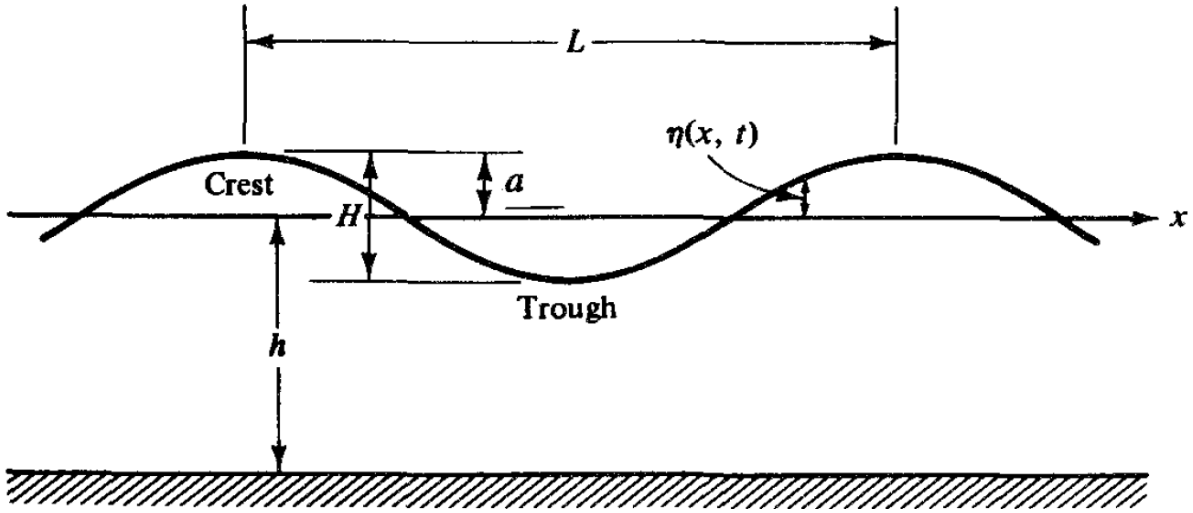

From now on, the reference system has the x direction like shown, the y one entering in the plane of the sheet and the zero for the z direction is at the still water level, so that the bottom is located at $z = -h$.

Referring to the sketch, the fundamental physical quantities for describing waves are:

- the length L, the distance between two crests or troughs;
- the height H, the distance between a crest and a trough;
- the water depth h, the distance between the still water level and the bottom.

Other important quantities are the wave amplitude a, the half of the wave height H, and the surface elevation η, the distance between still water level and interaction surface; moreover, we define the wave period T as the time spent by two successive crests or troughs to cross a certain point. Since the waves cross a distance L in the time T, we can define the speed of the wave as $C = L/T$; this quantity is called *celerity*. It is interesting to note that, despite this motion, the water above the surface does not translate along the wave propagation direction.

In real cases, the surface elevation η appear to be much different from the one showed in the sketch above; probably, for a fixed point of the sea surface, we will have the following record with respect to the time:

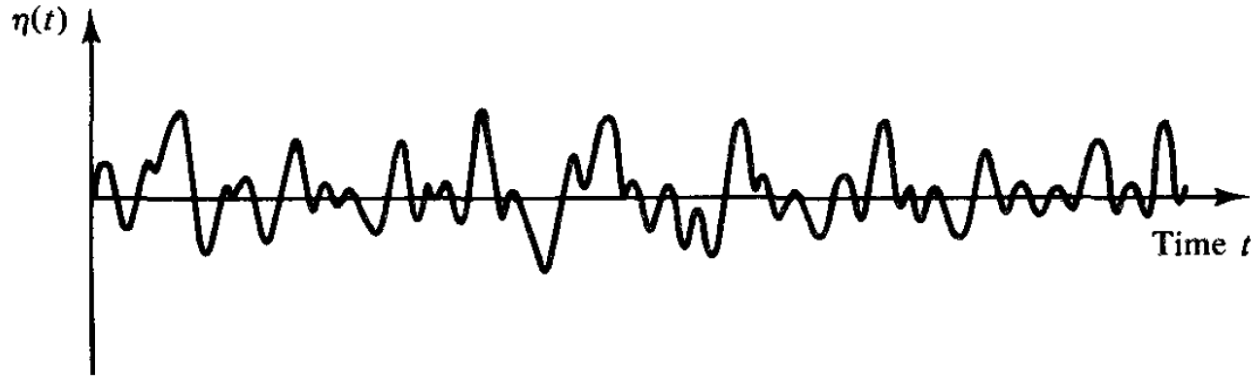

This trend can be seen like a superposition of sinusoids and it allows the use of Fourier analysis for describing water waves; moreover, to increase the analysis accuracy, statistical techniques are required to face the nature randomness.

However, in this work is used the linear, or small amplitude, water waves theory according which a wave can be modeled, with a good accuracy, by a sinusoid; this is mostly true for large waves, the so called *shallow water waves*, that present the ratio

$$\frac{h}{L} < \frac{1}{20}$$

In the following section, we will present the basis of this theory.

In general, the first two assumptions that we have to make for formulating the linear water waves theory are:

- irrotational fluid motion;
- incompressible fluid.

Referring to the first one, we can say that the motion of a volume of fluid is close to be irrotational, that means there is no vorticity inside the motion field, because the viscous effects, that give rotation to the fluid, are confined to the surface and the bottom. Let now see the consequences of this first assumption.

Let $\mathbf{u}$ be the velocity vector

$$\mathbf{u}(x,y,z,t) = u\mathbf{i} + v\mathbf{j} + w\mathbf{k}$$

The curl of the velocity vector is the vorticity $\boldsymbol{\omega}$

$$\nabla\times\mathbf{u} = \boldsymbol{\omega}$$

Since we made the hypothesis of irrotational fluid motion, we have no vorticity

$$\nabla\times\mathbf{u} = \mathbf{0}$$

This coincides with the independence of path condition for the result of a line integral in a three dimensional problem.

We introduce now the vector

$$d\mathbf{l} = dx\mathbf{i} + dy\mathbf{j} + dz\mathbf{k}$$

and we define the result of the line integral of $\mathbf{u}$ along a certain route that links the two general points P_0 and P_1 as

$$-\phi = \oint_{P_0}^{P_1} \mathbf{u}\cdot d\mathbf{l} = \oint_{P_0}^{P_1} (udx + vdy + wdz)$$

The respect of the above mentioned independence of path condition implies that the terms inside the integral have to be an exact differential, then

$$u = -\frac{\partial\phi}{\partial x} \quad v = -\frac{\partial\phi}{\partial y} \quad w = -\frac{\partial\phi}{\partial z}$$

This allows us to write

$$\mathbf{u}(x,y,z,t) = u\mathbf{i} + v\mathbf{j} + w\mathbf{k} = -\frac{\partial\phi}{\partial x}\mathbf{i} - \frac{\partial\phi}{\partial y}\mathbf{j} - \frac{\partial\phi}{\partial z}\mathbf{k}$$

that is

$$\mathbf{u} = -\nabla\phi$$

Summing up, since the fluid motion is quite irrotational, we can define a potential function ϕ the gradient of which is the velocity vector $\mathbf{u}$.

Let now see the consequences of the assumption of incompressible fluid.
From the theory, we can derive the continuity equation as follows

$$\frac{1}{\rho}\left(\frac{\partial \rho}{\partial t}+u\frac{\partial \rho}{\partial x}+v\frac{\partial \rho}{\partial y}+w\frac{\partial \rho}{\partial z}\right)+\frac{\partial u}{\partial x}+\frac{\partial v}{\partial y}+\frac{\partial w}{\partial z}=0$$

The definition of bulk modulus E of the fluid is

$$E \equiv \rho\frac{dp}{d\rho}$$

and for water is

$$E_{water} = 2.07 \cdot 10^9 Pa$$

Rewriting the definition as

$$d\rho = \frac{dp}{E}\cdot \rho$$

we can note that, for a pressure increase of $1 \cdot 10^6 Pa$ we have the 0.05% of density increase.
For this reason, we can clearly consider water incompressible and with $\rho = 1000\, kg/m^3$constant.

This allows to simplify the continuity equation reducing it to

$$\frac{\partial u}{\partial x}+\frac{\partial v}{\partial y}+\frac{\partial w}{\partial z}=0$$

or

$$\nabla \cdot \mathbf{u} = 0$$

This equation must be true everywhere in the fluid volume and a flow field $\mathbf{u}$ that satisfies this condition is called nondivergent flow.

Summing up, since we can consider the water incompressible, we can write the continuity equation in an easier way and the linked physical meaning is that is not allowed any fluid accumulation inside a volume of fluid.

Then, the continuity equation for an incompressible fluid states that

$$\nabla \cdot \mathbf{u} = 0$$

Substituting for $\mathbf{u}$ the result of the irrotational hypothesis we have

$$\nabla \cdot \nabla\phi = 0$$

and this yields to the Laplace equation, widespread in engineering problems

$$\boxed{\nabla^2\phi = \frac{\partial^2\phi}{\partial x^2}+\frac{\partial^2\phi}{\partial y^2}+\frac{\partial^2\phi}{\partial z^2}=0}$$

This is a second order linear differential equation and, in this case, it describes the fluid motion under a periodic two-dimensional water wave; this equation must be valid within the whole fluid domain, constituted by only one wave

$$\boxed{\begin{matrix}\nabla^2\phi = 0 \\ \begin{cases} 0 < x < L \\ -h < z < \eta \end{cases}\end{matrix}}$$

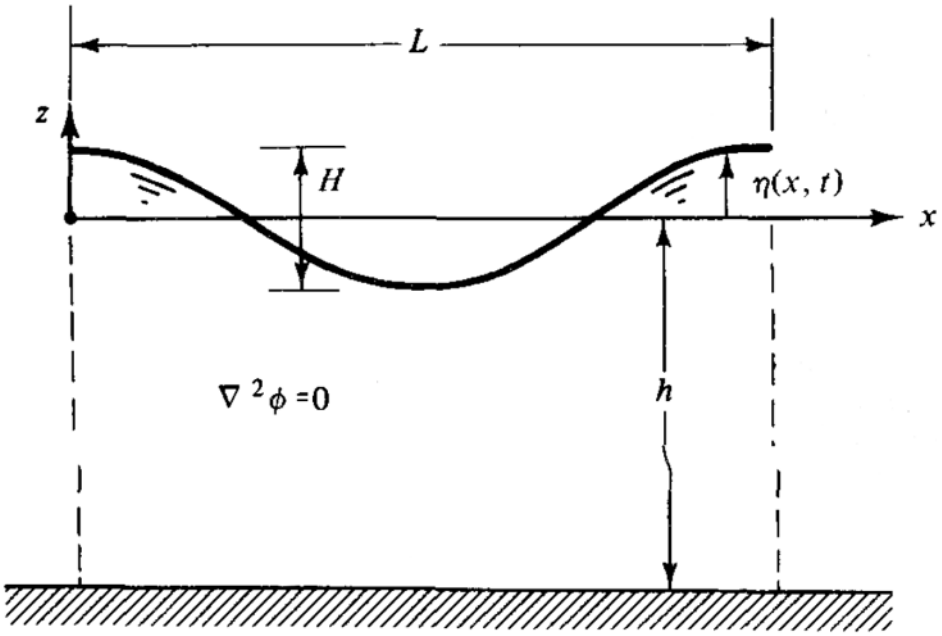

The are many solutions to this equation and now we have to find the ones that correctly describe our phenomenon setting up a boundary value problem and solving it. Before doing this, it is important to underline that this differential equation is linear and allows us to use the superposition property, in particular: if ϕ_1 and ϕ_2 are solution of the Laplace equation, then their linear combination $\phi_3 = A\phi_1 + B\phi_2$, where A and B are arbitrary constants, is still a solution. This give us the possibility to create new solutions with additions and subtractions between other solutions.

We have now to set up the following boundary value problem

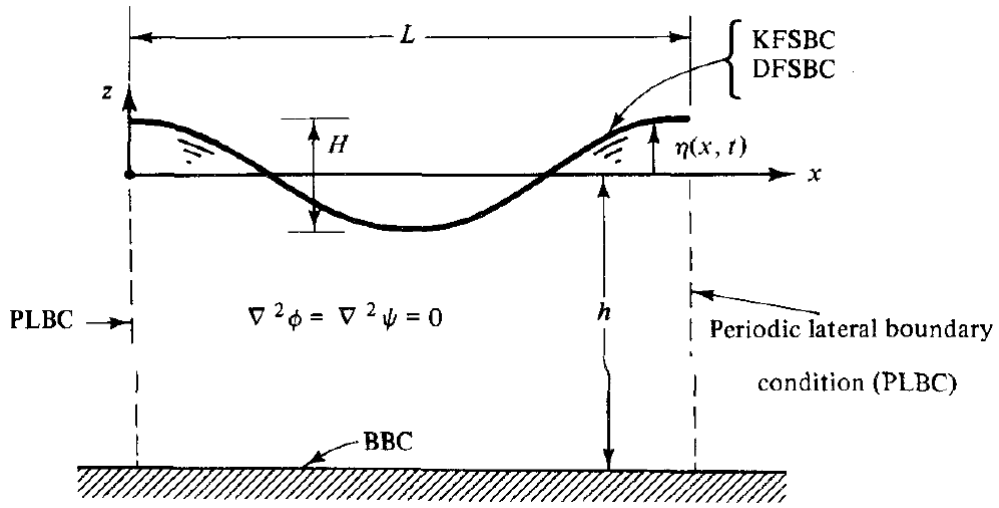

For the free surface and the bottom we have to introduce the so called *kinematic boundary conditions*, requirements on water particle kinematics. The concept is that there cannot be flow across this two boundaries; to translate this idea in an expression, we have to start from the mathematical description of these boundaries.

In general, a surface can be described by

$$F(x, y, z, t) = 0$$

Appling the total derivative to this surface expression and evaluating it on the surface, we have

$$\frac{DF(x,y,z,t)}{Dt} = \frac{\partial F}{\partial t} + u\frac{\partial F}{\partial x} + v\frac{\partial F}{\partial y} + w\frac{\partial F}{\partial z}\Big|_{on\ F(x,y,z,t)=0} = 0$$

because if we move with the surface we do not see any change.

The last equation can be rewritten as

$$-\frac{\partial F}{\partial t} = \mathbf{u} \cdot \nabla \mathrm{F}$$

and, since the gradient of a scalar field that describes a surface has the direction of the normal to this surface, we can introduce the unit vector normal

$$\mathbf{n} = \frac{\nabla \mathrm{F}}{|\nabla F|}$$

then

$$-\frac{\partial F}{\partial t} = \mathbf{u} \cdot \mathbf{n}|\nabla F|$$

Solving for $\mathbf{u} \cdot \mathbf{n}$, we obtain the general expression for the kinematic boundary condition

$$\mathbf{u} \cdot \mathbf{n} = \frac{-\frac{\partial F}{\partial t}}{|\nabla F|} \quad on\ F(x, y, z, t) = 0$$

with

$$|\nabla F| = \sqrt{\left(\frac{\partial F}{\partial x}\right)^2 + \left(\frac{\partial F}{\partial y}\right)^2 + \left(\frac{\partial F}{\partial z}\right)^2}$$

This equation states that the component of the fluid velocity field normal to the surface are linked to the surface local velocity

Now we apply this condition to the bottom and free surface boundaries.

Bottom boundary condition

In a two dimensional case, assuming no change in time for the bottom, we can describe its surface like

$$z = -h(x)$$

or

$$F(x, z) = z + h(x) = 0$$

and then

$$\frac{\partial F}{\partial t} = 0$$

Moreover, assuming the bottom impermeable, we have

$$\mathbf{u} \cdot \mathbf{n} = 0$$

where $\mathbf{n}$ is the normal to the bottom surface and has the following expression

$$\mathbf{n} = \frac{\nabla F}{|\nabla F|} = \frac{\frac{dh}{dx}\mathbf{i} + 1\mathbf{k}}{\sqrt{\left(\frac{dh}{dx}\right)^2 + 1}}$$

Developing the dot product and multiplying both sides of the equation by the square root at the denominator, we arrive to

$$\boxed{\frac{w}{u} = -\frac{dh}{dx} \quad on\ z = -h(x)}$$

According to this condition, the flow at the bottom has to be tangent to the bottom at each x; referring to the following image

$$-w = u\frac{dh}{dx} \quad on\ z = -h(x)$$

and summing the two vectors, one directed along x and the other along z, we can clearly observe the result of the bottom boundary condition.

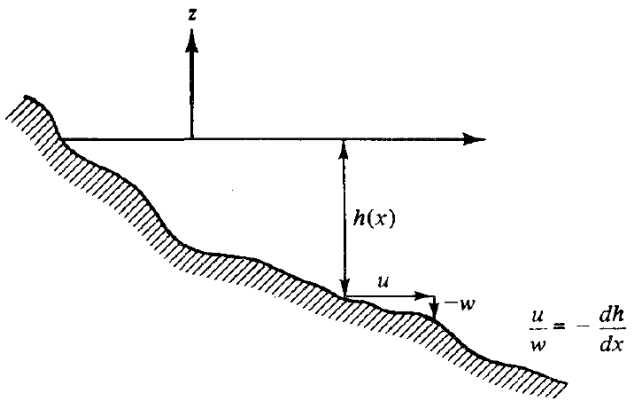

As shown in the reference sketch, in our problem we have a horizontal bottom and then

$$\frac{dh}{dx} = 0 \Rightarrow\ w = 0$$

Kinematic Free Surface Boundary Condition

Once studied the bottom, we move to the free surface.
Using the expression for the free surface displacement $\eta(x, y, t)$, the interaction surface between air and water can be described by

$$F(x, y, z, t) = \ z - \ \eta(x, y, t) = 0$$

Substituting this relation inside the general kinematic boundary condition we have

$$\mathbf{u}\cdot\mathbf{n}=\frac{\frac{\partial\eta}{\partial t}}{\sqrt{\left(\frac{\partial\eta}{\partial x}\right)^2+\left(\frac{\partial\eta}{\partial y}\right)^2+1}}\qquad on\ z=\eta(x,y,t)$$

where $\mathbf{n}$ is the normal to the free surface and has the following expression

$$\mathbf{n}=\frac{\nabla F}{|\nabla F|}=\frac{-\frac{\partial\eta}{\partial x}\mathbf{i}-\frac{\partial\eta}{\partial y}\mathbf{j}+1\mathbf{k}}{\sqrt{\left(\frac{\partial\eta}{\partial x}\right)^2+\left(\frac{\partial\eta}{\partial y}\right)^2+1}}$$

Developing the dot product and multiplying both sides of the equation by the square root at the denominator, we arrive to

$$\boxed{w=\frac{\partial\eta}{\partial t}+u\frac{\partial\eta}{\partial x}+v\frac{\partial\eta}{\partial y}\quad on\ z=\eta(x,y,t)}$$

Dynamic Free Surface Boundary Condition

The interaction surface between air and water is a free surface and, in reverse of surfaces fixed in the space, it cannot support pressure variations; for this reason, we need another boundary condition to impose the pressure distribution on the free surface. As shown by the following image, in our problem there is the atmospheric pressure acting on the water

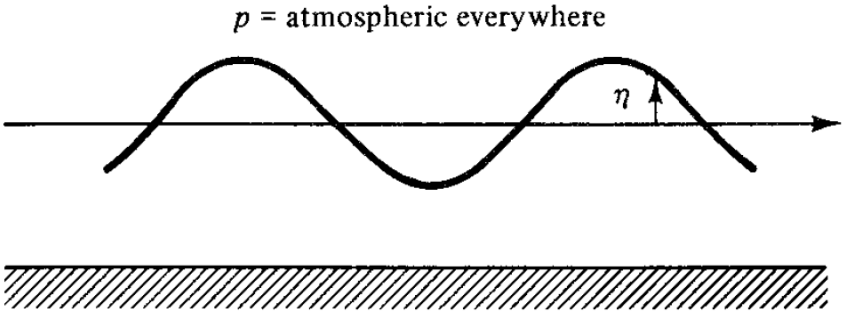

To impose this condition, we will use the *unsteady* Bernoulli equation.

Still under the hypothesis of irrotational motion and incompressible fluid, from the theory we can arrive to

$$-\frac{\partial\phi}{\partial t}+\frac{1}{2}(u^2+w^2)+\frac{p}{\rho}+gz=C(t)$$

Compared to the Bernoulli equation, the term $C(t)$ is not a constant and it is the cause of the "*unsteady*".

Coming back to the boundary condition, we apply the unsteady Bernoulli equation on the free surface

$$-\frac{\partial \phi}{\partial t}+\frac{1}{2}(u^2+w^2)+\frac{p_\eta}{\rho}+gz=C(t) \quad on \quad z=\eta(x,t)$$

where usually $p_\eta = 0$ because considered as gage pressure.

Substituting for u^2 and w^2 the results of the irrotational hypothesis, we obtain

$$\boxed{-\frac{\partial \phi}{\partial t}+\frac{p_\eta}{\rho}+\frac{1}{2}\left[\left(-\frac{\partial \phi}{\partial x}\right)^2+\left(-\frac{\partial \phi}{\partial z}\right)^2\right]+gz=C(t) \qquad on \quad z=\eta(x,t)}$$

that is the dynamic free surface boundary condition.

Lateral boundary condition

In order to finish the formulation of the problem, we have to impose the remaining two conditions to the lateral boundary. Since we are studying a general volume of water with the surface crossed by waves, we use the following periodic boundary condition used both in time and space

$$\boxed{\begin{array}{l}\phi(x,t)=\phi(x+L,t)\\ \phi(x,t)=\phi(x,t+T)\end{array}}$$

Set the boundary value problem, we have to solve it. The goal is to find a solution $\phi(x,z,t)$ for the Laplace equation and an expression for $\eta(x,t)$ both for standing and progressive waves; during the resolution will be carried out also another important equation, the dispersion relationship.

Since Laplace equation is a linear partial differential equation, we can try to solve it with separation of variables.

To apply this method, we first have to make the hypothesis that the solution has the following structure

$$\phi(x,z,t)=X(x)\cdot Z(z)\cdot T(t)$$

a product of terms, each one functions of one independent variable.

Since the lateral boundary condition imposes ϕ periodic also in time, we can set

$$T(t) = \sin \sigma t$$

where σ is the angular frequency of the wave.

To find a relation for σ, we use the time periodic boundary condition

$$\boxed{\phi(x,t) = \phi(x,t+T)}$$

then

$$\sin \sigma t = \sin \sigma (t+T)$$

$$\sin \sigma t = \sin(\sigma t + \sigma T)$$

which is true for $\sigma T = 2\pi$ and then, as usual

$$\boxed{\sigma = \frac{2\pi}{T}}$$

We have to note that, since we have a linear problem, the choice of $T(t) = \sin \sigma t$ as part of the solution can be replaced by $T(t) = \cos \sigma t$ or, in general, by the linear combination

$$T(t) = A\cos \sigma t + B \sin \sigma t$$

However, here we choose the first choice and then the velocity potential has now the following expression

$$\phi(x,z,t) = X(x) \cdot Z(z) \cdot \sin \sigma t$$

If we substitute this equation inside the Laplace one and then we divide by ϕ, not reporting the dependences, we obtain

$$\frac{1}{X}\frac{\partial^2 X}{\partial x^2} + \frac{1}{Z}\frac{\partial^2 Z}{\partial z^2} = 0$$

Considering now, for example, a variation in z while x is maintained constant, the second term of the equation could vary but the first one no and then the equation is not satisfied because we surely have not a sum equal to zero.

For this reason, last equation is satisfied if the two terms are equal to the same constant but with different sign

$$\frac{\frac{\partial^2 X(x)}{\partial x^2}}{X(x)} = -k^2$$

$$\frac{\frac{\partial^2 Z(z)}{\partial z^2}}{Z(z)} = k^2$$

where the constant k is called *wave number*; we have to note that it is not relevant which one of the two terms has the minus since k can also be a complex number.

The last equations are ordinary differential equations and we can solve it separately; the following table summarize the possible solutions

Character of k, the Separation Constant	Ordinary Differential Equations	Solutions
Real	$\frac{d^2X}{dx^2} + k^2X = 0$	$X(x) = A\cos kx + B\sin kx$
$k^2 > 0$	$\frac{d^2Z}{dz^2} - k^2Z = 0$	$Z(z) = Ce^{kz} + De^{-kz}$
$k = 0$	$\frac{d^2X}{dx^2} = 0$	$X(x) = Ax + B$
	$\frac{d^2Z}{dz^2} = 0$	$Z(z) = Cz + D$
Imaginary		
$k^2 < 0, k = i\lvert k\rvert$	$\frac{d^2X}{dx^2} - \lvert k\rvert^2X = 0$	$X(x) = Ae^{\lvert k\rvert x} + Be^{-\lvert k\rvert x}$
$\lvert k\rvert$ = magnitude of k	$\frac{d^2Z}{dz^2} + \lvert k\rvert^2Z = 0$	$Z(z) = C\cos\lvert k\rvert z + D\sin\lvert k\rvert z$

Since we have now a set of solutions to the Laplace equation, we have to understand which of these describes our phenomenon applying the above set of boundary conditions; this will give us also the possibility to find the several constants present in the solutions.

Lateral periodicity condition

The first boundary condition we are going to use is the lateral periodicity condition. According to this requirement, ϕ has to be periodic in space; observing the solutions reported in the above table, this is possible only if k is real and nonzero. Still from the table, for $k^2 > 0$ we have the following solutions for the above mentioned equations respectively

$$X(x) = A\cos kx + B\sin kx$$

$$Z(z) = Ce^{kz} + De^{-kz}$$

Consequently, we have the following velocity potential

$$\phi(x,z,t) = (A\cos kx + B\sin kx)(Ce^{kz} + De^{-kz})\sin\sigma t$$

To find a relation for k, we use the space periodic boundary condition

$$\boxed{\phi(x,t) = \phi(x,t+T)}$$

hence

$$A\cos kx + B\sin kx = A\cos k(x+L) + B\sin k(x+L) =$$
$$= A(\cos kx\cos kL - \sin kx\sin kL) + B(\sin kx\cos kL + \cos kx\sin kL)$$

The expression holds for $\cos kL = 1$ and $\sin kL = 0$ and this yields to $kL = 2\pi$ and then

$$\boxed{k = \frac{2\pi}{L}}$$

Since we are solving a linear problem, superposition principle is valid and it allows us to separate ϕ in different parts. From now on, it is useful for us to maintain the following terms from the previous potential equation

$$\phi = A\cos kx(Ce^{kz} + De^{-kz})\sin\sigma t$$

Thank to superposition, we can add back later the term $B\sin kx$.

Summing up, with the spatial periodicity condition we have restricted the possible solutions of the equations to the only ones for $k^2 > 0$ and we found an expression for k.

Bottom boundary condition for horizontal bottom

Proceeding in our development, we have now to use the bottom boundary condition. As already said, the condition states that

$$\boxed{\frac{w}{u} = -\frac{dh}{dx}}$$

Being the bottom horizontal in our problem, we have

$$\frac{dh}{dx} = 0$$

and then

$$w = -\frac{\partial\phi}{\partial z} = -Ak\cos kx(Ce^{kz} - De^{-kz})\sin\sigma t = 0$$

Evaluating the last expression in $z = -h$, we obtain

$$w = -\frac{\partial \phi}{\partial z} = -Ak \cos kx (Ce^{-kh} - De^{kh}) \sin \sigma t = 0$$

Since this equation has to be satisfied for any x and t, the quantity inside the parentheses must be zero; then, imposing this condition and resolving for C we have

$$C = De^{2kh}$$

Substituting now the last relation in the expression for the potential

$$\phi = A \cos kx \, (De^{2kh} e^{kz} + De^{-kz}) \sin \sigma t$$

$$\phi = A \, De^{kh} \cos kx \left(e^{k(h+z)} + e^{-k(h+z)}\right) \sin \sigma t$$

$$\phi = G \cos kx \cosh k(h+z) \sin \sigma t$$

with $G = 2ADe^{kh}$

Dynamic free surface boundary condition

We apply now the dynamic free surface boundary condition to determine the value of this new constant G. As already seen, we are going to use the unsteady Bernoulli equation

$$\boxed{-\frac{\partial \phi}{\partial t} + \frac{p_\eta}{\rho} + \frac{1}{2}\left[\left(-\frac{\partial \phi}{\partial x}\right)^2 + \left(-\frac{\partial \phi}{\partial z}\right)^2\right] + gz = C(t) \qquad on \quad z = \eta(x,t)}$$

Since the equation for the surface elevation is still not known now, this condition is applied on $z = \eta(x,t)$ evaluating this equation at $x = 0$ and using the truncated Taylor series

$$(Bernoulli\ equation)_{z=\eta} = (Bernoulli\ equation)_{z=0} + \eta \frac{\partial}{\partial z}(Bernoulli\ equation)_{z=0} + \cdots$$

Substituting the algebraic quantities

$$\left(gz - \frac{\partial \phi}{\partial t} + \frac{u^2 + w^2}{2}\right)_{z=\eta} = \left(gz - \frac{\partial \phi}{\partial t} + \frac{u^2 + w^2}{2}\right)_{z=0} + \eta \left[g - \frac{\partial^2 \phi}{\partial z \partial t} + \frac{1}{2}\frac{\partial}{\partial z}(u^2 + w^2)\right]_{z=0} + \cdots = C(t)$$

where $p = 0$ on $z = \eta$.

We have now to linearize. Referring to very small waves, η is small; then, we can assume that also velocities and pressures are small quantities.
Then the products of these terms are very small

$$\eta \ll 1 \quad \eta^2 \ll \eta \quad u\eta \ll \eta$$

Neglecting these quantities, we can write the linearized unsteady Bernoulli equation

$$\left(g\eta - \frac{\partial \phi}{\partial t}\right)_{z=0} = C(t)$$

Solving for η, we obtain the linear dynamic free surface boundary condition

$$\eta = \frac{1}{g}\frac{\partial \phi}{\partial t}\bigg|_{z=0} + \frac{C(t)}{g}$$

and substituting the velocity potential we have

$$\eta = \frac{G\sigma}{g}\cos kx \cosh k(h+z)\cos \sigma t\bigg|_{z=0} + \frac{C(t)}{g} = \left[\frac{G\sigma \cosh kh}{g}\right]\cos kx \cos \sigma t + \frac{C(t)}{g}$$

Setting $C(t) \equiv 0$ it results

$$\eta = \left[\frac{G\sigma \cosh kh}{g}\right]\cos kx \cos \sigma t$$

where the terms in the brackets are constant.

Referring to the reference sketch, that describes our physical model, we can write

$$\frac{H}{2} = \frac{G\sigma \cosh kh}{g}$$

and solving for G

$$G = \frac{Hg}{2\sigma \cosh kh}$$

Substituting this last relation inside the equation for η and ϕ, it yields

$$\eta = \frac{H}{2}\cos kx \cos \sigma t$$

$$\phi = \frac{Hg \cosh k(h+z)}{2\sigma \cosh kh}\cos kx \sin \sigma t$$

Summing up, using the bottom boundary condition and the dynamic free surface boundary condition, we have found an expression for the free surface elevation and for the velocity potential.

Kinematic free surface boundary condition

There is still another boundary condition to use, the kinematic free surface boundary condition

$$\boxed{w = \frac{\partial \eta}{\partial t} + u\frac{\partial \eta}{\partial x} + v\frac{\partial \eta}{\partial y} \quad on\ z = \eta(x, y, t)}$$

Using this last condition, we will find the relationship between σ and k.

Steel using the Taylor series expansion to relate the boundary condition at the unknown elevation $z = \eta(x, t)$ to $z = 0$, we have

$$\left(w - \frac{\partial \eta}{\partial t} - u\frac{\partial \eta}{\partial x}\right)_{z=\eta} = \left(w - \frac{\partial \eta}{\partial t} - u\frac{\partial \eta}{\partial x}\right)_{z=0} + \eta\frac{\partial}{\partial z}\left(w - \frac{\partial \eta}{\partial t} - u\frac{\partial \eta}{\partial x}\right)_{z=0} + \cdots = 0$$

With the same assumptions made before, we can linearize the last equation obtaining

$$w = \left.\frac{\partial \eta}{\partial t}\right|_{z=0}$$

or, expliciting w

$$-\left.\frac{\partial \phi}{\partial z}\right|_{z=0} = \frac{\partial \eta}{\partial t}$$

Substituting the expressions for ϕ and η in the last relation

$$-\frac{H}{2}\frac{gk}{\sigma}\frac{\sinh k(h+z)}{\cosh kh}\cos kx \sin \sigma t\Big|_{z=0} = -\frac{H}{2}\sigma \cos kx \sin \sigma t$$

and then, simplifying, we obtain the *dispersion relationship*

$$\boxed{\sigma^2 = gk \tanh kh}$$

Fixed the values of σ and h, we have only one k that satisfies this equation; this is shown in the graph below, in which is plotted the following equation

$$\frac{\sigma^2 h}{gkh} = \tanh kh$$

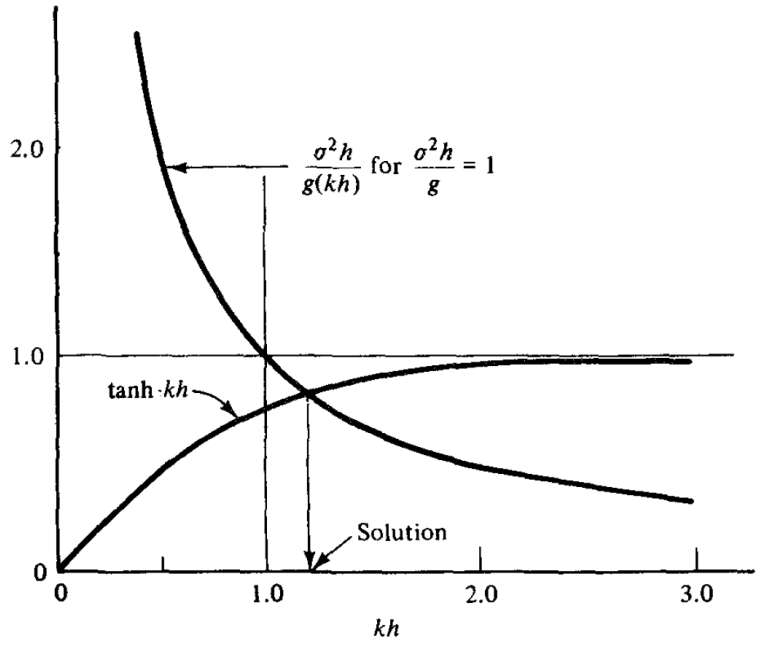

Remembering that

$$\sigma = \frac{2\pi}{T} \qquad k = \frac{2\pi}{L}$$

after some algebra, we can obtain an expression for speed of wave propagation C

$$C^2 = \frac{L^2}{T^2} = \frac{g}{k}\tanh kh$$

$$C = \sqrt{\frac{g}{h}\tanh kh}$$

and the expression for the wave length

$$L = \frac{g}{2\pi}T^2 \tanh\frac{2\pi h}{L}$$

Standing waves

Summing up the results obtained until now, we have

$$\phi = \frac{H}{2}\frac{g}{\sigma}\frac{\cosh k(h+z)}{\cosh kh}\cos kx \sin \sigma t$$

$$\eta(x,t) = \frac{1}{g}\frac{\partial \phi}{\partial t}\bigg|_{z=0} = \frac{H}{2}\cos kx \cos \sigma t$$

$$\sigma^2 = gk \tanh kh$$

These results describes a so called *standing wave* because it does not propagate; it can model a wave completely reflected by a vertical wall.
Now we have to find the same results for *progressive waves*.

Progressive waves

We consider the following velocity potential

$$\phi(x,z,t) = \frac{H}{2}\frac{g}{\sigma}\frac{\cosh k(h+z)}{\cosh kh}\sin kx \cos \sigma t$$

it differs from the other velocity potential because the x and the t terms are 90° out of phase but this is steel a solution to the Laplace equation and it respects all the boundary conditions.
Appling the linearized Dynamic Free Surface Boundary Condition we obtain

$$\eta(x,t) = \frac{1}{g}\frac{\partial \phi}{\partial t}\Big|_{z=0} = -\frac{H}{2}\sin kx \sin \sigma t$$

Since Laplace equation is linear and superposition is valid, we can subtract the new potential to the precedent one steel obtaining a solution

$$\phi = \frac{H}{2}\frac{g}{\sigma}\frac{\cosh k(h+z)}{\cosh kh}(\cos kx \sin \sigma t - \sin kx \cos \sigma t) = -\frac{H}{2}\frac{g}{\sigma}\frac{\cosh k(h+z)}{\cosh kh}\sin(kx - \sigma t)$$

Appling again the linearized Dynamic Free Surface Boundary Condition we obtain

$$\eta(x,t) = \frac{1}{g}\frac{\partial \phi}{\partial t}\Big|_{z=0} = \frac{H}{2}\cos(kx - \sigma t)$$

from which we understand that we have now a time moving wave.

Summing up, we obtained

$$\boxed{\begin{array}{c} \phi = -\frac{H}{2}\frac{g}{\sigma}\frac{\cosh k(h+z)}{\cosh kh}\sin(kx - \sigma t) \\ \eta(x,t) = \frac{1}{g}\frac{\partial \phi}{\partial t}\Big|_{z=0} = \frac{H}{2}\cos(kx - \sigma t) \\ \sigma^2 = gk \tanh kh \end{array}}$$

These results describes a *progressive wave*.

2.2 Simplifications for shallow and deep water waves

In these expressions, often occur hyperbolic functions of kh; for large and small values of kh, simplifications are admitted. Before introducing them, we have to define *shallow*, *intermediate* and *deep water waves*.

We define:

- *shallow water waves*, that waves that have a length much bigger than the backdrop depth on which they propagate ($L > 20h$);
- *intermediate water waves,* that waves that have a length comprised between $2h < L < 20h$;
- *deep water waves*, that waves that have a length inferior than twice the backdrop depth on which they propagate ($2h > L$).

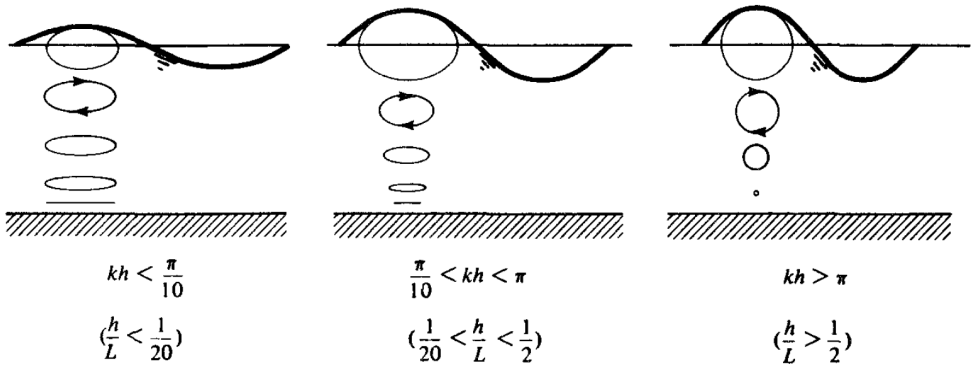

The following graph shows the trends of $\sinh kh$, $\cosh kh$ and $\tanh kh$

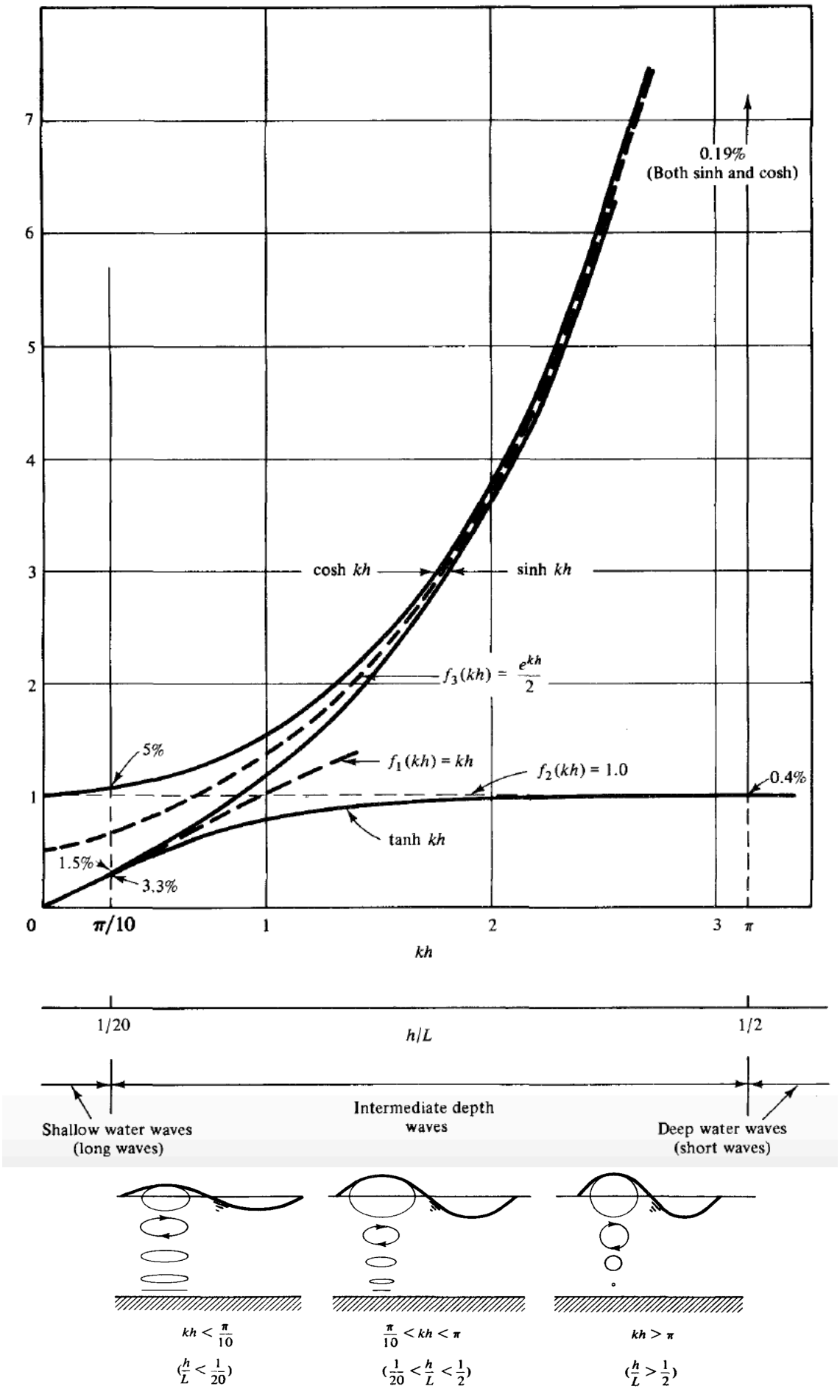
7
6
5
4
3
2
1
0
π/10
1
2
3
π
kh
0.19%
(Both sinh and cosh)
cosh kh
sinh kh
$f_3(kh) = \frac{e^{kh}}{2}$
$f_1(kh) = kh$
$f_2(kh) = 1.0$
tanh kh
5%
1.5%
3.3%
0.4%
1/20
h/L
1/2
Shallow water waves
(long waves)
Intermediate depth
waves
Deep water waves
(short waves)
$kh < \frac{\pi}{10}$
$(\frac{h}{L} < \frac{1}{20})$
$\frac{\pi}{10} < kh < \pi$
$(\frac{1}{20} < \frac{h}{L} < \frac{1}{2})$
$kh > \pi$
$(\frac{h}{L} > \frac{1}{2})$

The following table sums up the results

Function	Large kh	Small kh
cosh kh	$e^{kh}/2$	1
sinh kh	$e^{kh}/2$	kh
tanh kh	1	kh

Chapter 3

First order wavemaker theory

In this chapter it is presented the first order wavemaker theory. The chapter includes the main passages to obtain the transfer function H/S for piston and flap type wavemaker and the evaluation of forces and power for the configuration with water on only one side and on both sides. The chapter is closed by the main passages to derive the general transfer function for oblique waves generation. The main reference for this part is [2].

3.1 First order wavemaker theory

From now on, we will refer to the following sketch

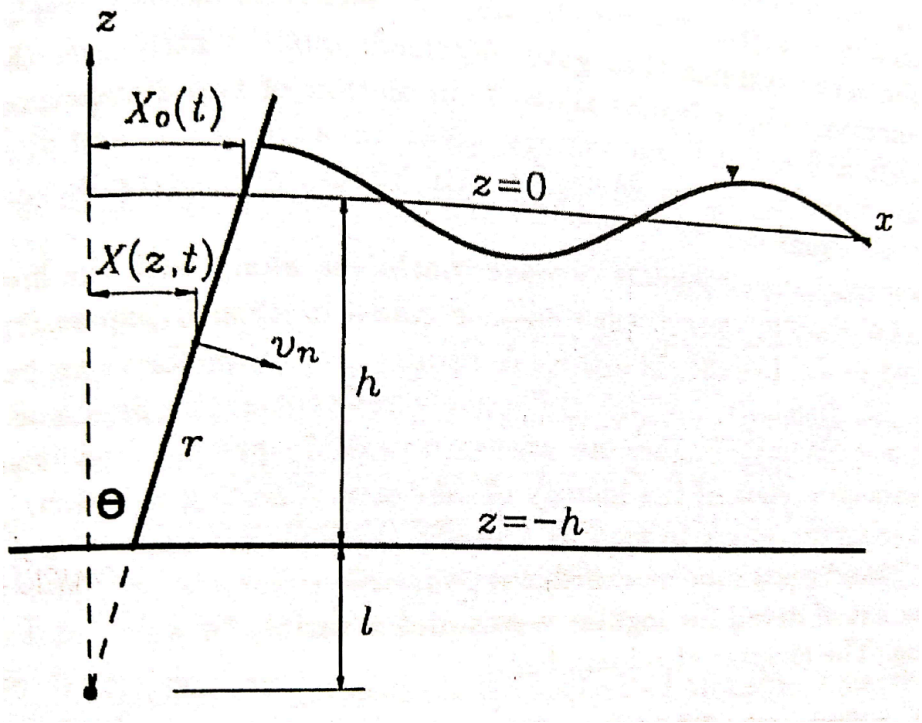

The wave board motion here is given by a combination of rotation and translation

Then, assuming irrotational fluid, its behavior in a wave tank is described by Laplace equation

$$\frac{\partial^2\phi}{\partial x^2}+\frac{\partial^2\phi}{\partial z^2}=0$$

with the appropriate boundary conditions.

As already seen in the second chapter, we have:

- Bottom Boundary Condition for horizontal bottom

$$\frac{\partial \phi}{\partial z} = 0 \qquad at\ z = -h$$

- Kinematic Free Surface Condition

$$\frac{\partial \eta}{\partial t} + \frac{\partial \phi}{\partial x}\frac{\partial \eta}{\partial x} - \frac{\partial \phi}{\partial z} = 0 \qquad at\ z = \eta$$

- Dynamic Free Surface Boundary Condition

$$\frac{\partial \phi}{\partial t} + \frac{1}{2}\left[\left(\frac{\partial \phi}{\partial x}\right)^2 + \left(\frac{\partial \phi}{\partial z}\right)^2\right] + g\eta = 0 \qquad at\ z = \eta$$

Now we have to formulate the wave board boundary condition; assuming that the wave board is:

- flat;
- solid;
- impermeable

the fluid velocity normal to the paddle and the paddle have the same velocity. Then, the boundary condition for this side becomes (Flick and Guza 1980; Barthel, et al.1983)

$$r\frac{\partial \theta}{\partial t} = v_n$$

Working on the geometry of the reference sketch, we can write

$$r = \sqrt{\left(X(z,t)\right)^2 + (l + h + z)^2} = (l + h + z)\sqrt{1 + (\tan\theta)^2}$$

$$v_n = u\cos\theta - w\sin\theta$$

$$X(z,t) = \left(1 + \frac{z}{h + l}\right)X_o(t)$$

Substituting these relations inside the boundary condition, we obtain

$$(l + h + z)\sqrt{1 + (\tan\theta)^2}\frac{\partial \theta}{\partial t} = u\cos\theta - w\sin\theta$$

Assuming θ to be small, it is possible to write:

$u\cos\theta \approx u$

$w\sin\theta \approx 0$

$(\tan\theta)^2 \ll 1$

$\theta \approx \frac{X(z,t)}{(l+h+z)}$

Substituting, we obtain the General Wave Board Boundary Condition:

$$\boxed{\frac{\partial\phi}{\partial x} = \left(1 + \frac{z}{h+l}\right)\frac{\partial X_o(t)}{\partial t} \qquad at\ x = X(z,t)}$$

- $l = 0$, boundary condition for a flap type wavemaker hinged at the bottom;
- $l \to \infty$, boundary condition for a piston type wavemaker.

Summing up, the wavemaker problem is given by the following set of equations:

- $\frac{\partial^2\phi}{\partial x^2} + \frac{\partial^2\phi}{\partial z^2} = 0$ Laplace equation
- $\frac{\partial\phi}{\partial z} = 0 \qquad at\ z = -h$ Bottom Boundary Condition for horizontal bottom
- $\frac{\partial\eta}{\partial t} + \frac{\partial\phi}{\partial x}\frac{\partial\eta}{\partial x} - \frac{\partial\phi}{\partial z} = 0 \qquad at\ z = \eta$ Kinematic Free Surface Condition
- $\frac{\partial\phi}{\partial t} + \frac{1}{2}\left[\left(\frac{\partial\phi}{\partial x}\right)^2 + \left(\frac{\partial\phi}{\partial z}\right)^2\right] + g\eta = 0 \qquad at\ z = \eta$ Dynamic Free Surface Boundary Condition
- $\frac{\partial\phi}{\partial x} = \left(1 + \frac{z}{h+l}\right)\frac{\partial X_o(t)}{\partial t} \qquad at\ x = X(z,t)$ General Wave Board Boundary Condition

We can solve the wavemaker problem using standard perturbation techniques.

We assume to express the following terms with power series:

$\phi = \sum_{n=1}^{\infty}\epsilon^n\phi_n = \epsilon\phi_1 + \epsilon^2\phi_2 + \epsilon^3\phi_3 + O(\epsilon^4)$

$\eta = \sum_{n=1}^{\infty}\epsilon^n\eta_n = \epsilon\eta_1 + \epsilon^2\eta_2 + \epsilon^3\eta_3 + O(\epsilon^4)$

$\theta = \sum_{n=1}^{\infty}\epsilon^n\theta_n = \epsilon\theta_1 + \epsilon^2\theta_2 + \epsilon^3\theta_3 + O(\epsilon^4)$

$X_o = \sum_{n=1}^{\infty}\epsilon^n X_{o_n} = \epsilon X_{o_1} + \epsilon^2 X_{o_2} + \epsilon^3 X_{o_3} + O(\epsilon^4)$

where ϵ, the perturbation parameter, is proportional to the wave steepness H/L.

In the following, we retain only terms up to $O(\epsilon)$ for having the first order approximation. Substituting the expression for ϕ inside Laplace equation and bottom boundary condition, we have respectively

$$\frac{\partial^2 \phi_1}{\partial x^2} + \frac{\partial^2 \phi_1}{\partial z^2} = 0$$

$$\frac{\partial \phi_1}{\partial z} = 0 \qquad at\ z = -h$$

Representing the velocity potential evaluated at $z = \eta$ by a Taylor series expansion about $z = 0$

$$\phi(\eta, x, t; \epsilon) = \epsilon\phi_1 + \epsilon^2 \left(\phi_2 + \eta_1 \frac{\partial \phi_1}{\partial z}\right) + O(\epsilon^3)$$

and substituting this expression and the power series representation for η in the Kinematic Free Surface Condition and in the Dynamic Free Surface Boundary Condition, we obtain

Kinematic Free Surface Condition

$$\frac{\partial \eta_1}{\partial t} - \frac{\partial \phi_1}{\partial z} = 0 \qquad at\ z = 0$$

Dynamic Free Surface Boundary Condition

$$\frac{\partial \phi_1}{\partial t} + g\eta_1 = 0 \qquad at\ z = 0$$

It is possible to combine these last two expressions obtaining from them only one condition and avoiding the partial derivative of η_1 (Flick and Guza, 1980)

$$\begin{cases} \frac{\partial \eta_1}{\partial t} - \frac{\partial \phi_1}{\partial z} = 0 & at\ z = 0 \\ \frac{\partial \phi_1}{\partial t} + g\eta_1 = 0 & at\ z = 0 \end{cases} \xrightarrow{\eta_1 = -\frac{1}{g}\frac{\partial \phi_1}{\partial t}} \frac{\partial^2 \phi_1}{\partial t^2} + g\frac{\partial \phi_1}{\partial z} = 0 \qquad at\ z = 0$$

Moving on the paddle, we approximate the velocity potential evaluated on the surface of the wave board by the following Taylor series expansion in cylindrical coordinates about $\theta = 0$

$$\phi(\theta, z, t; \epsilon) = \epsilon\phi_1 + \epsilon^2 \left(\phi_2 + \theta_1 \frac{\partial \phi_1}{\partial \theta}\right) + O(\epsilon^3)$$

Referring to the main sketch, we can write it in Cartesian coordinates

$$\phi(x, z, t; \epsilon) = \epsilon\phi_1 + \epsilon^2 \left[\phi_2 + \theta_1 \left((l + h + z)\frac{\partial \phi_1}{\partial x} - x\frac{\partial \phi_1}{\partial z}\right)\right] + O(\epsilon^3)$$

Substituting now this equation for ϕ, the power expressions for θ and X_o, and θ_1 with the small angle approximation inside the general Wave Board Boundary Condition

$$\frac{\partial \phi_1}{\partial x} = f(z)\frac{dX_{o_1}}{dt} \qquad at\ x = 0$$

$$with\ f(z) = \left(1 + \frac{z}{h+l}\right)$$

Summing up, the wavemaker problem with the first order approximation is given by the following equations:

- $\frac{\partial^2 \phi_1}{\partial x^2} + \frac{\partial^2 \phi_1}{\partial z^2} = 0$ Laplace equation
- $\frac{\partial \phi_1}{\partial z} = 0 \qquad at\ z = -h$ Bottom Boundary Condition for horizontal bottom
- $\frac{\partial^2 \phi_1}{\partial t^2} + g\frac{\partial \phi_1}{\partial z} = 0 \qquad at\ z = 0$ Kinematic and Dynamic Free Surface Boundary Condition
- $\frac{\partial \phi_1}{\partial x} = f(z)\frac{dX_{o_1}}{dt} \qquad at\ x = 0$ General Wave Board Boundary Condition

  $f(z) = \left(1 + \frac{z}{h+l}\right)$

First order wave generation

To find the solution for the wavemaker problem, we assume to write ϕ_1 in the following manner

$$\phi_1(x, z, t) = X(x)Y(y)T(t)$$

Making this assumption, it is possible to divide the Laplace equation into ordinary differential equations with a known solutions. Since all them have to be contained in the potential function, we write it as follows ([1])

$$\phi_1(x, z, t) = \phi_{k_1} + \phi_{k_2} + \phi_{k_3}$$

where the elements in the sum are the solutions we have when the separation constant is respectively real, zero and imaginary. In particular:

- $k_1^2 > 1$

$$\phi_{k_1} = [A_1 \cos(k_1 x + \alpha_1)](C_1 e^{k_{1z}} + D_1 e^{-k_{1z}})T_1(t)$$

- $k_2 = 0$

$$\phi_{k_2} = (A_2 x + B_2)(C_2 z + D_2)T_2(t)$$

- $k_3^2 < 1$

$$\phi_{k_3} = \left(A_3 e^{|k_3|x} + B_3 e^{-|k_3|x}\right)(C_3 \cos|k_3|z + D_3 \sin|k_3|z)T_3(t)$$

Substituting these velocity potentials inside the Bottom Boundary Condition and evaluating it at

$z = -h$ we obtain

$$C_1 = D_1 e^{2k_1 h} \qquad C_2 = 0 \qquad C_3 = -D_3 \frac{\cos|k_3|h}{\sin|k_3|h}$$

In the expression of ϕ_{k_3} we set $A_3 = 0$ because it multiplies a term which would give an exponential increase of the u velocity component with x and this is not realistic.

The three potentials are now

$$\phi_{k_1} = [A_1 \cos(k_1 x + \alpha_1)] 2D_1 e^{k_1 h} \cosh[k_1(h+z)]\, T_1(t)$$

$$\phi_{k_2} = (A_2 x + B_2) D_2 T_2(t)$$

$$\phi_{k_3} = \left(B_3 e^{-|k_3|x}\right)\left(\frac{-D_3}{sin|k_3|h}\right) cos[|k_3|(z+h)] T_3(t)$$

Substituting these three potentials inside the combined kinematic and dynamic free surface boundary condition and evaluating it at $z = 0$, we obtain ordinary differential equations which can be solved for the three unknown time functions.
The velocity potentials become

$$\phi_{k_1} = (2A_1 D_1 e^{k_1 h}) \cosh[k_1(h+z)] \cos(k_1 x + \alpha_1)\, [B_1 \sin(\sigma_1 t + \beta_1)]$$

$$\phi_{k_2} = (A_2 x + B_2) D_2 (E_2 t + F_2)$$

$$\phi_{k_3} = \left(\frac{-B_3 D_3}{sin|k_3|h} e^{-|k_3|x}\right) cos[|k_3|(z+h)][E_3 \cos(\sigma_3 t + \alpha_3)]$$

with

$(\sigma_1)^2 = g k_1 \tanh(k_1 h)$

$(\sigma_3)^2 = -g|k_3| \tan(|k_3|h)$

The last relation will be elaborated on later.

ϕ_{k_2} increases monotonically with time; this is unrealistic and then we put $E_2 = 0$.

Using a trigonometric identity in ϕ_{k_1} and regrouping we have

$$\phi_{k_1} = A \cosh[k_1(h+z)][\sin(k_1 x - \sigma_1 t + \gamma_1) + \sin(k_1 x + \sigma_1 t + \epsilon_1)]$$

$$\phi_{k_2} = (Bx + D)$$

$$\phi_{k_3} = C e^{-|k_3|x} \cos[|k_3|(z+h)] \cos(\sigma_3 t + \alpha_3)$$

Observing the expression for ϕ_{k_1}, we can note that it is the sum of two progressive waves moving in opposite directions; since we have assumed that the wave board is a solid, we can reject the wave moving toward the paddle.

ϕ_{k_2} will give, after the application of the vector differential operator ∇, a constant horizontal velocity component; as already said, since it is not possible to have flow through the paddle, we can set B equal to zero. The remaining constant D is arbitrary and so we choose it again equal to zero.

Moreover, $\sigma_1 = \sigma_3 = \sigma_{wavemaker} = \sigma$ and then

$$\sigma = gk_1 \tanh(k_1 h) = -gk_3 \tan(k_3 h)$$

As shown by the following two graphs, fixing a value for σ and h, we have only one solution k_1 for the dispersion relationship and infinite solutions k_3 for the last equation.

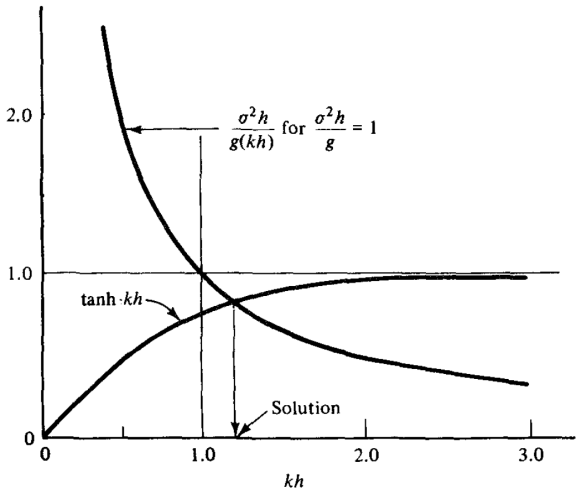

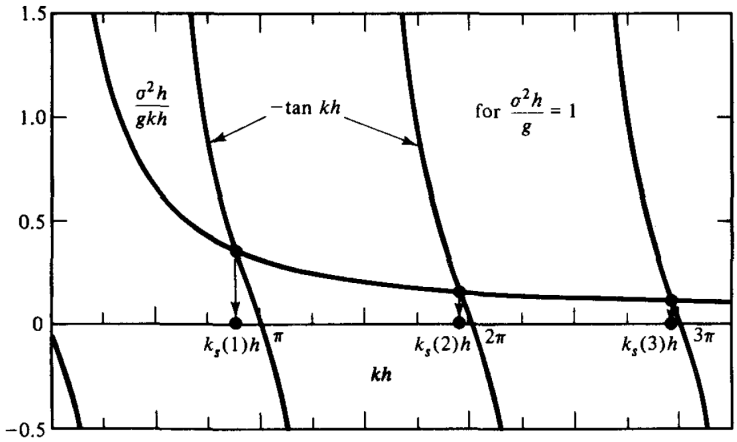

As already seen in chapter two, k_1 is the wave number of a progressive wave while the infinite values of k_3 ,that satisfy the last equation for fixed σ and h, are wave numbers of standing waves; these last quantities yield to many values for ϕ_{k_3} that we have to consider with a summation. The origin of this standing waves is due the fact that the solid wave board does not exactly follow the velocity motion beneath a progressive first order wave.

Furthermore, referring to the equations for ϕ_{k_1} and ϕ_{k_3}, since the quantities γ_1 and α_{3_n} are arbitrary, we can set them zero.

Summing up the last results, we have

$$\phi_1(x,z,t) = \phi_{k_1} + \phi_{k_2} + \phi_{k_3}$$

$$\phi_1(x,z,t) = A\cosh[k_1(h+z)]\sin(k_1 x - \sigma t) + \cos(\sigma t)\sum_{n=1}^{\infty} C_n e^{-k_{3_n} x}\cos\left[k_{3_n}(z+h)\right]$$

The first term of the potential ϕ_1 is a progressive wave that propagates in the positive x direction with its wave number k_1; the second term is a series of standing waves, each one of them with its wave number k_{3_n}. As it can be seen, these standing waves exponentially decay with the distance x from the paddle: according to [1], the amplitude of the first standing wave, the most important, will decrease by 99% at $x = 3h$.

We have now to find the expressions for the coefficient A and C_n.
We assume that the wave board follows the following sinusoidal motion

$$X_{o_1} = \frac{S_o}{2}\sin(\sigma t)$$

with S_o the wave board stroke at $z = 0$.

Remembering the wave board boundary condition

$$\frac{\partial \phi_1}{\partial x} = f(z)\frac{dX_{o_1}}{dt} \qquad at\ x = 0$$

$$with\ f(z) = \left(1 + \frac{z}{h+l}\right)$$

we substitute in the expression for ϕ_1 and X_{o_1} obtaining

$$Ak_1 \cosh[k_1(h+z)] - \sum_{n=1}^{\infty} C_n\, k_{3_n} \cos\left[k_{3_n}(z+h)\right] = f(z)\frac{\sigma S_o}{2}$$

Multiplying both sides of the last equation by $\cosh[k_1(h+z)]$,integrating it between $z = -h$ and $z = 0$ and resolving for A, we obtain

$$A = \frac{\sigma S_o}{2k_1}\frac{\int_{-h}^{0} f(z)\cosh[k_1(h+z)]\,dz}{\int_{-h}^{0}(\cosh[k_1(h+z)])^2\,dz}$$

where the summation terms have gone to zero due to the orthogonality considerations given by the Sturm-Liouville theory ([1]).

Then, we multiply both sides of the equation that comes from the wave board boundary condition by $\cos\left[k_{3_n}(z+h)\right]$ and we integrate it between the above mentioned integrations extremes; this yields the progressive waves terms to go to zero and then, solving for C_n, we obtain

$$C_n = -\frac{\sigma S_o}{2k_{3_n}}\frac{\int_{-h}^{0} f(z)\cos\left[k_{3_n}(z+h)\right]dz}{\int_{-h}^{0}\left(\cos\left[k_{3_n}(z+h)\right]\right)^2 dz}$$

To complete the analysis, we have to find the expression of the surface elevation η_1 and the general transfer function between wave board stroke S_o and wave height H.

Substituting the expression for ϕ_1 inside the first order Dynamic Free Surface Boundary Condition and evaluating it at $z = 0$, we obtain the surface elevation in the wave tank

$$\eta_1(x,t) = \frac{\sigma A}{g}\cosh(k_1 h)\cos(k_1 x - \sigma t) + \sin(\sigma t)\sum_{n=1}^{\infty}\frac{\sigma C_n}{g}e^{-k_{3_n}x}\cos\left(k_{3_n}h\right)$$

As above said, starting from a distance of $x = 3h$ from the wavemaker, there are not disturbances; for this reason, far from the wavemaker, we can neglet the summation terms that mathematically describe this phenomenon. Then, the surface elevation can be described by the already mentioned progressive wave solution

$$\eta_1(x,t) = \frac{H}{2}\cos(k_1 x - \sigma t)$$

Equating the last two expressions for η_1 without consider the series terms, we obtain the general transfer function between wave board stroke S_o and wave height H

$$H = \frac{2\sigma A}{g}\cosh(k_1 h)$$

where the stroke S_o is contained in A.

This is a general expression from which we can find the relation for different types of wavemaker substituting in $f(z)$ the function that describes the particular wave board geometry.

We have to note that, since we have neglected the summation terms, the last equation gives the wave height H enough far from the wavemaker.

Piston-type and Flap-type wavemakers

Referring to the main sketch, we know that the wave board geometry is described by

$$f(z) = \left(1 + \frac{z}{h+l}\right)$$

As already said, this expression can describe the geometry of both piston-type and flap-type wavemakers:

- $l = 0$, flap type wavemaker hinged at the bottom;
- $l \to \infty$, piston type wavemaker.

Developing the expressions for A and C_n, we obtain

$$A = \frac{2\sigma S_o}{k(\sinh 2kh + 2kh)}\left[\sinh kh + \frac{(1-\cosh kh)}{k(h+l)}\right]$$

$$C_n = -\frac{2\sigma S_o}{k_n(\sinh 2k_n h + 2k_n h)}\left[\sin k_n h + \frac{(cosk_n h - 1)}{k_n(h+l)}\right]$$

where k stands for k_1 and k_n for k_{3_n}.

Substituting the expression for A in the expression for H and using the dispersion relationship to explicit σ^2, we obtain the General First-Order Wavemaker Solution

$$\boxed{\frac{H}{S_o} = \frac{4\sinh kh}{\sinh 2kh + 2kh}\left[\sinh kh + \frac{(1-\cosh kh)}{k(h+l)}\right]}$$

From this relation, we can find the transfer function for both piston and flap type wavemakers:

- $l \to \infty$ First-Order Piston Wavemaker Solution

$$\frac{H}{S_o} = \frac{2(\cosh 2kh - 1)}{\sinh 2kh + 2kh}$$

$l = 0$ First-Order Flap Wavemaker Solution

$$\frac{H}{S_o} = \frac{4\sinh kh}{\sinh 2kh + 2kh}\left[\sinh kh + \frac{(1-\cosh kh)}{kh}\right]$$

Wave Board Pressure

Assuming water on only one side of the wave board, we have a first order expression for the pressure distribution on the paddle from the linearized Bernoulli equation

$$p(x,z,t) = -\rho\frac{\partial \phi_1}{\partial t} - \rho g z$$

in which we can note the dynamic and the hydrostatic term.

Substituting the expression for ϕ_1 and evaluating the result at $x = 0$, we have the general relation for the instantaneous pressure acting on the wave board.

We can derive particular expressions for piston and flap type wavemaker using $l \to \infty$ or $l = 0$ respectively

$$p_o(z,t) = [\rho\sigma A\cosh k(h+z)]\cos\sigma t + \left[\rho\sigma\sum_{n=1}^{\infty} C_n \cos k_n(h+z)\right]\sin\sigma t - \rho g z$$

The first element is the *resistive* part of the dynamic pressure fluctuation and it is in phase with the paddle velocity. The second element is the *inertia* part of the dynamic pressure fluctuation; this term is in phase with the paddle acceleration. The third element is the hydrostatic pressure acting on the paddle and it is usually the most relevant of the three terms.

If in our problem there is water of the same depth on both sides of the board, we have to add the contribution that comes from a wavemaker velocity potential for waves that propagates in the negative x-direction, still evaluated at $x = 0$. This yields to the doubling of the dynamic pressure term and it yields also the deleting of the hydrostatic term.
Then we have

$$p_{oo}(z,t) = 2[\rho\sigma A \cosh k(h+z)] \cos\sigma t + 2\left[\rho\sigma \sum_{n=1}^{\infty} C_n \cos k_n(h+z)\right] \sin\sigma t$$

In this case, water of the same depth on both sides, in the real application it will be necessary to dissipate waves generated behind the paddle in order to avoid the return of wall reflected waves.

Wave Board Force

Assuming again water on only one side, the total istantaneous force acting per unit width of paddle is

$$F_{T_o}(t) = \int_{-h}^{0} p_o(z,t)\, dz$$

and this yields to

$$F_{T_o}(t) = \left(\frac{\rho\sigma A \sinh kh}{k}\right) \cos\sigma t + \left(\rho\sigma \sum_{n=1}^{\infty} \frac{C_n}{k_n} \sin k_n h\right) \sin\sigma t + \frac{\rho g h^2}{2}$$

If there is water of equal depth on both sides of the board, we write

$$F_{T_{oo}}(t) = \int_{-h}^{0} p_{oo}(z,t)\, dz$$

and then

$$F_{T_{oo}}(t) = 2\left(\frac{\rho\sigma A \sinh kh}{k}\right) \cos\sigma t + 2\left(\rho\sigma \sum_{n=1}^{\infty} \frac{C_n}{k_n} \sin k_n h\right) \sin\sigma t$$

From the general equations, we can obtain the particular relations for flap and piston type wavemaker substituting the respective values for l.

Wave board power

Neglecting friction and mechanical losses, starting again with water on only one side of the paddle, the instantaneous power per unit width of board is given by

$$P_o(t) = \int_{-h}^{0} p_o(z,t)\, u_o(z,t) dz$$

with u_o the horizontal wave board velocity at $x = 0$.

This quantity is found from the First-Order Wave Board Boundary Condition as

$$u_o = \left(\frac{\partial \phi_1}{\partial t}\right)_{x=0} = f(z)\frac{dX_{o1}}{dt}$$

Substituting then the expressions for $f(z)$ and $\frac{dX_{o1}}{dt}$ respectively, we obtain

$$u_o = \frac{\sigma S_o}{2}\left(1 + \frac{z}{h+l}\right)\cos\sigma t$$

Making now the appropriate substitutions, we can solve the above mentioned integral

$$\begin{aligned} P_o(t) = {} & \left(\frac{\rho\sigma^2 S_o A}{2k}\right)\left[\sinh kh + \frac{(1-\cosh kh)}{k(h+l)}\right](\cos\sigma t)^2 \\ & + \left(\frac{\rho\sigma^2 S_o}{2}\right)\sum_{n=1}^{\infty}\frac{C_n}{k_n}\left[\sin k_n h + \frac{(\cos k_n h - 1)}{k_n(h+l)}\right]\sin\sigma t\cos\sigma t \\ & + \left(\frac{\rho g\sigma S_o}{2}\right)\left[\frac{h^2}{2} - \frac{h^3}{3(h+l)}\right]\cos\sigma t \end{aligned}$$

If we have water on both sides of the waves board, we write

$$P_{oo}(t) = \int_{-h}^{0} p_{oo}(z,t)\, u_o(z,t) dz$$

and making now the appropriate substitutions, we can solve the integral

$$\begin{aligned} P_{oo}(t) = {} & 2\left(\frac{\rho\sigma^2 S_o A}{2k}\right)\left[\sinh kh + \frac{(1-\cosh kh)}{k(h+l)}\right](\cos\sigma t)^2 \\ & + 2\left(\frac{\rho\sigma^2 S_o}{2}\right)\sum_{n=1}^{\infty}\frac{C_n}{k_n}\left[\sin k_n h + \frac{(\cos k_n h - 1)}{k_n(h+l)}\right]\sin\sigma t\cos\sigma t \end{aligned}$$

It is also possible to obtain the expression for the mean wave board power over a wave cycle writing

$$P_o = \frac{1}{T}\int_{-T/2}^{+T/2} P_o(t)\, dt$$

and then, substituting the dispersion relationship

$$P_o = \frac{\pi \rho g S_o^2}{kT} \left(\frac{\tanh kh}{\sinh 2kh + 2kh} \right) \left[\sinh kh + \frac{(1 - \cosh kh)}{k(h + l)} \right]^2$$

For water on both sides of the paddle we have

$$P_{oo} = 2 \frac{\pi \rho g S_o^2}{kT} \left(\frac{\tanh kh}{\sinh 2kh + 2kh} \right) \left[\sinh kh + \frac{(1 - \cosh kh)}{k(h + l)} \right]^2$$

Again, we can obtain the particular relations for flap and piston type wavemaker substituting the respective values for l inside the above mentioned equations.

According to [1], the piston type wavemakers are more efficient in shallow water because their motion approximate better the nearly uniform vertical distribution of the horizontal fluid particles. Instead, the flap type wavemakers are more efficient for generating deep water waves.

3.2 First order oblique regular wave generation

Until now we have referred to a wavemaker with only one paddle; if we use in our tank more wave boards independently controlled, we can create a so called *snake wavemaker* and then generate oblique waves. These devices are particularly useful when we want to study the model reaction to waves incoming from different directions: in fact, the possibility to vary the wave angle avoids continuous model set up changes during the tests, saving time and then money. Moreover, some of these wavemakers can also generate a random directional sea and then providing a very realistic simulation environment.

As already seen in chapter 1, we can have several configurations. The easiest provides a snake wavemaker on only one side of the tank; then, since we want to avoid wall reflected waves and also extend the testing capabilities, often there are snake wavemakers also on other sides.

From now on, we will refer also to the following sketch

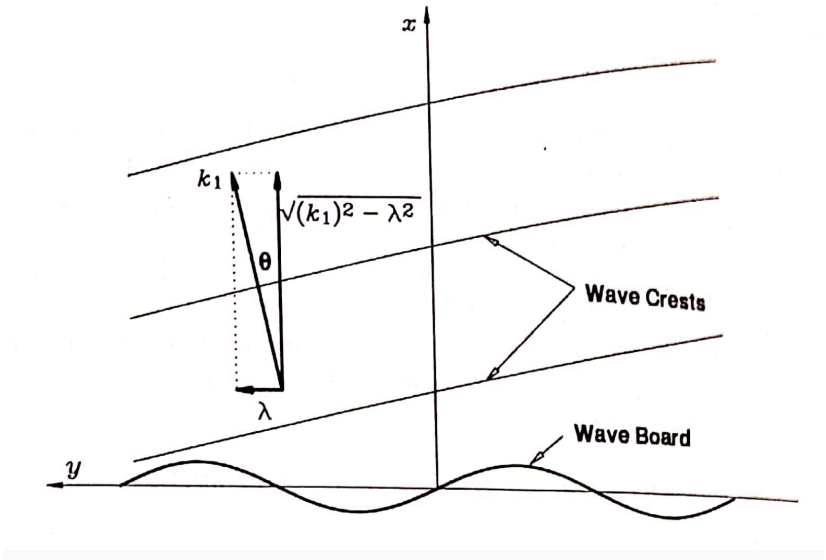

The reference system is the one shown in the above sketch, with the z axis that comes out from the sheet plane and has its zero at the still water level.

The governing equation is the three dimensional Laplace equation

$$\frac{\partial^2 \phi_1}{\partial x^2} + \frac{\partial^2 \phi_1}{\partial y^2} + \frac{\partial^2 \phi_1}{\partial z^2} = 0$$

and the fluid domain in which it stands is

$$\begin{cases} 0 \leq x < \infty \\ -\infty < y < +\infty \\ -h \leq z \leq 0 \end{cases}$$

Regarding the boundary conditions, we still use the above mentioned equations. Also the Wave Board Boundary Condition is the same but here we have to change the equation that describes the wavemaker motion. Assuming a sinusoidal motion in the y direction for the paddles of the snake wavemaker, we can write

$$X_{o_1} = \frac{S_o}{2} \sin(\sigma t - \lambda y)$$

where λ is the wavenumber of the snake wavemaker sinusoidal motion. This implies that the wavemaker is modeled like a continuous line and this is a significant difference from the reality.

Deriving respect to the time, we obtain the wave board velocity

$$\frac{dX_{o_1}}{dt} = \frac{\sigma S_o}{2} \cos(\lambda y - \sigma t)$$

As already made with the two dimensional problem, we can found a solution for the first order velocity potential ϕ_1 with the separation of variables ([1])

$$\phi_1(x,y,z,t) = A\cosh[k_1(h+z)]\sin\left(\sqrt{\left({k_1}^2-\lambda^2\right)}\,x+\lambda y-\sigma t\right)+\cos(\lambda y-\sigma t)\sum_{n=1}^{\infty}C_n e^{-\sqrt{{k_{3_n}}^2+\lambda^2}\,x}\cos\left[k_{3_n}(z+h)\right]$$

In the last equation, k_1 is the wavenumber of the generated progressive wave in the propagation direction and it comes from the dispersion relationship; k_{3_n} are the wavenumbers of the already seen standing waves.

Studying the progressive part of the last equation, we note that it must be $k_1 \geq \lambda$; referring to the reference sketch, this means that it is not possible to generate waves with θ bigger than $90°$.

Still studying the relation between wavenumbers, we can write

$$\lambda = k_1 \sin\theta$$

$$\sqrt{\left({k_1}^2-\lambda^2\right)} = k_1\cos\theta$$

where

$$k_1 = \frac{2\pi}{L} \qquad \lambda = \frac{2\pi}{NB}$$

Substituting now the equation for ϕ_1 and dX_{o_1}/dt in the Wave Board Boundary Condition, we obtain

$$A\sqrt{\left({k_1}^2-\lambda^2\right)}\cosh[k_1(h+z)]-\sum_{n=1}^{\infty}C_n\sqrt{{k_{3_n}}^2+\lambda^2}\cos\left[k_{3_n}(z+h)\right]=f(z)\frac{\sigma S_o}{2}$$

Multiplying both sides of the last equation by $\cosh[k_1(h+z)]$ and integrating over the depth, all the summation terms are sent to zero according to the orthogonally conditions; then, we can solve for A

$$A=\frac{\sigma S_o}{2\sqrt{\left({k_1}^2-\lambda^2\right)}}\frac{\int_{-h}^{0}f(z)\cosh[k_1(h+z)]\,dz}{\int_{-h}^{0}(\cosh[k_1(h+z)])^2dz}$$

As already done for the two dimensional case, we can find an expression for C_n.

Developing the last equation and using the equation for $f(z)$, we obtain the expression for A

$$A=\frac{2\sigma S_o}{k\cos\theta\,(\sinh 2kh+2kh)}\left[\sinh kh+\frac{(1-\cosh kh)}{k(h+l)}\right]$$

in which k stands for k_1.

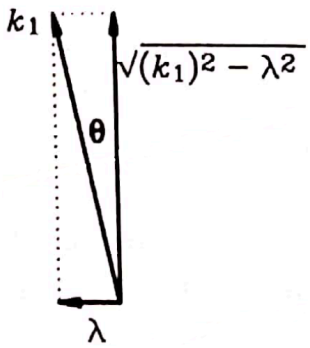

The expression for the surface elevation is

$$\eta_1(x,y,t) = -\frac{1}{g}\frac{\partial \phi_1}{\partial t} \qquad at\ z = 0$$

$$\eta_1(x,y,t) = \frac{\sigma A}{g}\cosh(k_1 h)\cos[(k_1\cos\theta)x + (k_1\sin\theta)y - \sigma t] + \sin(\lambda y - \sigma t)\sum_{n=1}^{\infty}\frac{\sigma C_n}{g}e^{-\sqrt{{k_3}_n{}^2+\lambda^2}\,x}\cos\left({k_3}_n h\right)$$

If we are enough far from the wavemaker, at least $x = 3h$, the effects of the standing waves are negligible and then

$$\eta_1(x,y,t) = \frac{\sigma A}{g}\cosh(kh)\cos[(k\cos\theta)x + (k\sin\theta)y - \sigma t]$$

in which, again, k stands for k_1 and

$$\frac{H}{2} = \frac{\sigma A}{g}\cosh(kh)$$

is the wave amplitude.

Substituting the expression for A in the last equation, we obtain the transfer function between the wave height and the board stroke

$$\frac{H}{S_o} = \frac{4\sinh kh}{\cos\theta\,(\sinh 2kh + 2kh)}\left[\sinh kh + \frac{(1-\cosh kh)}{k(h+l)}\right]$$

This equation differs from the other one for the $\cos\theta$ at the denominator. As we can note, this allows to use less stroke than 2D case for generating the same wave height H.

We have now to introduce the differences between theory and reality. As we can see from the following sketch, a directional wavemaker has a finite length and it is composed by several paddles each one of which with a finite width

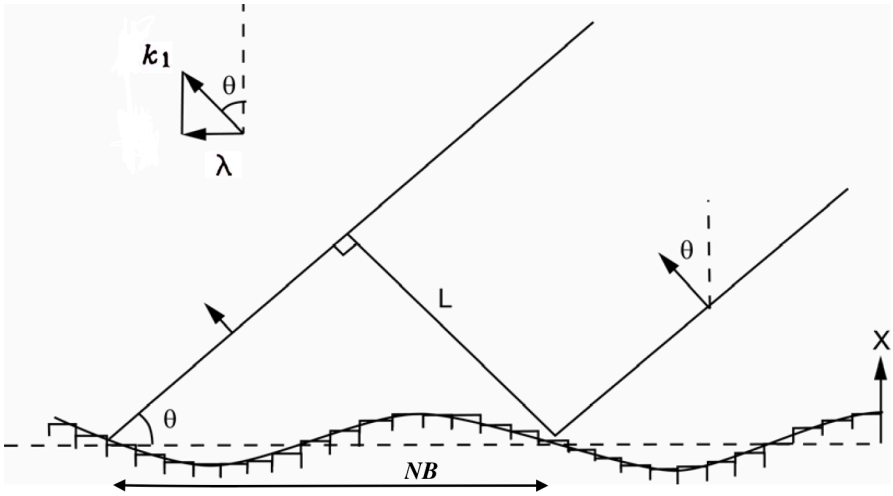

These practical solutions do not match the hypothesis of infinitely long wavemaker and paddles with an infinitesimal width. From the above sketch, in addition to the quantities already defined, we introduce:

L, the wave length in the propagation direction;

B, the paddle width;

N, the number of paddles included in a wavelength of the sinusoid made by the snake wavemaker.

Then, the expression for the wave number in the y direction is

$$\lambda = \frac{2\pi}{NB}$$

Substituting the last relation in $\lambda = k_1 \sin\theta$ and expliciting the expression for k_1, we can find the expression for the wave angle

$$\sin\theta = \frac{L}{NB}$$

The phase shift between adjacent paddles is

$$\phi = \frac{2\pi}{N}$$

which can be substituted in the previous equation. This yields to a relation that links the wave angle to the phase shift

$$\sin\theta = \frac{L\phi}{2\pi B}$$

Remembering that $0° \leq \theta < 90°$, if we want to increase the wave angle we have to increase the phase shift.

In generating oblique waves, we have also to consider the undesired presence of spurious waves; these problem is the consequence of the paddle finite width. The relation found by Sand and Mynett (1987) for minimizing this problem states that

$$\frac{L}{B} > 2$$

with L the shortest wave length that we want to generate.

Oblique waves generation leads also to several effects that influence the tests, still studied by Sand and Mynett (1987). The following sketch shows in which areas of the tank these phenomena occur

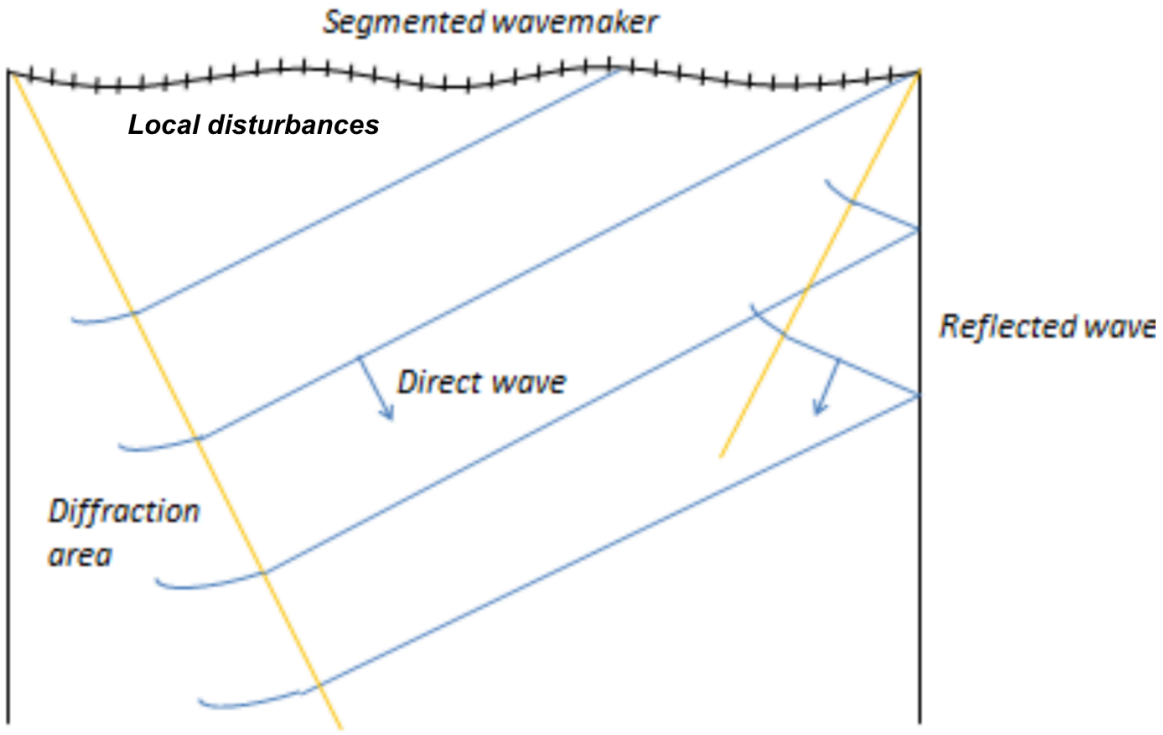

Diffraction reduces the wave height and so also the useful testing area; to avoid this problem we can use *wave guides*, solid boundaries that cross the tank perpendicular to the wave crest starting from the wavemaker sides but we can have reflection problems. Another strategy is to compensate the diffraction effects by generating bigger waves than the ones theoretically required in order to have the required wave height where desired. As we can see from the sketch, oblique waves impacting on the tank boundaries can create reflected waves that disturb the testing area. It is possible to solve this problem using others wavemakers on the lateral sides of the tank, using them to absorb the impacting waves. We have already talked about local disturbances created by the mismatching between wave board motion and water motion. This phenomena creates a deformed wave shape but its effects end at a distance of three times the water depth from the wavemaker.

Chapter 4

Wavemaker design with first order water waves theory

In this chapter it is presented the wavemaker design method followed, based on the linear water waves theory. We first analyzed the wave generation potentialities of our tank: given a period range of interest, it was evaluated the maximum stroke reachable for every period and the corresponding maximum wave height. Several other values for strokes and wave heights are given to have a complete overview of the system features; the plots of the wave length and celerity respect to the period, complete this first analysis. To generate waves, we have to make a first design of the paddle and a first dimensioning of the actuation system. For these reasons, we analyzed velocities and forces acting on the paddle to generate the desired waves. The results of this analysis were used to make a first dimensioning of the actuation system: in particular, it was chosen an electric cylinder driven by a brushless motor for its simplicity and flexibility but, as we will see later, this choice implies a new limitation in wave generation. Subsequently, we focused on the consequences of the choice made on the actuation system: in particular, we determined the new features of the really generable waves. The work is closed by the analysis of transmission and suitable brushless motors.

4.1 Problem definition

The water tank that has to be equipped with the wavemaker is $30\ m\ x\ 2.2\ m\ x\ 0.88\ m$.

The wave period range of interest is between $0.5\ s$ and $2.5\ s$. Since we are interested in generating deep water waves, we have considered only the flap type wavemaker: in fact, its motion more closely resembles the field of motion of deep water waves.

From now on, we will refer to the following two sketches:

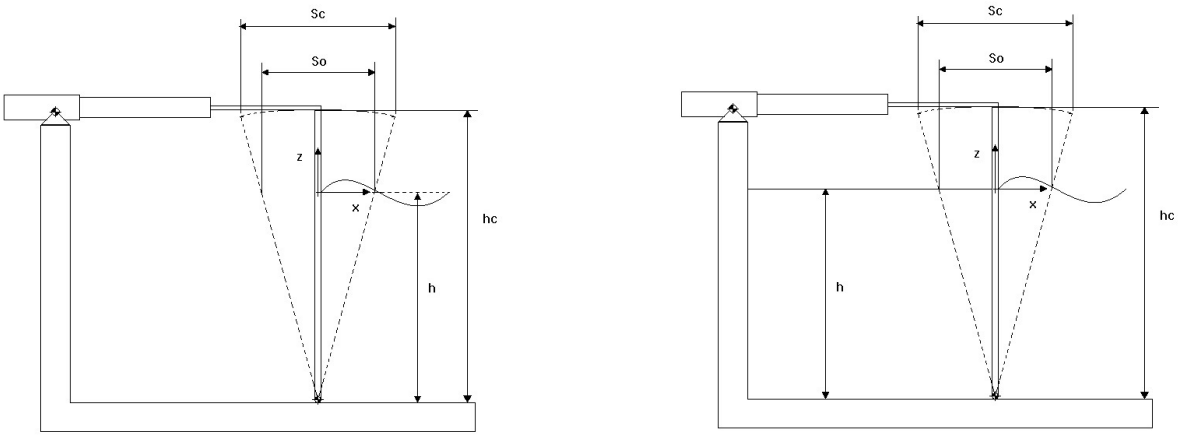

in which $h = 0.7\ m$ and $h_c = 1.1\ m$; this last value was assumed in order to leave a certain safety distance between the sloshing water and the actuator with the electric engine.
Both the configurations will have an actuation system made of an electric cylinder driven by a brushless motor; in this way, the rotational motion of the motor is converted in a translation that drives the flap motion.

Both the configurations, water on only one side and water on both sides, will be discussed during the evaluation of the forces due to the water but, further on, we will focus only on the configuration with water on both sides.
The following arguments were developed using the software Matlab.

4.2 Analysis of wave generation potentialities and first dimensioning of the actuation system

4.2.1 Waves ideally generable in our tank

Summing up, the input data are:

- Tank geometry: $30\ m\ x\ 2.2\ m\ x\ 0.88\ m$
- Wave period range of interest: $T = 0.5\ s\ \div 2.5\ s$
- Water depth: $h = 0.7\ m$
- Height of the link between flap and electro cylinder: $h_c = 1.1\ m$
- Flap type wavemaker

First, we evaluate the wave generation capability of the tank. For each wave period of the above mentioned range, we will have a maximum wave height expected according to the linear water waves theory; to find these information, we have to introduce the following limits that constrain our system:

- Wave break limit $\left(\frac{H}{L} < \frac{1}{7}\right)$,
  If we overcome this ratio, we will not have regular shaped wave and it probably breaks.

- Maximum wave height in the tank,
  Referring to the above sketches, the maximum wave height reachable in our system is set to

  $H_{max} = 0.4\ m$

- Maximum actuator stroke,

  $S_c = 0.5\ m$

  This limit arises from another limit on the control system. If we want to control the position of the flap, the maximum recommended angle excursion is set to $+/-\ 12°$; controlling the force, it is possible to reach a maximum angle of $+/-\ 18°$ [Edinburgh Design]. Since we are interested in controlling the position, we consider:

  $\theta = 12°$

  $h_c = 1.1\ m$

  $\frac{S}{2} = h_c \cdot \tan\theta = 0.23\ m \Rightarrow S = 0.46\ m$

  that, for practical convenience, was carried to

  $$S_c = 0.5\ m$$

- Ballscrew maximum acceleration,

  $a_{max} = 1g$

  This value was assumed in first instance, as made in [5]

To apply this limitations to our system, we use the First order Flap Type Wavemaker Solution

$$\boxed{\frac{H}{S_o} = \frac{4\sinh kh}{\sinh 2kh + 2kh}\left[\sinh kh + \frac{(1-\cosh kh)}{kh}\right]}$$

It is important to underline that, as we can see from the two sketches, the quantity S_o is the wave board stroke at $z = 0\ m$; since the link between the actuator and the flap is located at $z = 0.4\ m$, we have to report S_o at the same level of the actuator to make a consistent comparison between the introduced four limits. In general, raising up the connection point between actuator and flap respect to the still water level, we will have a lost in wave height: connecting actuator and flap at $z = 0.4\ m$ from the still water level, we have lost the 20% of the maximum wave height that we would have making the connection at $z = 0\ m$.

Then, we have:

- Wave break limit

$$\frac{H}{L} < \frac{1}{7} \xrightarrow{substituting\ in\ TF} S_{\max wb} = S_0 = \frac{\pi h}{14 \sinh kh} \cdot \frac{\sinh 2kh + 2kh}{kh \cdot \sinh kh - \cosh kh + 1} \qquad at\ z = 0$$

$$\tan\theta = \frac{S_0}{2h}$$

$$S_{\max wb}{}^{*} = S_c = 2 \cdot (h_c \cdot \tan\theta)$$

- Maximum wave heigth in the tank

$$H_{max} = 0.4\ m \xrightarrow{substituting\ in\ TF} S_{\max wh} = S_0 = 0.4 \cdot \frac{\sinh 2kh + 2kh}{4 \cdot \sinh kh \cdot \left[\sinh kh + \frac{(1 - \cosh kh)}{kh}\right]} \quad at\ z = 0$$

$$\tan\theta = \frac{S_0}{2h}$$

$$S_{\max wh}{}^{*} = S_c = 2 \cdot (h_c \cdot \tan\theta)$$

- Ballscrew maximum acceleration

$$S(t) = \frac{S_c}{2} \sin\omega t \xrightarrow{Deriving\ twice\ respect\ to\ the\ time} a(t) = -\frac{S_c}{2} \omega^2 \sin\omega t$$

$$\frac{S_c}{2} \omega^2 \leq 9.81 \rightarrow S_c = \frac{g}{2\pi^2} T^2$$

- Maximum actuator stroke

$$S_c = 0.5\ m$$

To plot the first two equations, we need to solve the dispersion relation for each period of the range

$$\sigma^2 = gk \tanh kh$$

As already seen in chapter two, if we have a fixed period and a constant water depth, there is only one k that satisfies this equation; this value is obtained through an iteration procedure, solving the last equation for each period in which the period range of interest was divided.

From the comparison between the above limits expressed in terms of actuator strokes, we obtain, for each period, the maximum actuator strokes $S_{c\,max}$ that we can use

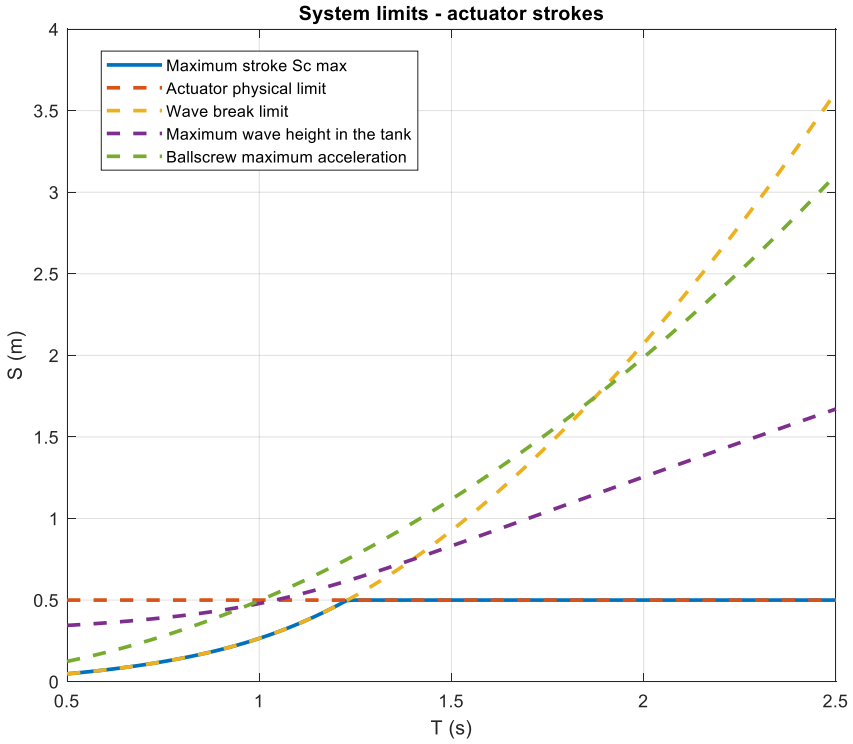

As we can see from the graph, the maximum actuator strokes $S_{c\,max}$ is limited by the wave break limit until $T = 1.23\ s$ and then by the actuator physical limit.

Now we bring back the quantity $S_{c\,max}$ at the still water level, $z = 0$:

$$\tan\theta = \frac{S_{c\,max}}{2h_c}$$

$$S_{0\,max} = 2(h\tan\theta)$$

The following graph shows various strokes at $z = 0$

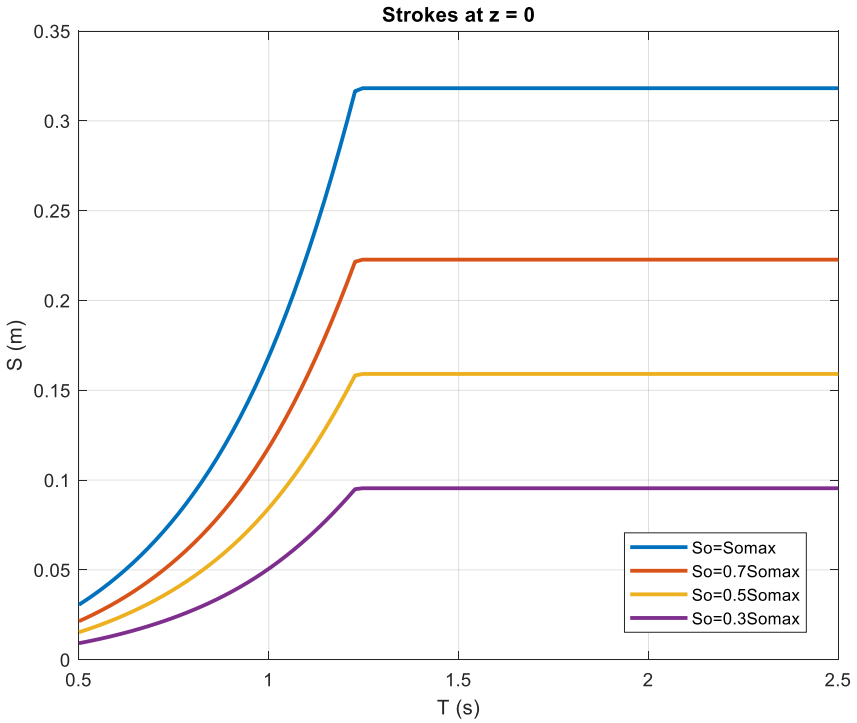

The several values for S_0 are used in the flap type transfer function to obtain the maximum wave height for each period; the following wave heights values are expected at a certain distance away from the wavemaker, minimum three times the water depth, in order to let extinguish the local disturbances introduced by the flap motion

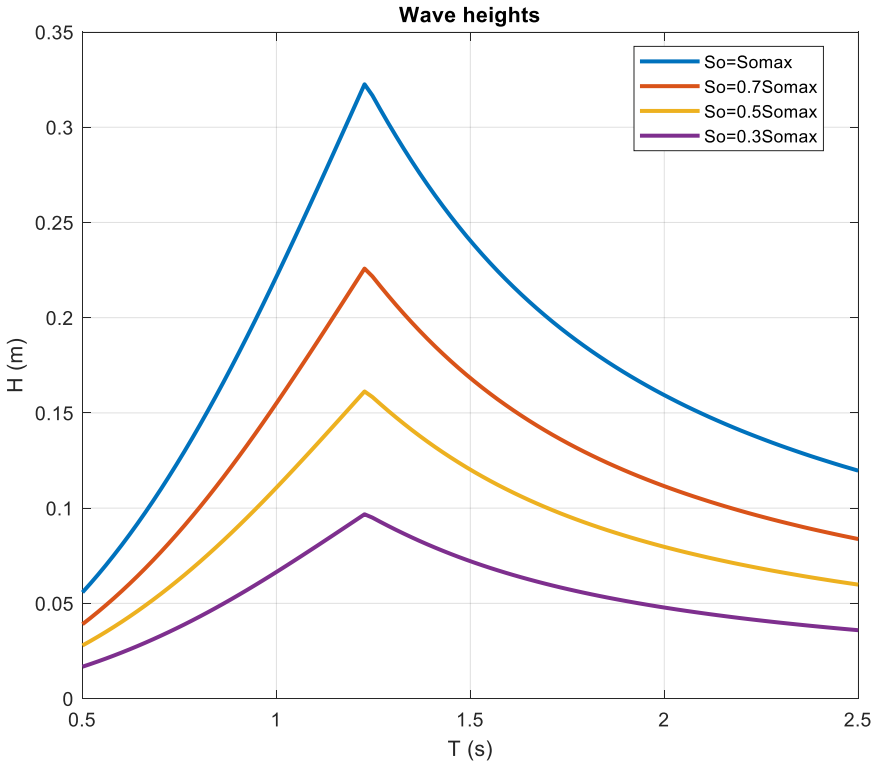

To complete the potentialities overview of our tank, we have to analyze the wave length and the celerity that is the propagation speed of a single wave. The expression for these two quantities is the already mentioned dispersion relationship opportunely rearranged

$$\sigma^2 = gk \tanh kh$$

$$L = \frac{g}{2\pi} T^2 \tanh kh$$

$$C = \frac{g}{k} \tanh kh$$

We report now the obtained values for the wave lengths and celerity for each period of the range

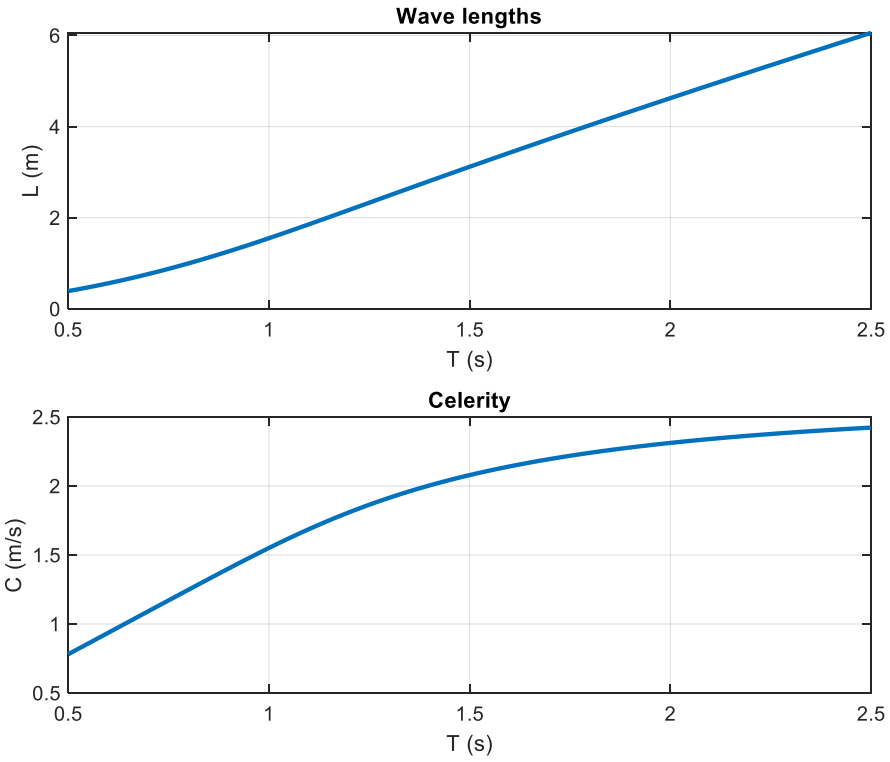

Summing up, given the period range of interest, we evaluated the maximum actuator stroke and the corresponding maximum wave height expected for each period; to have an overview of the wave generation capabilities of the system, we plotted also several values of stroke at $z = 0$ and the corresponding wave height values. To complete the analysis, we reported for each period of the range the expected wave length and celerity.

4.2.2 Velocities, forces and power requirement

Once understood the potentialities of our tank, we have to design the actuation system that better approaches the ideal capabilities. To do this, we have to determine the velocity field, the forces acting on the flap and then the power requirement. In the first two following sections, we will deepen the action of the water on the paddle for the two above mentioned configurations; this because, as we will show later, this force gives the larger contribution in the equilibrium of the flap and so it is very close to the force necessary to drive the paddle during a work cycle. Still in these two first sections, it is made a preliminary analysis of the power required by our system. Then, we will focus on the case with water on both sides: here it will be made a more detailed analysis of the forces and velocities during a work cycle.

Water on one side

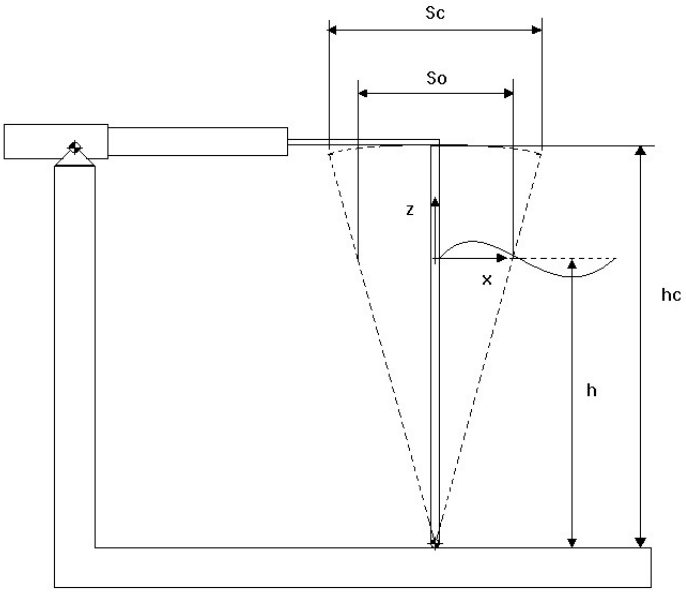

The instantaneous pressure acting on the paddle, is given by the already mentioned expression

$$p_o(z,t) = [\rho\sigma A \cosh k(h+z)]\cos\sigma t + \left[\rho\sigma \sum_{n=1}^{\infty} C_n \cos k_n(h+z)\right]\sin\sigma t - \rho g z$$

with

$$A = \frac{2\sigma S_o}{k(\sinh 2kh + 2kh)}\left[\sinh kh + \frac{(1-\cosh kh)}{k(h+l)}\right]$$

$$C_n = -\frac{2\sigma S_o}{k_n(\sinh 2k_n h + 2k_n h)}\left[\sin k_n h + \frac{(cosk_n h - 1)}{k_n(h+l)}\right]$$

in which we set $l = 0$ to study the flap type wavemaker.

As already seen, the total istantaneous force acting per unit width of paddle is given by the following integral

$$F_{T_o}(t) = \int_{-h}^{0} p_o(z,t)\, dz$$

This yields to

$$F_{T_o}(t) = \left(\frac{\rho\sigma A \sinh kh}{k}\right)\cos\sigma t + \left(\rho\sigma \sum_{n=1}^{\infty} \frac{C_n}{k_n}\sin k_n h\right)\sin\sigma t + \frac{\rho g h^2}{2}$$

where it is possible to find in order the *dynamic resistive term*, the *dynamic inertia term* and the *hydrostatic term*. The subscript "T" in F_{T_o} stands for *total force*; from now on we will use only *force* for convenience.

To plot the above equation, we need to solve

$$\sigma = -gk_3 \tan(k_3 h)$$

for each period of the range and for the fixed water depth.
In this way, we obtain the k_n terms in the expressions for C_n and F_{T_o}. In fact, we are now studying the interaction between water and flap, that is we are very close to the wavemaker; as seen, in this situation we cannot neglect the already mentioned disturbances terms.

The last equation has an infinite number of roots; it is possible to solve it using the Matlab function f zero and stopping the solutions research to the third one. In fact, going on in finding more solutions yields to negligible values in the summation in F_{T_o} expression: $k_n$is at the denominator in both the C_n and in the inertia term and the solutions k_n are even more bigger as shown below

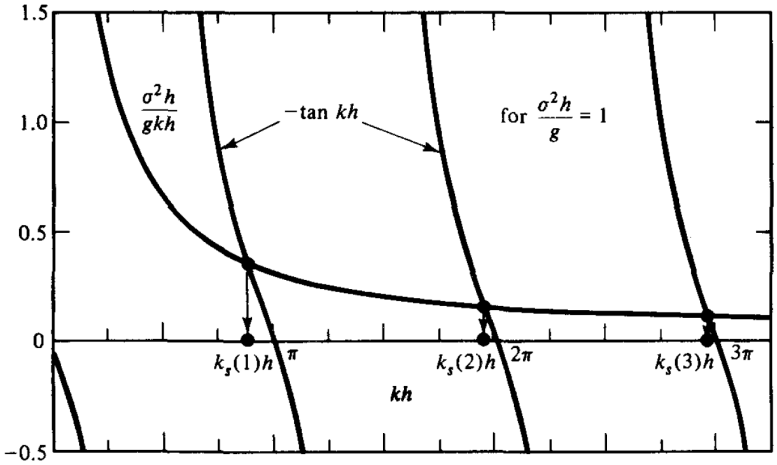

Said this, it is possible to see the graphs made in the present work.
The following graph shows the maximum and minimum force required to face the water action for each period; it was obtained running expression for F_{T_o} period by period and saving the maximum and minimum values

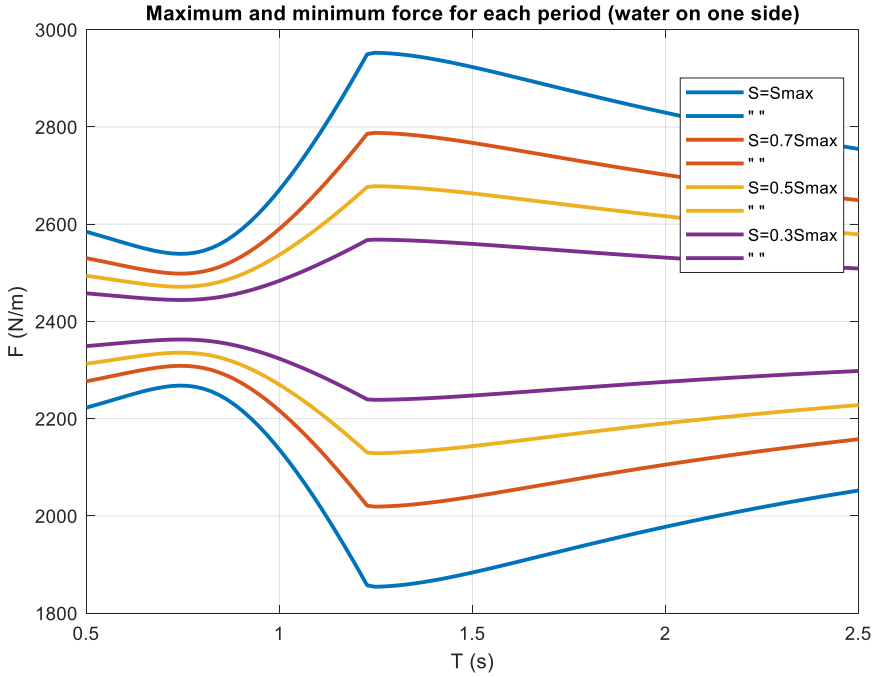

The maximum force is reached for $T = 1.23\ s$. The graph below reports the force components trends respect to the time for this particular period and for the maximum possible stroke. It is important to note that for $t = 0\ s$ the flap is vertical and it is moving.

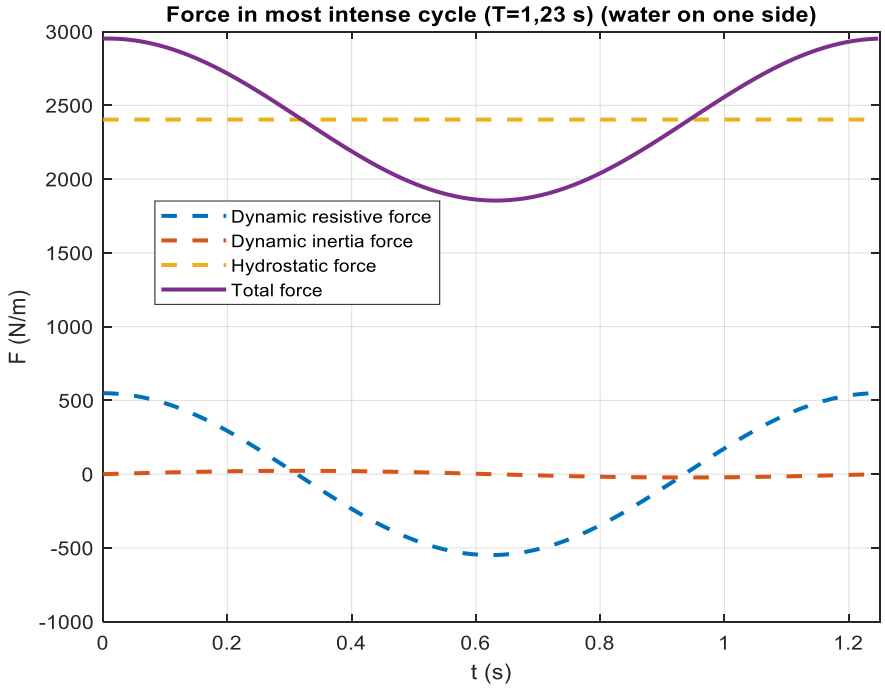

As it is possible to see, the hydrostatic term is much bigger than the others two components; the oscillating trend is given by dynamic resistive term while the inertia one is almost negligible in this period.

To have an overview of the force trend evolution through the period range of interest, we report the following graphs that show the force trend for the extreme period range values and for the period in which the maximum force is reached

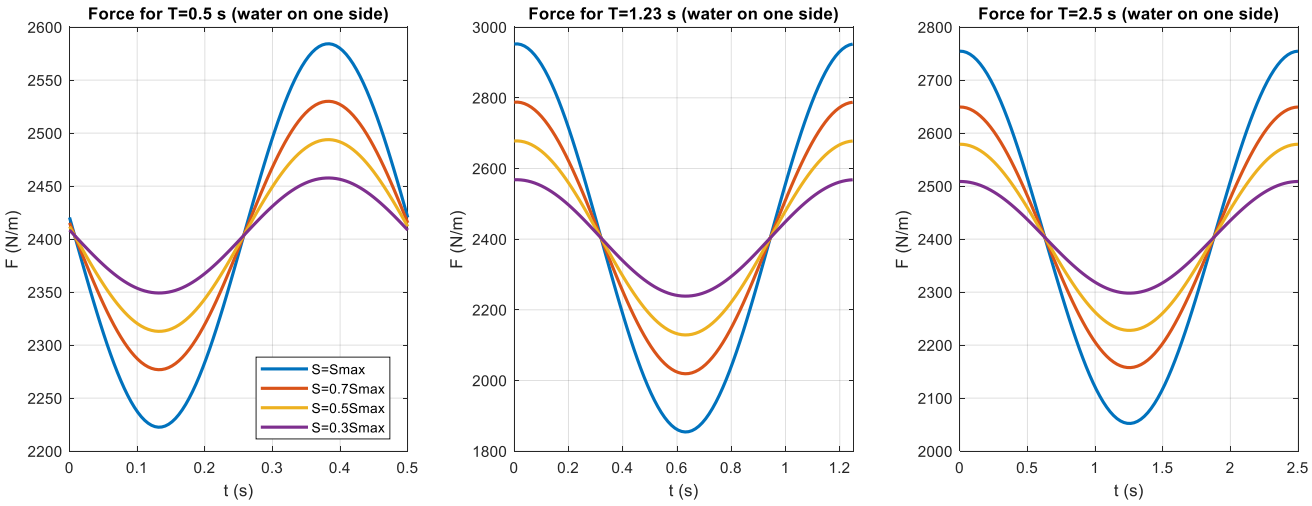

From the graphs we note that the force is always positive for each one of the three particular periods analyzed; this because there is water on only one side and then we have to apply always a positive force, respect to the chosen reference system, to move the paddle or to contain the action of the hydrostatic component. Furthermore, as guessed, force values slack off reducing the stroke.

It is also interesting to compare the force value with the relative position of the connection point between actuator and paddle over a cycle

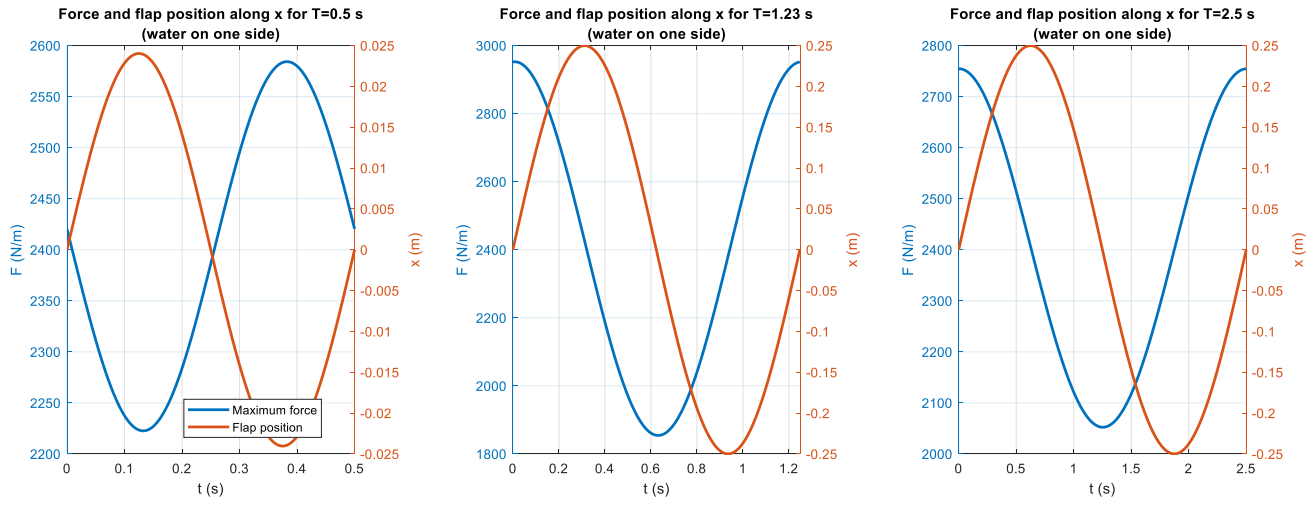

Observing the last two graphs for $T = 0.5\ s$, it is possible to note that the maximum force does not occur at the period beginning, that is when the flap is vertical, but later; this is linked to the inertia effects that are not negligible for small periods, like shown by the series of the following three graphs

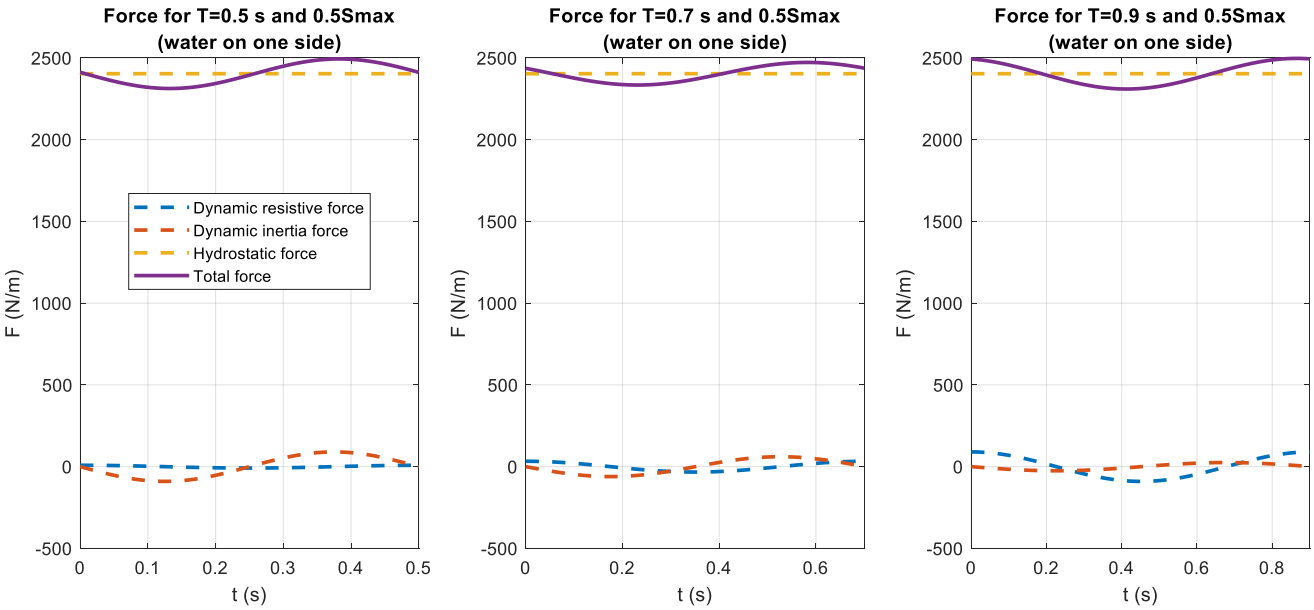

Passing by $T = 0.5\ s$ to $T = 0.9\ s$, it is possible to note that the dynamic inertia term loses importance while the dynamic resistive term becomes relevant. In particular, for $T = 0.5\ s$ we have smaller force values but the trend is governed by the inertia term; on the contrary, for $T = 0.9\ s$ we have bigger force values and the trend is given by the resistive term. This means that, for very small periods, the inertia term is not negligible because it gives the sinusoidal trend to the total force while it becomes irrelevant for bigger periods.

We evaluate now the wavemaker power requirement; following the first order wavemaker problem, friction and mechanical losses are neglected.

As already seen in chapter three, the instantaneous power expression is obtained carrying out the following integral

$$P_o(t) = \int_{-h}^{0} p_o(z,t)\, u_o(z,t) dz$$

that yields to

$$P_o(t) = \left(\frac{\rho\sigma^2 S_o A}{2k}\right)\left[\sinh kh + \frac{(1-\cosh kh)}{k(h+l)}\right](\cos\sigma t)^2 + \left(\frac{\rho\sigma^2 S_o}{2}\right)\sum_{n=1}^{\infty}\frac{C_n}{k_n}\left[\sin k_n h + \frac{(\cos k_n h - 1)}{k_n(h+l)}\right]\sin\sigma t\cos\sigma t + \left(\frac{\rho g\sigma S_o}{2}\right)\left[\frac{h^2}{2} - \frac{h^3}{3(h+l)}\right]\cos\sigma t$$

where the considerations above made for the force about A, C_n and k_n are still valid; again, it is possible to find in order the *dynamic resistive power*, the *dynamic inertia power* and the *hydrostatic power*.
It is useful to remember the expression for the mean power over a cycle that arises from the following integral

$$P_o = \frac{1}{T}\int_{-T/2}^{+T/2} P_o(t)\, dt$$

Its resolution yields to

$$P_o = \frac{\pi \rho g S_o^2}{kT}\left(\frac{\tanh kh}{\sinh 2kh + 2kh}\right)\left[\sinh kh + \frac{(1-\cosh kh)}{k(h+l)}\right]^2$$

The last expression is used to have an overview of our system needs period by period

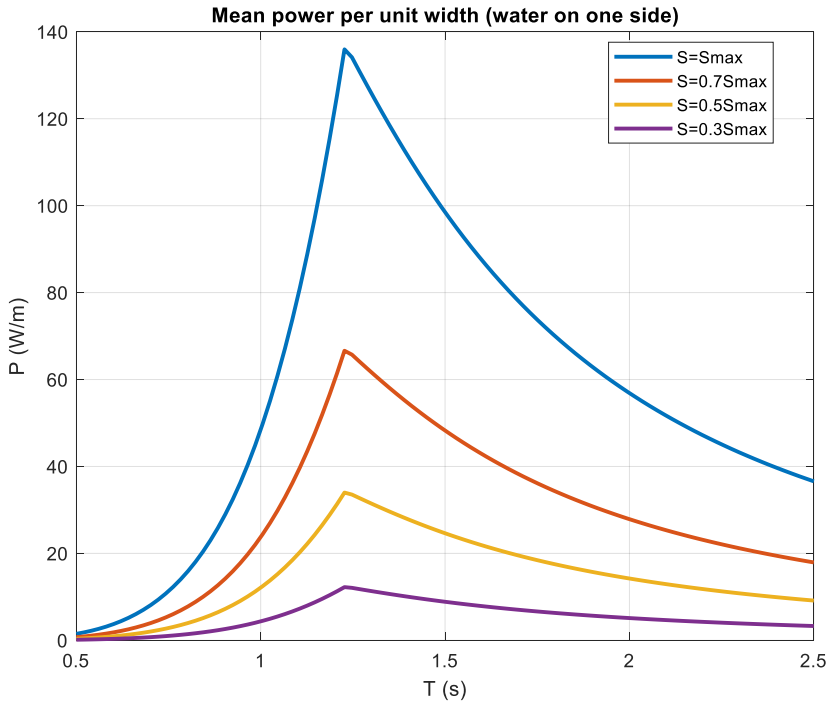

The maximum mean power value occurs for the same period in which there is the maximum force.

The following graph let us understand which are the real power requirement for each period, that is values not affected by media operation; the graph was obtained evaluating the instantaneous power expression for every period of the analyzed range and saving the maximum and the minimum power values for each period

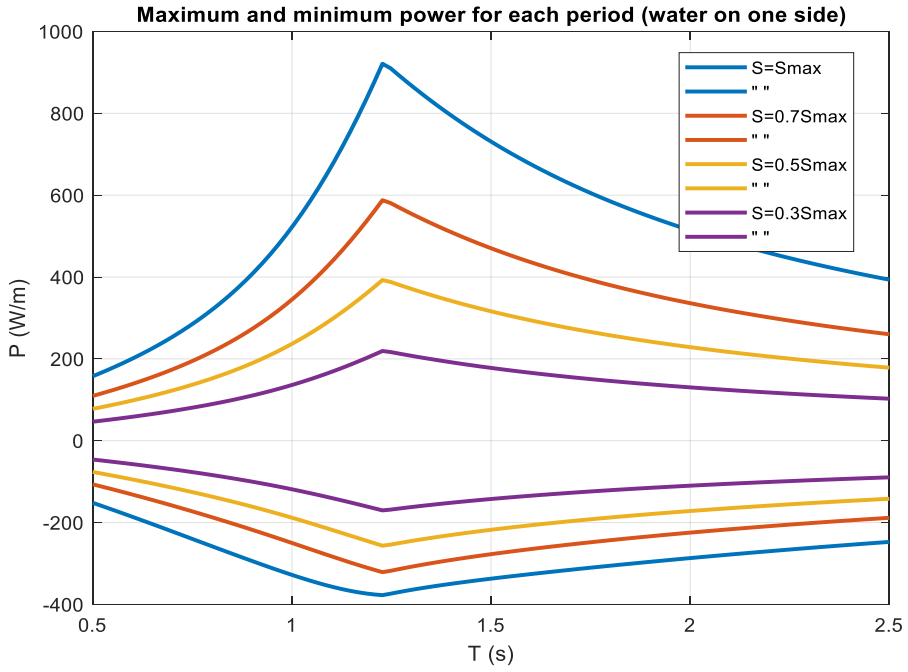

It is possible to note that the power reaches also negative values; this because the force given by the actuator to the paddle acts always along the positive x direction while the paddle follows a sinusoidal motion, that is the velocity is not always positive. The maximum power requirement is reached still for $T = 1.23\ s$ and the following graph shows the instantaneous power component trend for this period and for the maximum stroke

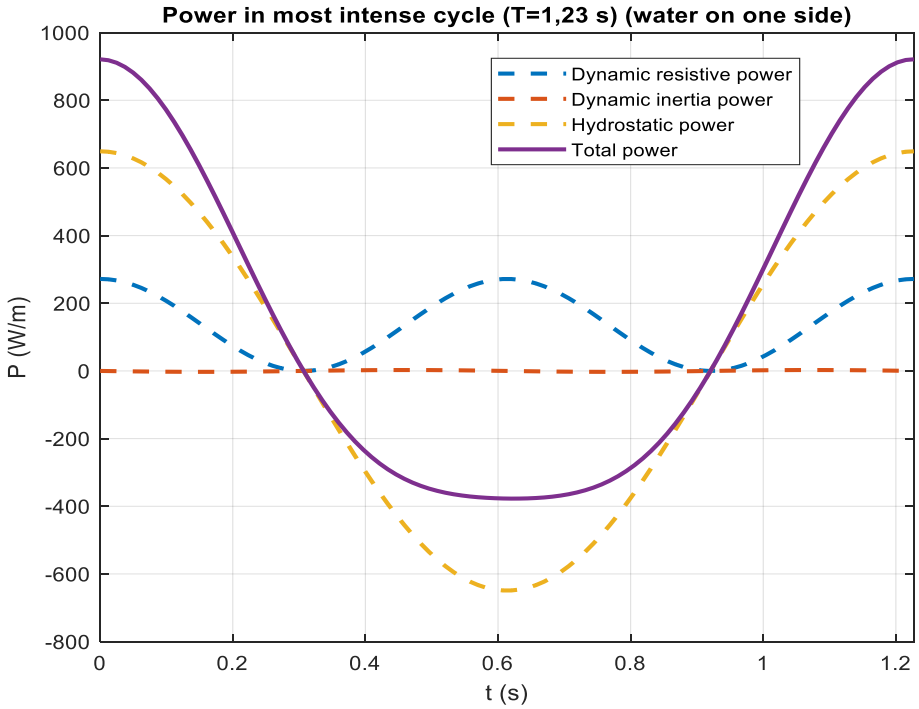

Water of the same depth on both sides

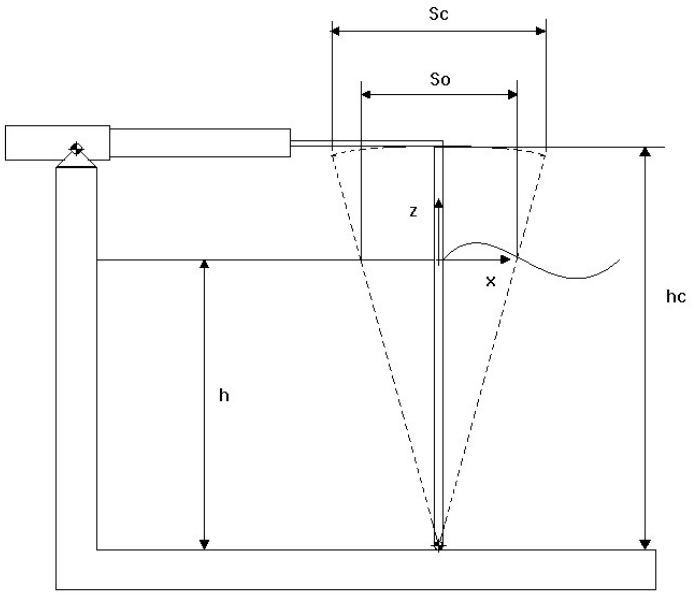

If in our problem there is water of the same depth on both sides of the board, the instantaneous pressure acting on the paddle is given by the following expression

$$p_{oo}(z,t) = 2[\rho\sigma A \cosh k(h+z)]\cos\sigma t + 2\left[\rho\sigma \sum_{n=1}^{\infty} C_n \cos k_n(h+z)\right]\sin\sigma t$$

with again

$$A = \frac{2\sigma S_o}{k(\sinh 2kh + 2kh)}\left[\sinh kh + \frac{(1-\cosh kh)}{k(h+l)}\right]$$

$$C_n = -\frac{2\sigma S_o}{k_n(\sinh 2k_n h + 2k_n h)}\left[\sin k_n h + \frac{(cosk_n h - 1)}{k_n(h+l)}\right]$$

in which we set $l = 0$ since we are studying a flap type wavemaker.

To evaluate the force to apply to face the water action, we have to develop the following integral

$$F_{T_{oo}}(t) = \int_{-h}^{0} p_{oo}(z,t)\,dz$$

$$F_{T_{oo}}(t) = 2\left(\frac{\rho\sigma A \sinh kh}{k}\right)\cos\sigma t + 2\left(\rho\sigma \sum_{n=1}^{\infty} \frac{C_n}{k_n}\sin k_n h\right)\sin\sigma t$$

As we can see, we have a doubling of the dynamic resistive and inertia terms while the hydrostatic term disappears. What said about the resolution of equation

$$\sigma = -gk_3 \tan(k_3 h)$$

for water on only one side, is still valid in the actual case.

Following the scheme already used for water on one side case, we present now the graphs about forces and power.

The following graph shows the maximum and minimum force for each period; it was obtained running the expression for $F_{T_{oo}}$ period by period and saving the maximum and minimum values

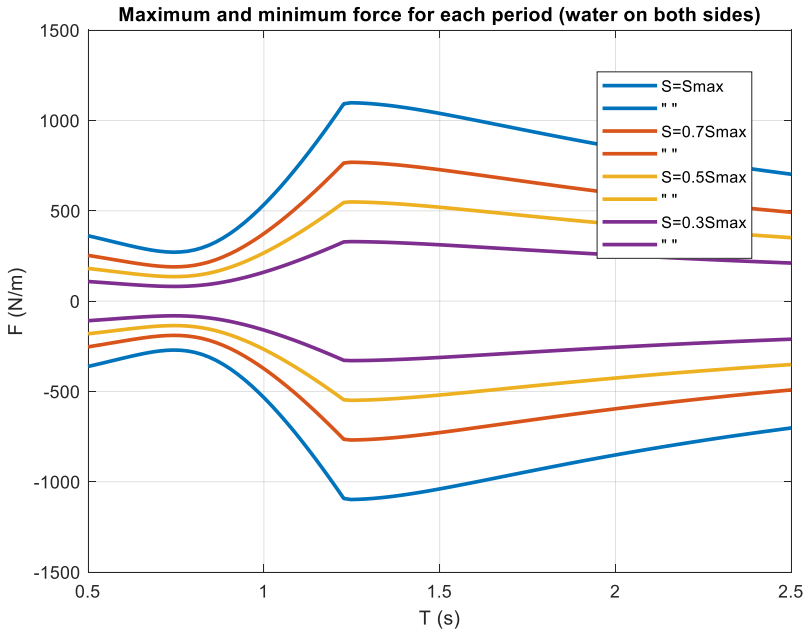

The maximum force is still reached for $T = 1.23\ s$ but the values are lower. Comparing to the other case, we can also start to note the force symmetric trend respect to zero; the following graph, in which are reported the force components trends respect to the time for the period in which the maximum value is reached, clarifies this aspect

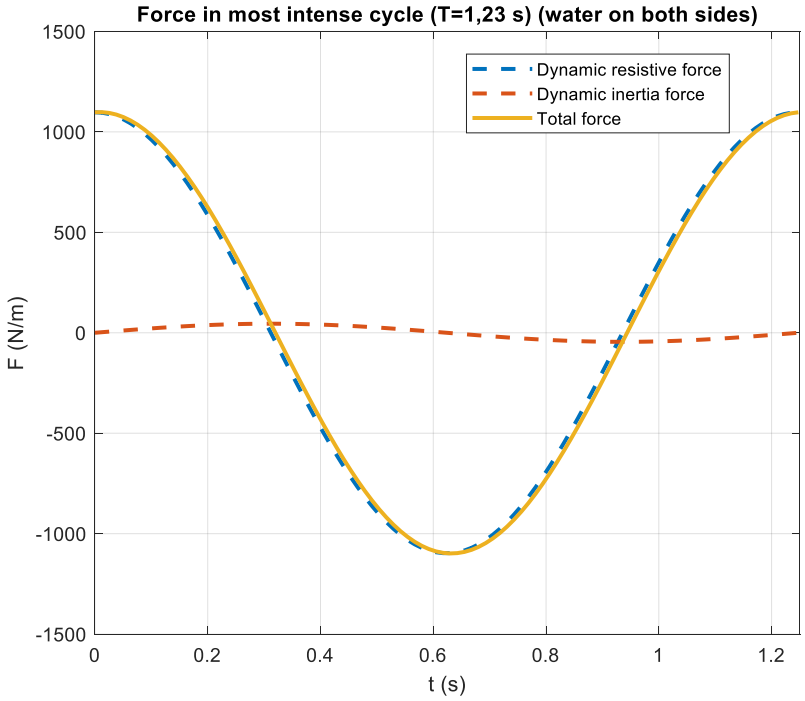

This trend is caused by the presence of water of the same depth on both sides of the paddle: in fact, water is pushed by the paddle in both directions and to do this we have to apply a positive and negative force that generate, respectively, positive and negative velocity of the flap. Also in this case the inertia term is negligible, coherently with its low influence for periods bigger than about $1\ s$.

To have an overview of the force trend evolution through the period range of interest, we report the following graphs that show the force trend for the extreme period range values and for the period in which the maximum force is reached

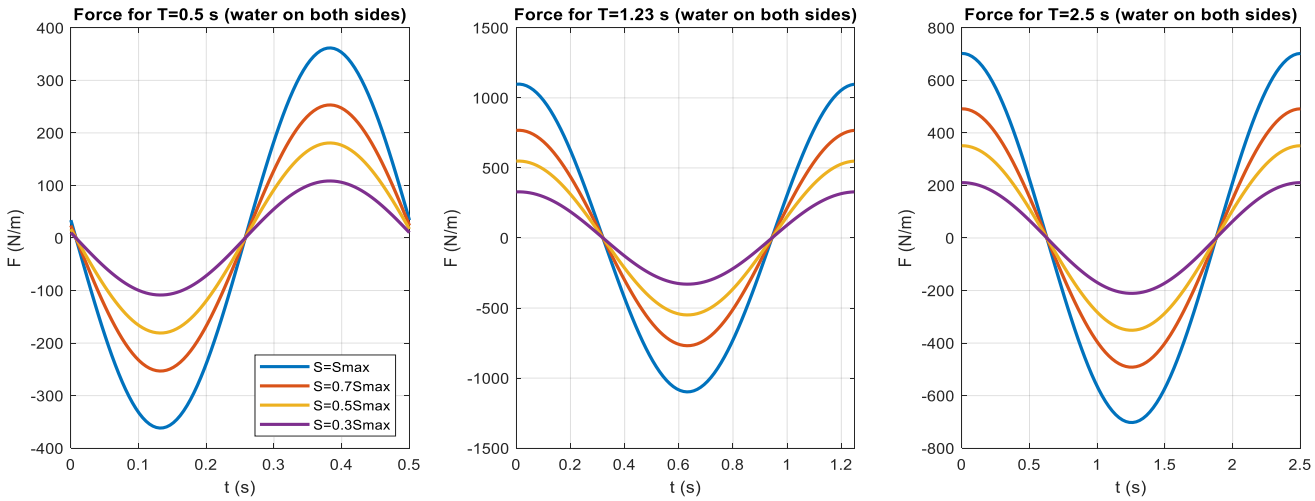

Again, we propose a comparison between the force value and the relative position of the connection point between actuator and paddle over a cycle

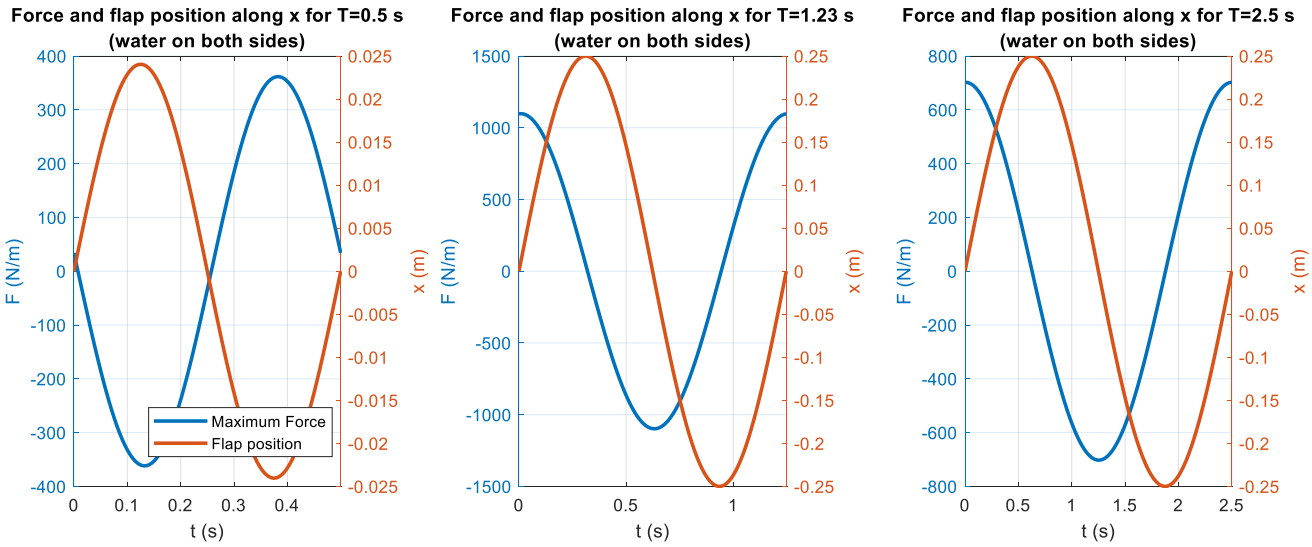

Also in this case, we can note the effect of the inertia term on the total force observing the trends for three different time periods and for the half of the maximum stroke available for this period

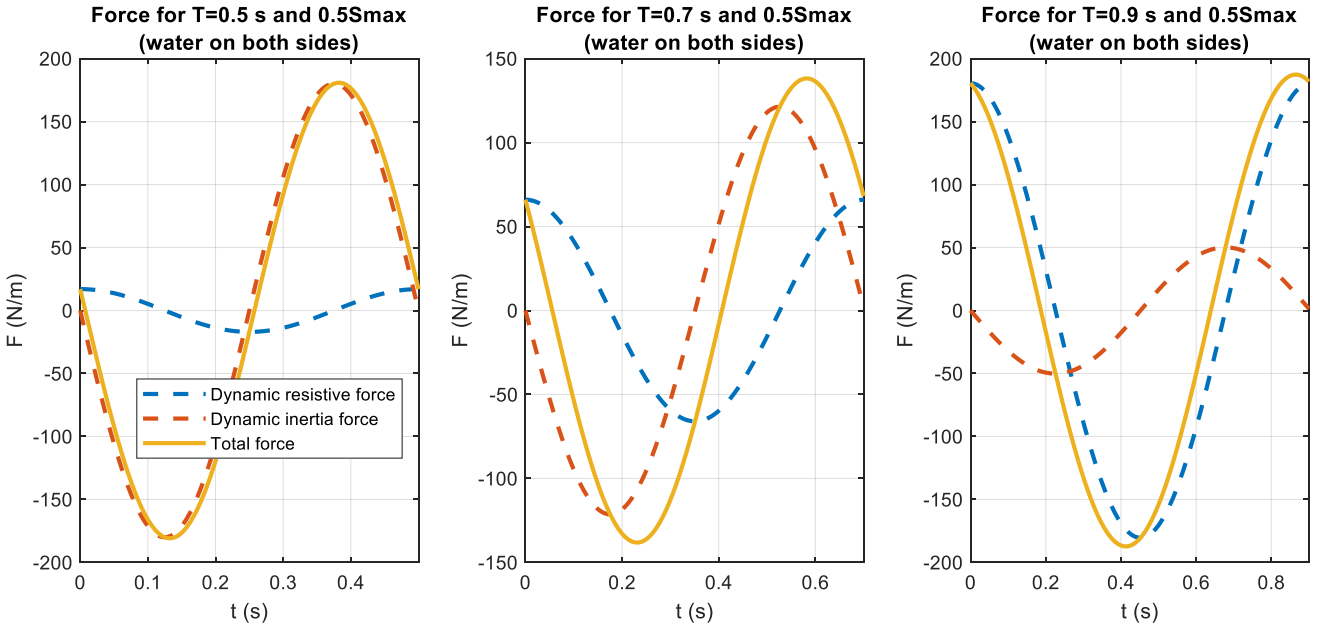

Since in this case there is not the hydrostatic component, the inertia term for small period is more relevant respect to the other case. In particular, for very small period, the total force trend is very close to the inertia component; increasing the period, the resistive term rises up until it becomes predominant for period less than $1\ s$.

Passing to the power analysis, the instantaneous power required is given by the following integral

$$P_{oo}(t) = \int_{-h}^{0} p_{oo}(z,t)\, u_o(z,t) dz$$

that developed becomes

$$P_{oo}(t) = 2\left(\frac{\rho\sigma^2 S_o A}{2k}\right)\left[\sinh kh + \frac{(1-\cosh kh)}{k(h+l)}\right](\cos\sigma t)^2 + 2\left(\frac{\rho\sigma^2 S_o}{2}\right)\sum_{n=1}^{\infty}\frac{C_n}{k_n}\left[\sin k_n h + \frac{(\cos k_n h - 1)}{k_n(h+l)}\right]\sin\sigma t\cos\sigma t$$

where the considerations previously made about A, C_n and k_n are still valid. Furthermore, like for the force expression, it is possible to note the doubling of the dynamic resistive and inertia terms and the disappearing of the hydrostatic term.

The expression for the mean power over a cycle is again given by the following integral

$$P_{oo} = \frac{1}{T}\int_{-T/2}^{+T/2} P_{oo}(t)\, dt$$

that yields to

$$P_{oo} = 2\frac{\pi\rho g S_o^2}{kT}\left(\frac{\tanh kh}{\sinh 2kh + 2kh}\right)\left[\sinh kh + \frac{(1-\cosh kh)}{k(h+l)}\right]^2$$

To have an overview of our system power requirement period by period, it is possible to use the last expression; the following graph reports P_{oo} respect to period

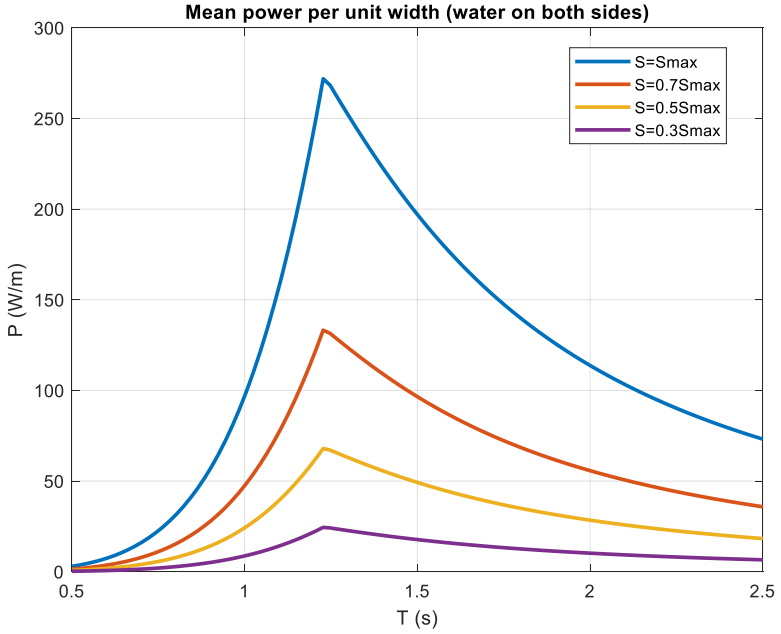

Also in this case, the period that on average requires more power is the same in which the maximum force occurs.

The next graph it is useful to understand what are the real power requirement for each period; like in the case for water on one side, it was obtained evaluating the expression for the instantaneous power for each period and saving the maximum and minimum values

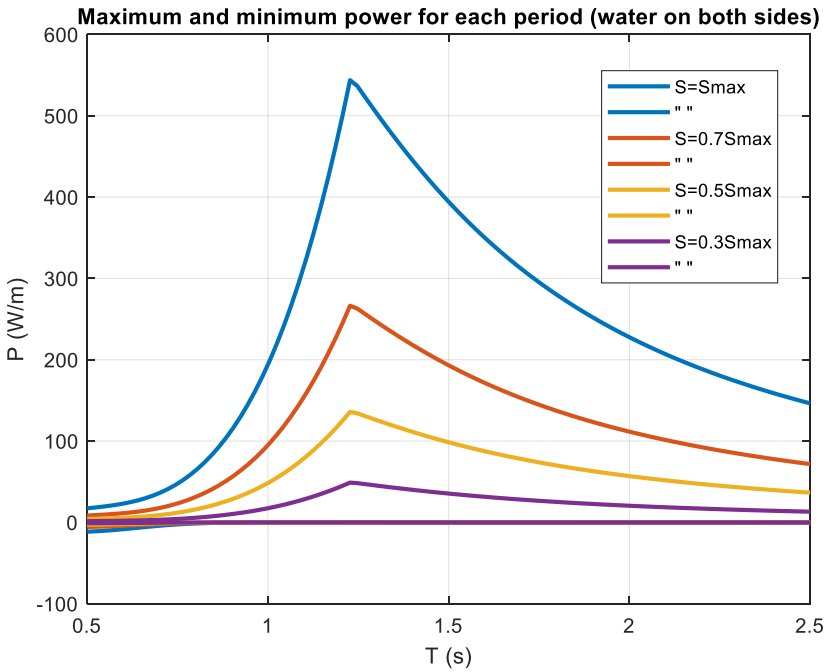

It is possible to note that the maximum values reached in this case are lower than the one for water on only one side; this because, being in this case water on both sides, the hydrostatic component is balanced. Furthermore, we can note that the power is practically always positive since the force to apply to push the water and the paddle velocity have the same direction. Again, for $T = 1.23\ s$ we reach the maximum power requirement and the following graph offers a detail of the power component trends

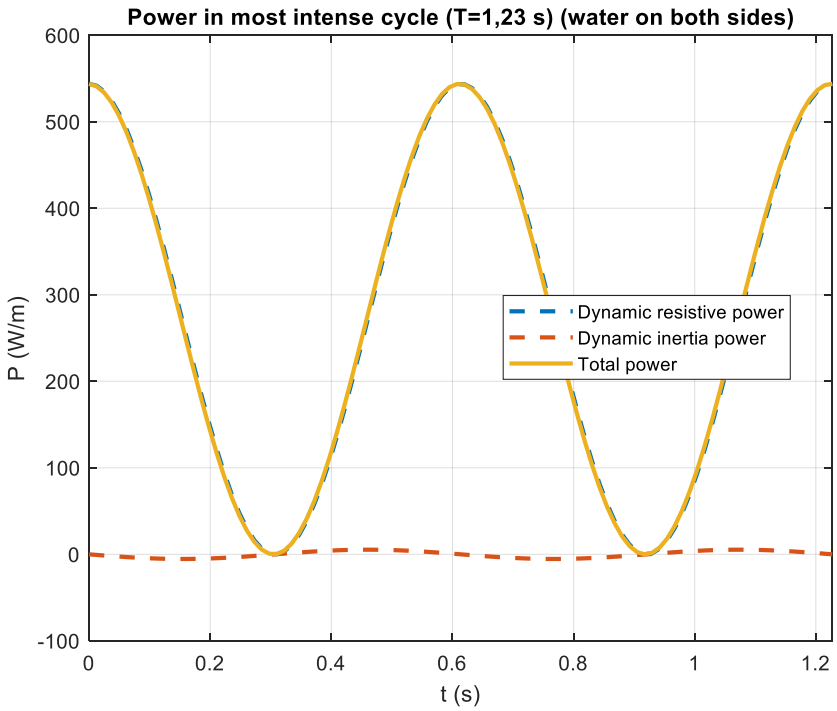

After this analysis of the water force and power requirement according to the first order wavemaker theory, we introduce now some practical considerations. As it is possible to see from the graphs above, forces and power values are smaller in the case with water on both side: this is due to the balancing of the hydrostatic term. The configuration with water on only one side requires the use of seals to avoid the passage of water in the dry back of the flap. For practical reasons, we decided for the option with water on both sides. This choice implies the necessity of a sort of beach also in the area back to the flap to reduce the effects of wave reflection. It is possible to balance the hydrostatic term also with water on only one side designing a device to hold it but, again for simplicity, we decided for the other option. Then, from now on, we will consider only the case with water of the same depth on both sides.

Since we want to have a more detailed analysis of the forces acting during a work cycle to make a more reliable choice of the actuation system, we deepen the problem considering the other forces acting on the flap.

First, the flap has to move according to the following equations

$$\theta = \theta_{max} \sin\left(2\pi \frac{t}{T}\right)$$

$$\dot{\theta} = \theta_{max} \frac{2\pi}{T} \cos\left(2\pi \frac{t}{T}\right)$$

$$\ddot{\theta} = -\theta_{max} \frac{4\pi^2}{T^2} \sin\left(2\pi \frac{t}{T}\right)$$

where θ_{max} is half of the angle subtended by the particular stroke.

The following image represents the free body diagram of the flap

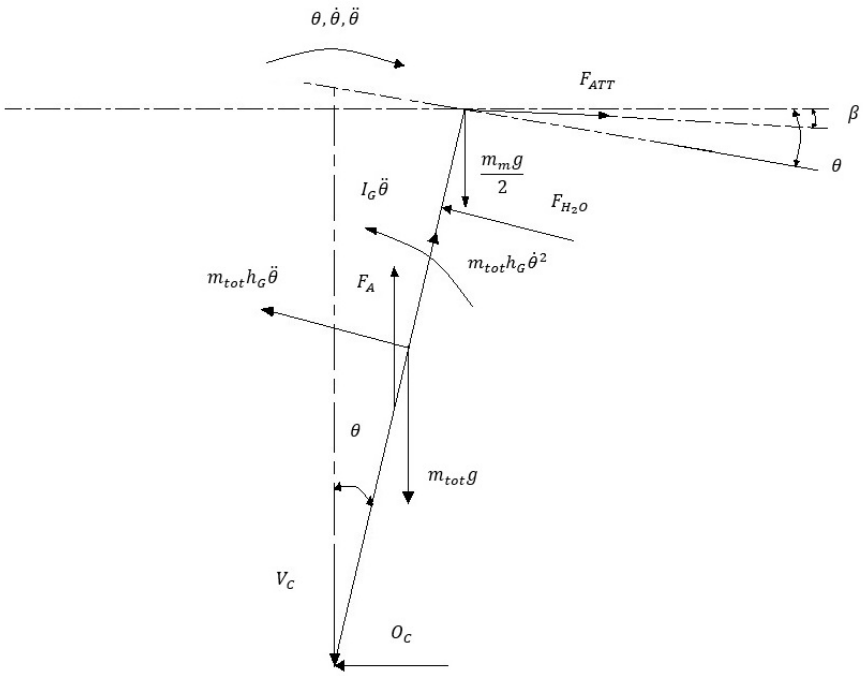

Taking the clockwise as positive, the rotational equilibrium around the bottom hinge C is

$$F_{ATT}\cos(\theta-\beta)h_{flap}+\frac{m_m g}{2}\sin\theta\, h_{flap}-F_{H_2O}h_{max}-I_G\ddot{\theta}-m_{tot}h_G\ddot{\theta}h_G+m_{tot}g\sin\theta\, h_G-F_A\sin\theta\, h_{G'}=0$$

$F_{ATT}\cos(\theta-\beta)$, is the component of the force exerted by the actuator which gives moment respect to C; since we consider the linking point between flap and actuator at the top of the flap, the force component is multiplied by the flap height h_{flap}. The angle β is the one formed by the horizontal direction and the axis of the linear actuator; the values of these angle are very small and further on we will neglect it. The position of the second hinge was chosen considering that the maximum water force occurs when the flap is vertical: in this way, the actuator can directly face this force without using components.

Since we were oriented to mount the actuator with a double hinge, we considered the action of half of the weight of motor and actuator; also this force acts at the connection point between flap and actuator and m_m was estimated to be

$m_m \cong 44\ kg$

already oversized for safety.

F_{H_2O} is the force exerted by the water. As made in [], we considered this force applied at the maximum height reachable by the water: in this way, the importance of this force in the rotational equilibrium is overestimated but we are in safety.

m_{tot} is the mass of the flap and of the steel structure used to support it. Since we want to minimize the inertia, we designed the flap with Divinycell, a polymer foam characterized by low density ($\rho \cong 400\ kg/m^3$) and widely used in marine applications. Knowing the dimensions of the paddle, $2.2\ m\ x\ 1.1\ m\ x\ 0.03\ m$, it is possible to calculate the mass of the flap

$\rho = 400\ kg/m^3$

$V_{flap} = 2.2 \cdot 1.1 \cdot 0.03\ = 0.0726\ m^3$

$m_{flap} = \rho \cdot V_{flap}\ = 29\ kg$

As already said, the flap will be supported by a structure of stainless steel and then we consider also this weight estimated to be around $5\ kg$

$m_{tot} = m_{flap} + m_{steel} = 34\ kg$

F_A is the bouncy force. In fact, the flap will be partially submerged by water and then we consider the bouncy force acting on it.

The minimum submerged volume considering the maximum ideal wave height, is estimated to be

$V_{submerged} = 0.0356\ m^3$

and the center of gravity of this submerged part is

$h'_g = 0.27\ m$

Now, assuming negligible the angle β, we have

$$F_{ATT} = \frac{1}{\cos\theta\ h_{flap}}\left(F_{H_2O}h_{max} - \frac{m_m g}{2}\sin\theta\ h_{flap} + I_G\ddot{\theta} + m_{tot}h_G\ddot{\theta}h_G - m_{tot}g\sin\theta\ h_G + F_A\sin\theta\ h_{G'}\right)$$

that is the force exerted by the actuator along its axis.

The following graph shows the trends of F_{ATT} and all of the other components in the last equation

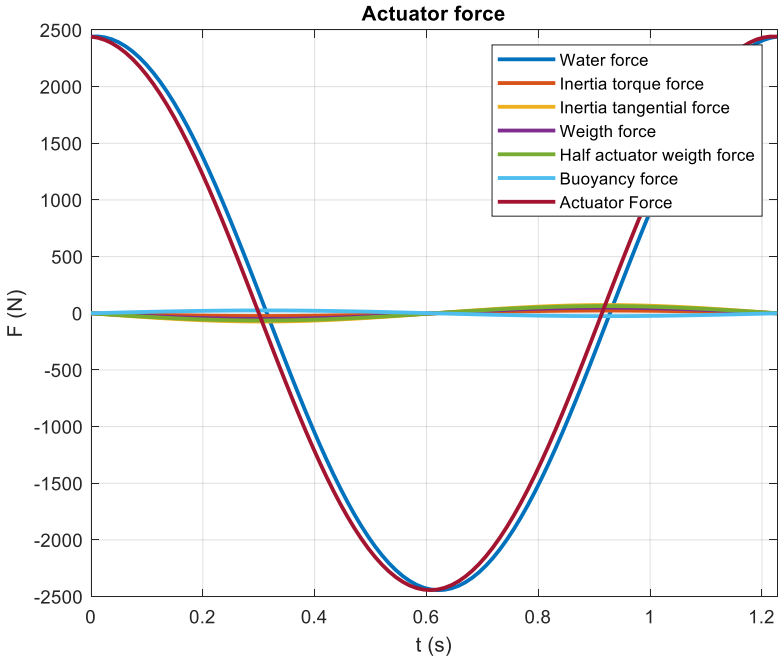

It is possible to see that the most important component is the one of the water force and all the others are quite negligible. Using others materials for the flap, like aluminum, we would probably have an increase of the inertia and then an increase of the corresponding forces.

To choose the linear actuator for our system, we have to evaluate also the velocity of the stem of the actuator. To find this expression, we define a new mobile reference system located on the cylinder and in rotation with it

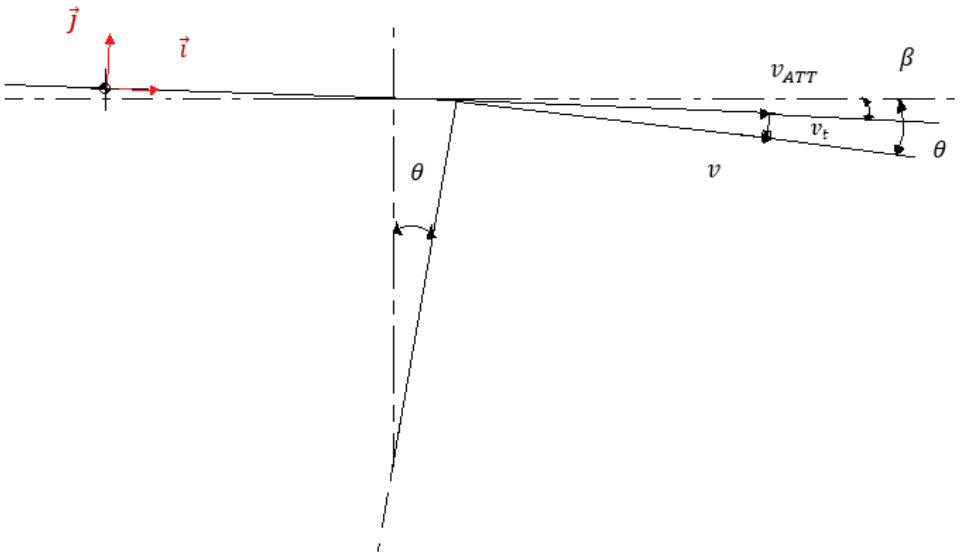

Writing the equation for motion composition for the superior extremity of the flap, we have

$$\vec{v} = \overrightarrow{v_r} + \overrightarrow{v_t}$$

$$\vec{v} = \overrightarrow{v_{ATT}} + \overrightarrow{v_t}$$

where $\vec{v}$ is the velocity of the superior extremity of the flap, $\overrightarrow{v_{ATT}}$ is the velocity of the cylinder stem and $\overrightarrow{v_t}$ is the drag velocity; from the sketch above we obtain

$$v_{ATT} = v\cos(\theta - \beta)$$

Also in this expression, we neglect the angle β since it is assumed to be very small and then we have

$$v_{ATT} = \dot{\theta} h_{flap} \cos\theta$$

Summing up, we evaluated the force exerted by the water on the flap during its motion and the power requirement according to the first order wavemaker theory. Practical reasons brought us to the configuration with water on both sides and then this case was studied evaluating all the forces acting during a work cycle. The rotational equilibrium of the flap showed that in our case the most important force is the one given by the water confirming the approach of the linear wavemaker theory. Since we want to choose a linear actuator to move our flap, it is important to know the actuator stem velocity; this was obtained using motion composition.

4.2.3 Actuator dimensioning

We have now to make a first dimensioning of the actuation system. Several solutions were considered but quite soon we moved on the electric cylinder for its simplicity and flexibility. Then, we analyzed catalogues of several companies to find a good solution for our problem; at the end, the electro cylinders of Pamoco appears to be very interesting for our application since they introduce low reductions in wave generation and they have an IP 65 that allows these actuator to work in proximity of sloshing water.

After some evaluations, we decided for a configuration with an electric cylinder with double hinge has shown in the sketch above

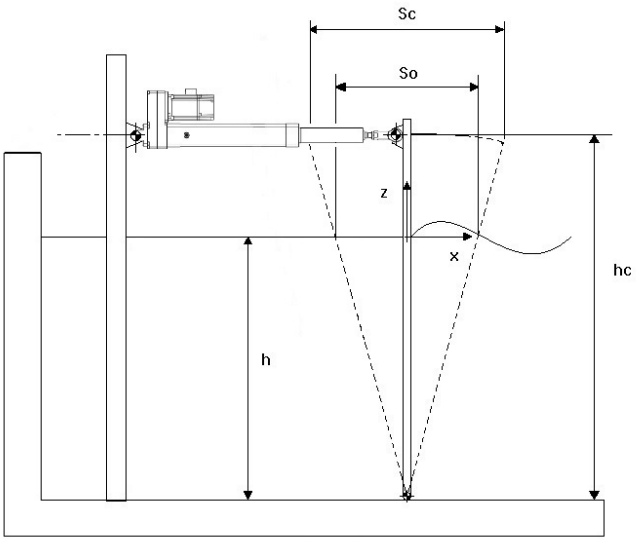

Then, we studied the working conditions of the actuator through the period range of interest. The following graphics show the maximum and minimum cylinder stem velocity and force for each period

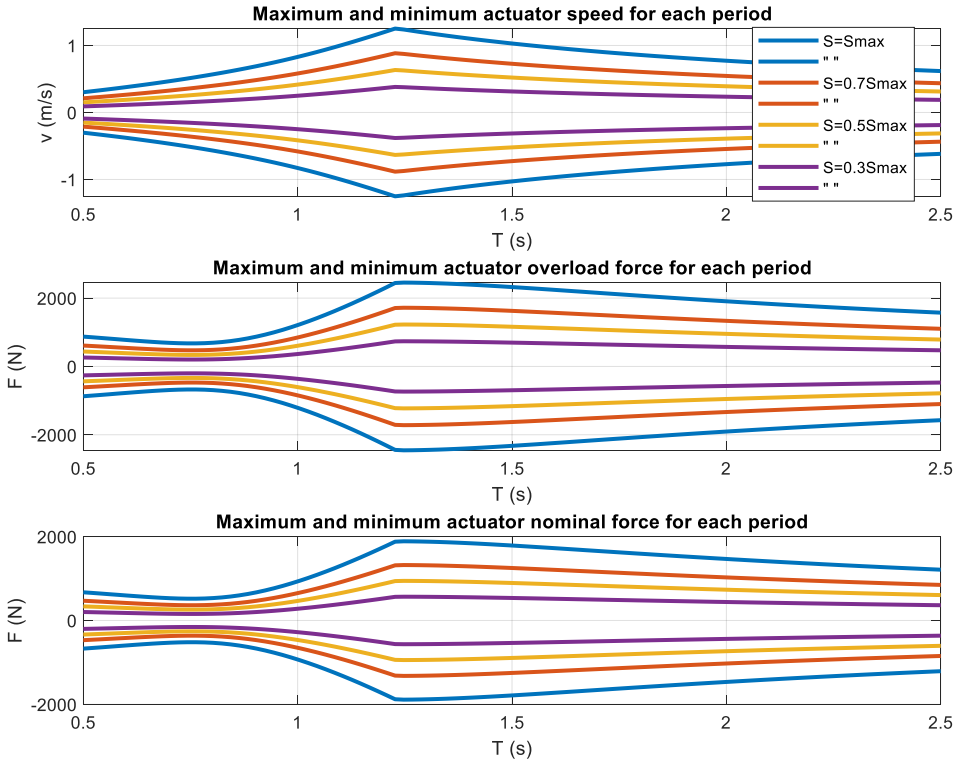

From the graphs above it results that the most intense cycles in terms of velocities and forces are the ones made with the maximum stroke possible. For this reason, we concentrate only on these working cycles.

The following graph represents the F- v characteristic that we would like to realize when we use the maximum possible stroke for each period and in overload conditions. From what said, this is the limit working area and all the others working areas corresponding to smaller strokes are contained inside this one. Then, to generate all our ideal waves above mentioned, we need an actuator that covers with its characteristic this limit working area

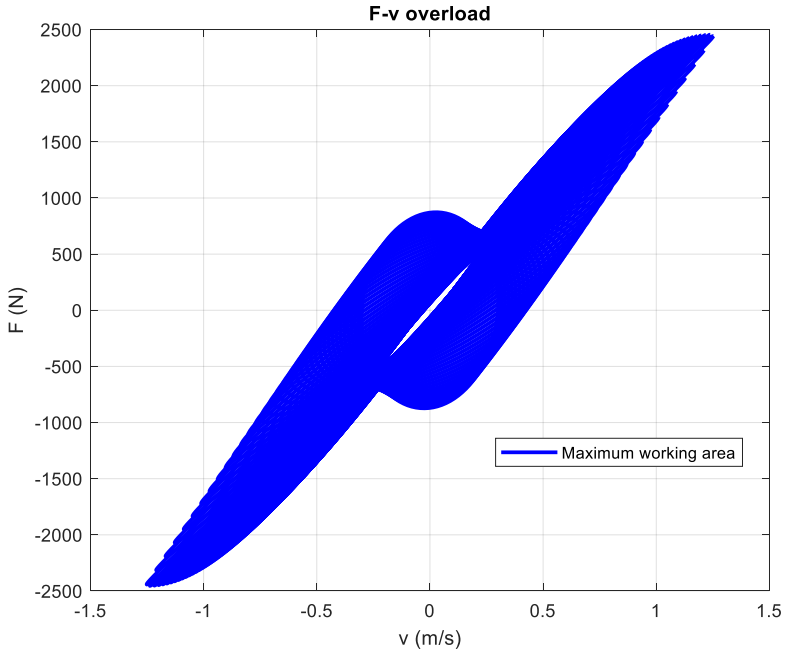

For completeness, we report the following three graphs that show the trend of velocity, overload force and nominal force in the period corresponding to the most intense cycle; the difference between overload and nominal is a safety factor of 1.3 on the forces values, as made in [6]

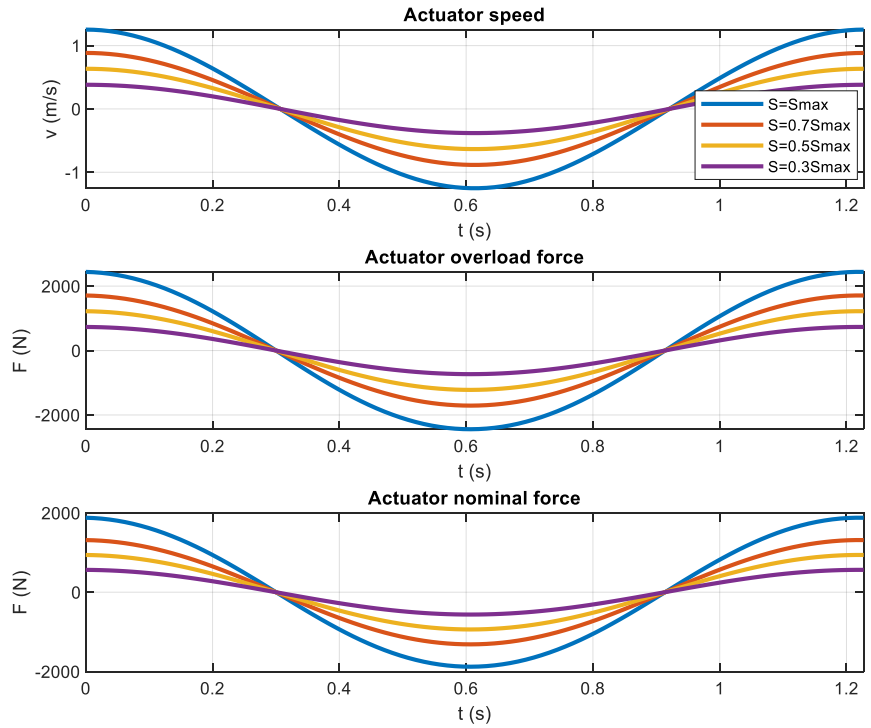

The electro cylinders offered by Pamoco appear to be the most suitable, between the analyzed providers, for this application since they better cover the working are of interest and have IP65.

From a first analysis of the catalogue, we focused on the following two actuators:

- PNCE 50 20 x 20

  Maximum axial load $F_{max} = 3900\ N$

  Maximum travel speed $v_{max} = 1.1\ {}^{m}/_{s}$

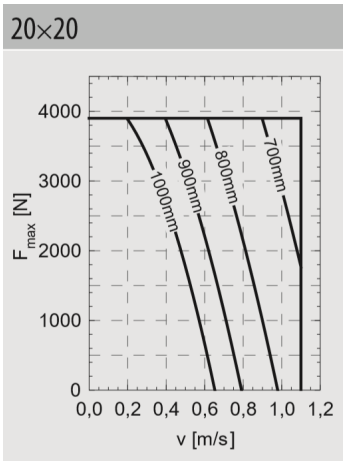

- PNCE 63 25 x 25
  Maximum axial load $F_{max} = 7940\ N$

  Maximum travel speed $v_{max} = 1.13\ {}^{m}/_{s}$

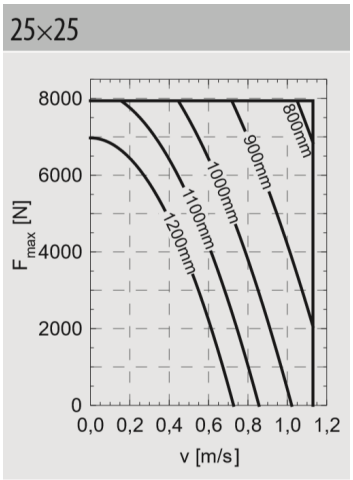

Our F-v characteristics and the one of the two actuators found in the catalogue are reported in the following graph to have an overview.

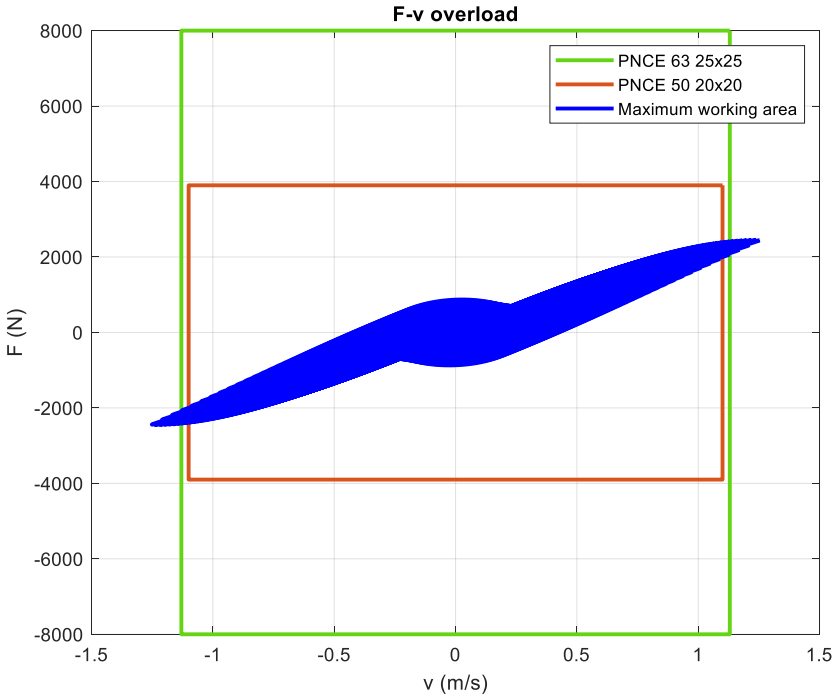

As can be guessed, in the catalogue the are several other values such as maximum and minimum stroke, maximum acceleration and so on; all these values and limits are not reported here because our application largely passes these verifies or they are not taken into account in this first dimensioning.

Both the real values of F_{max} and v_{max} depend on the particular application; so, to choose between the two actuators, we followed the procedure provided in the catalogue. To do this, we first have to define more quantities.

Referring to the following image

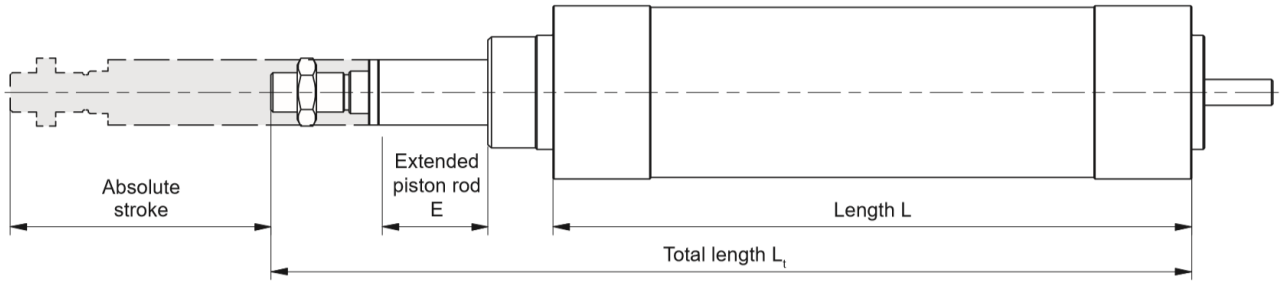

In our application, for both the actuators, we have

- $E = 0\ mm$
- $Absolute\ stroke = 600\ mm$

that is

$Absolute\ stroke = Effective\ stroke + 2\ x\ Safety\ stroke = 500\ mm + 2\ x\ 50\ mm = 600\ mm$

- Mounting case: simple - simple mount

For both the actuators, we need the following mounting attachments

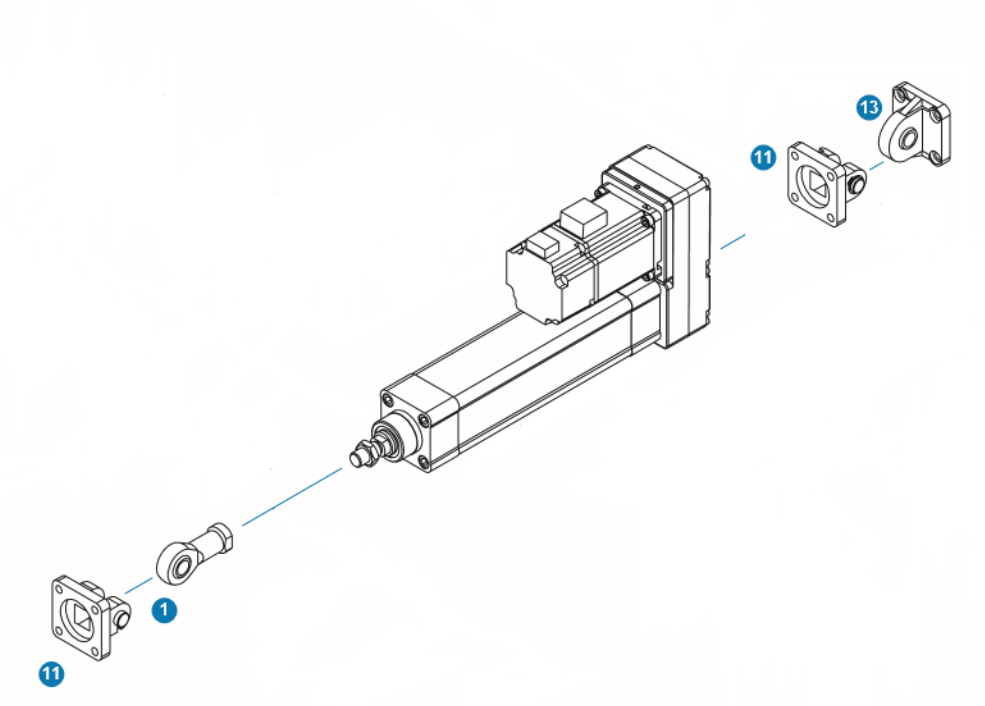

These accessories introduce limits on the maximum axial load.

For both the actuators we started to evaluate the use of a speed reducer, still provided by Pamoco and designed for these particulars electro cylinder, to reduce the dimensions of the motor:

- MSD T2 $(i = 2)$, for PNCE 50 20 x 20
- MSD T1 $(i = 2)$, for PNCE 63 25 x 25

Now it is possible to follow the dimensioning procedure that aims to evaluate the maximum axial force that the actuator can support in this particular application.

PNCE 50 20 x 20

Entering data:

- $Absolute\ stroke = 600\ mm$
- $E = 0\ mm$
- Travel speed $v_{max} = 1.1\ m/s$, that in our case is the maximum allowed by the electro cylinder.
- Using motor side drive MSD - PNCE50 - T2 with gear ratio $i = 2$
- Mounting: simple - simple mount

F_{max} function of absolute stroke and mounting case

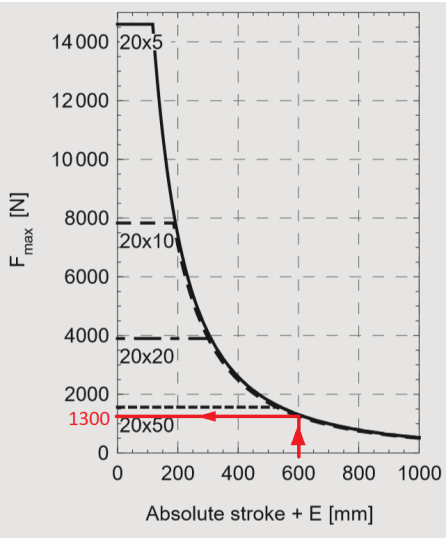

$F_{max} = 1300\ N$

F_{max} function of travel speed, ball screw lead and absolute stroke

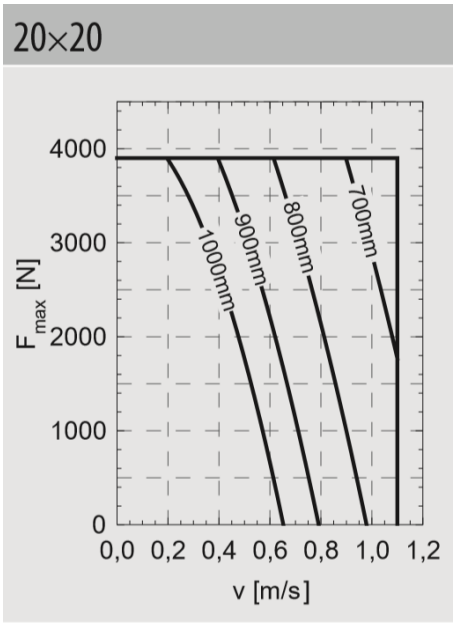

$F_{max} = 3900\ N$

F_{max} limit from maximum drive torque $M_{p,MSD}$ on motor side drive

From the catalogues, we have the expression of the load torque

$M_{load} = \frac{F_{axial} \cdot l}{2000 \cdot \pi \cdot \eta \cdot i}$

From technical data of MSD - PNCE50 - T2 we have the maximum drive torque

$M_{p,MSD} = 4.5\ Nm$

Substituting this value in M_{load} and solving for F_{axial} we have

$$F_{axial} = \frac{M_{load} \cdot 2000 \cdot \pi \cdot \eta \cdot i}{l} = 2545\ N$$

$F_{max} = 2545\ N$

Maximum axial load for mounting attachments

$F_{max} = F_{PNCE} = 3900\ N$

Finally, the maximum axial load is given by the lowest value of F_{max}

$$F_{max} = 1300\ N < F_{ATT,max}$$

Surely, we have to discard the PNCE 50 20 x 20.

PNCE 63 25 x 25

As already done for the other cylinder, we have:

- $Absolute\ stroke = 600\ mm$
- $E = 0\ mm$
- Travel speed $v_{max} = 1.13\ m/s$, that in our case is the maximum allowed by the electro cylinder.
- Using motor side drive MSD - PNCE63 - T1 with gear ratio $i = 2$
- Mounting: simple - simple mount

F_{max} function of absolute stroke and mounting case

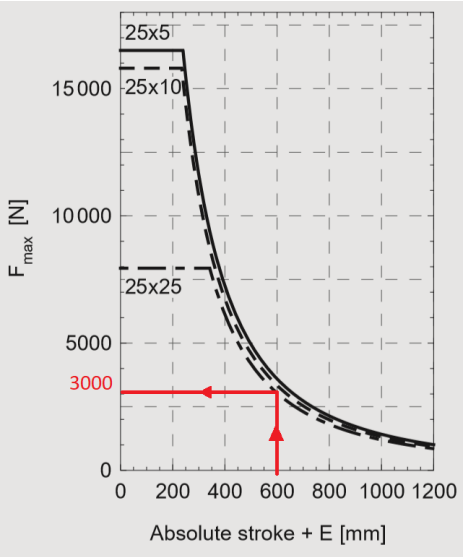

$F_{max} = 3000\ N$

F_{max} function of travel speed, ball screw lead and absolute stroke

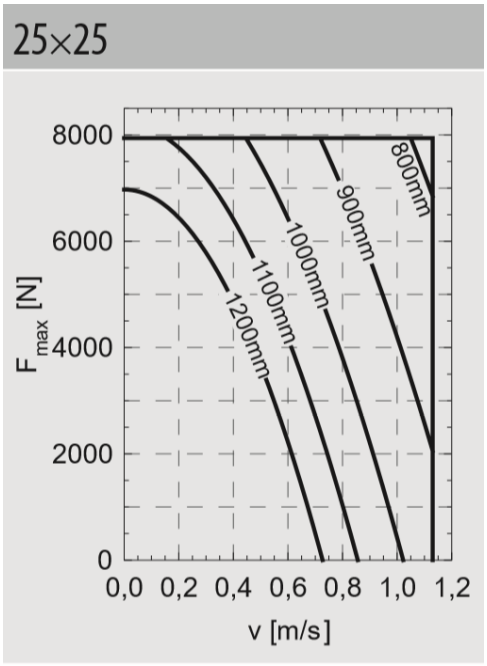

$F_{max} = 7940\ N$

F_{max} limit from maximum drive torque $M_{p,MSD}$ on motor side drive

$M_{load} = \frac{F_{axial} \cdot l}{2000 \cdot \pi \cdot \eta \cdot i}$

From technical data of MSD - PNCE63 - T1 we have the maximum drive torque

$M_{p,MSD} = 8.9\ Nm$

Substituting this value in M_{load} and solving for F_{axial} we have

$$F_{axial} = \frac{M_{load} \cdot 2000 \cdot \pi \cdot \eta \cdot i}{l} = 4026\ N$$

$F_{max} = 4026\ N$

Maximum axial load for mounting attachments

$F_{max} = F_{PNCE} = 7940\ N$

Finally, the maximum axial load is given by the lowest value of F_{max}

$$F_{max} = 3000\ N > F_{ATT,max}$$

PNCE 63 $25\ x\ 25$ could be used in our application.

As already seen in the first F-v characteristic, it is not possible to reach our maximum velocities with this actuator; this yields to a cut on the wave generation capabilities that will be analyzed in the following section.

Since we have the actuator, it is possible to evaluate the length of the cylinder in the two extreme positions. Considering all the accessories and the speed reducer, we have

$L_{tot\ IN} = 1066\ mm$, total length at rest

$L_{tot\ OUT} = 1666\ mm$, maximum length

Using this data and working on the sketch geometry it is possible to evaluate the angle β; in particular, it results

$\beta = 6.08°$, when the cylinder is at rest

$\beta = 3.56°$, when the cylinder is completely out.

This shows that β is small and, when it should interact with θ inside a cosine for the projection, it does not change too much the value of the cosine and of the corresponding physical quantity.

Still from the catalogue, it is possible to evaluate the mass of the actuator, accessories and speed reducer; we have

$m = 14.3\ kg$

The last value does not take into account the weight of the motor.

Summing up, once analyzed the velocities and forces of the actuator, we focused on the cycles with maximum stroke. For each period of the range, we reported the characteristic F-v when the maximum stroke is used: the result is the largest working area of the actuator in the period range of interest. This information allows us to search actuators; we moved on the electro cylinder of Pamoco because they cover quite well the working area and has an IP65. After following the dimensioning procedure provided in the catalogue, we chose the electric cylinder PNCE 63 $25\ x\ 25$ with MSD - PNCE63 - T1. As shown in the following chapter, this choice yields anyway to a reduction of wave generation capabilities. At last, once known the actuator, it is also possible to evaluate the mass and the lengths and this allows us to evaluate the angle β to verify that is very small.

4.2.4 Consequences of the actuator choice

As already said in the previous section, even if this actuator represents a suitable choice, it introduces cuts in wave generation since it is not possible to reach the velocities required to generate the desired waves. In particular, this limit on the velocities yields to a limit on the strokes and then consequences on the forces; for these reasons, it is necessary to evaluate again the possible strokes for each period and all the quantities that depend from them. In particular, we evaluated again the wave heights and the forces exerted by the actuator to quantify the reduction that could be interesting for the motor choice.

The maximum velocity of actuator PNCE 63 is set to $1.13\ m/s$; for safety, this limit was reduced to $1\ m/s$.

The velocity of the stem of the actuator is, neglecting the angle β

$$v_{EC} = \dot{\theta} h_{flap} \cos\theta$$

The angular velocity of the flap is given by

$$\dot{\theta} = \theta_{max} \frac{2\pi}{T} \cos\left(2\pi \frac{t}{T}\right)$$

where θ_{max} is half of the angle subtended by a general stroke
Substituting the last equation in the expression for v_{EC} we have

$$v_{EC} = \left(\theta_{max} \frac{2\pi}{T} \cos\left(2\pi \frac{t}{T}\right)\right) h_{flap} \cos\theta$$

For a fixed period and a fixed stroke, v_{EC} is max when the value of the two cosines is one that is for $t = 0\ s$ being

$$\theta = \theta_{max} \sin\left(2\pi \frac{t}{T}\right)$$

Then, for a particular period and stroke, the maximum velocity of the stem of the actuator is given by

$$v_{EC\ MAX} = \theta_{max} \frac{2\pi}{T} h_{flap}$$

The velocity of the actuator was set to $1\ m/s$; imposing this value in the last expression and evaluating it for every period of the range, we obtain, for each period, the angle θ_{max} that allows the respect of the condition on the maximum stem velocity for the given period T

$$\theta_{max} = \frac{v_{EC\ MAX} \cdot T}{2\pi \cdot h_{flap}}$$

It is possible now to use the last expression to introduce a new limit on the strokes. The general expression for a stroke is given by

$$S = 2 \cdot h_{flap} \cdot \tan(\theta)$$

$$S = 2 \cdot h_{flap} \cdot \tan\left(\frac{v_{EC\,MAX} \cdot T}{2\pi \cdot h_{flap}}\right)$$

In this way, the limit on the angle is transformed into a limit on the stroke. The following graph reports this new limit together with the others already mentioned in the first section

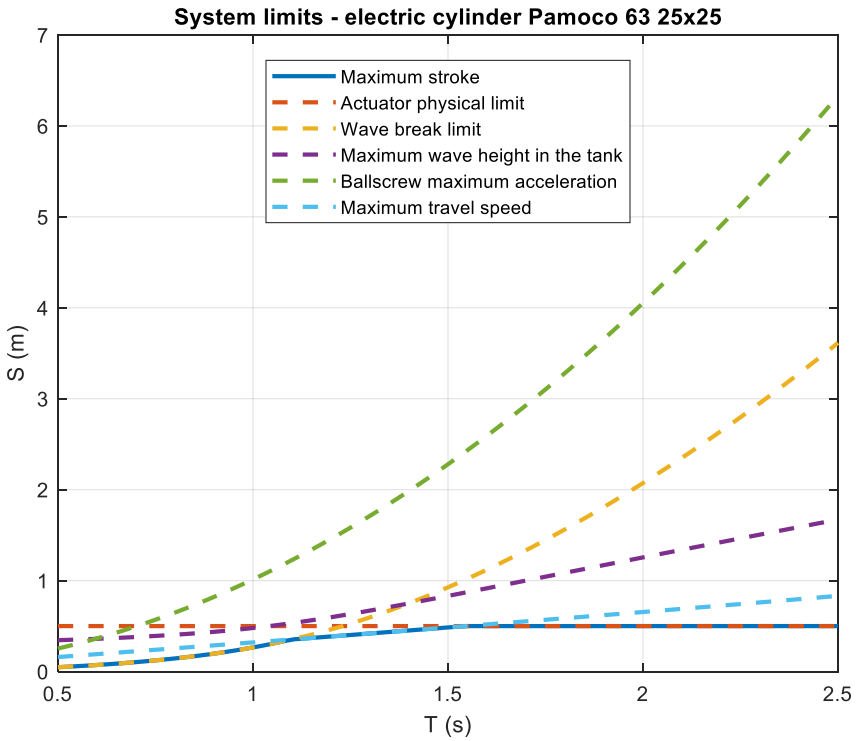

As it is possible to see, the new limit intervenes between the limits on the wave breaking and on the maximum actuator stroke determining a cut of our maximum wave height generable. The value of the maximum acceleration of the ball screw is now $20\ m/s$, according to the information in the catalogue. The corresponding new strokes and wave heights are summarized in this graph

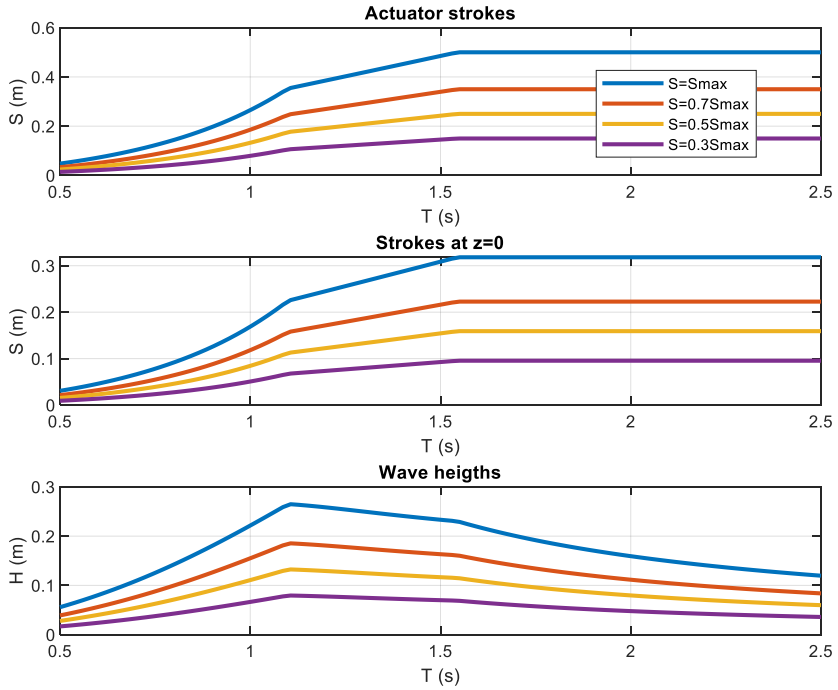

As it is possible to see, the new maximum wave height is $H_{Max} = 0.265\ m$; respect to the ideal case, in which the maximum wave height was $0.323\ m$, the choice of the actuator caused a reduction of the $18\ \%$ of the maximum wave height.

It is interesting to see that the wave length and celerity are not affected by this new constrain: in fact, they both depend on the dispersion relationship that describes how waves disperse.

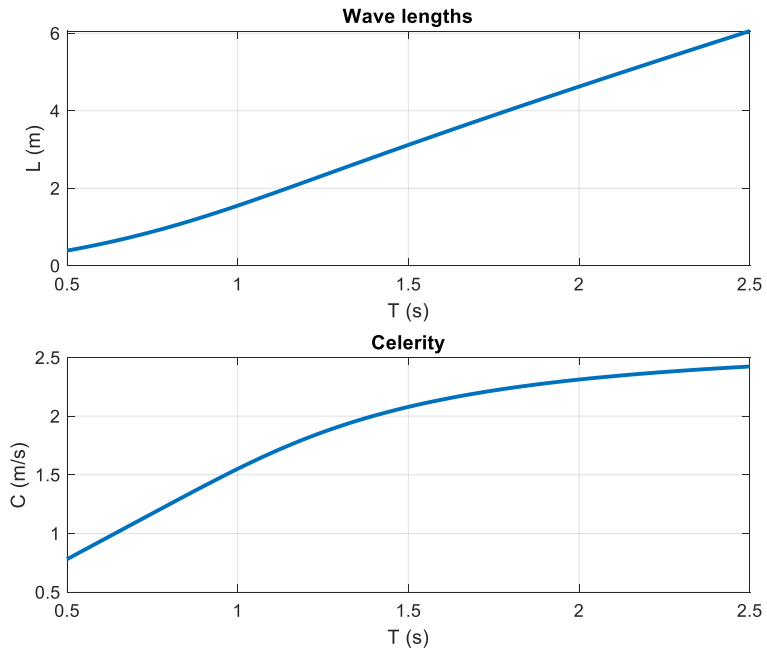

The new limit on the actuator velocity introduces a limit on the strokes and this has consequences also on the forces. Then, it could be interesting to calculate again the forces in action during all the cycles of the period range made with the maximum possible stroke for that period. The equilibrium is the one already seen in the previous section. Theoretically, we have to update in the equation the value of the maximum wave height reachable but, respect to z axis, there is a very small change; moreover, considering the first value, we are in safety and so we decided to not update.

The following graph is the new F-v characteristics which arises from this new calculation

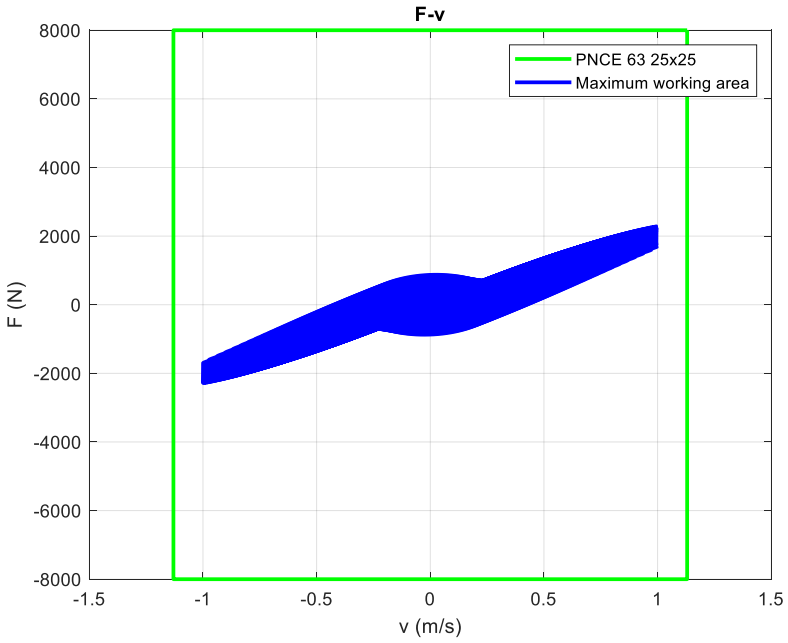

Comparing with the previous characteristic, we have a lost in the forces values and the velocity is limited to $1\ m/s$. As before, we reported also the general actuator characteristic that could seem too much large but it does not take into account the mounting limitations.

Summing up, the choice of the actuator introduces a limit on the velocities that yields to a limit on the maximum stroke reachable in each period. Then, we analyzed the consequences of this new constrain on wave generation capabilities and on the actuator forces obtaining a new F-v characteristic that takes into account the chosen actuator; this last characteristic is the starting point for the motor choice.

4.2.5 Motor choice

Now that we have the actuator and the new F-v characteristic, we have to find a suitable motor to drive it; to do this, we need the torque and angular velocity on the motor shaft.

To evaluate the torque on the motor shaft it is possible to use the equation provided by the catalogue

$$M_{load} = \frac{F_{axial} \cdot l}{2000 \cdot \pi \cdot \eta \cdot i}$$

For the angular velocity it is possible to use the relation for the screw transmission with rectangular thread

$$v' = v \tan \alpha$$

$$v' = \omega_{vite} \frac{d_{vite}}{2} \tan \alpha \;\Rightarrow\; \omega_{vite} = \frac{v'}{\frac{d_{vite}}{2} \tan \alpha}$$

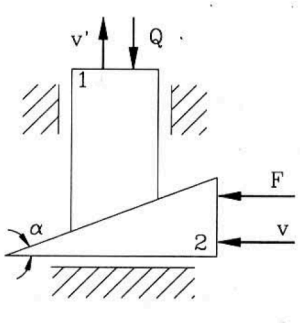

To obtain the velocity on the motor shaft we introduce the gear ratio i

$$\omega_{load} = i \left(\frac{v'}{\frac{d_{vite}}{2} \tan \alpha} \right)$$

The following graph represents the characteristic C-n that our motor has to be able to provide to drive the actuator

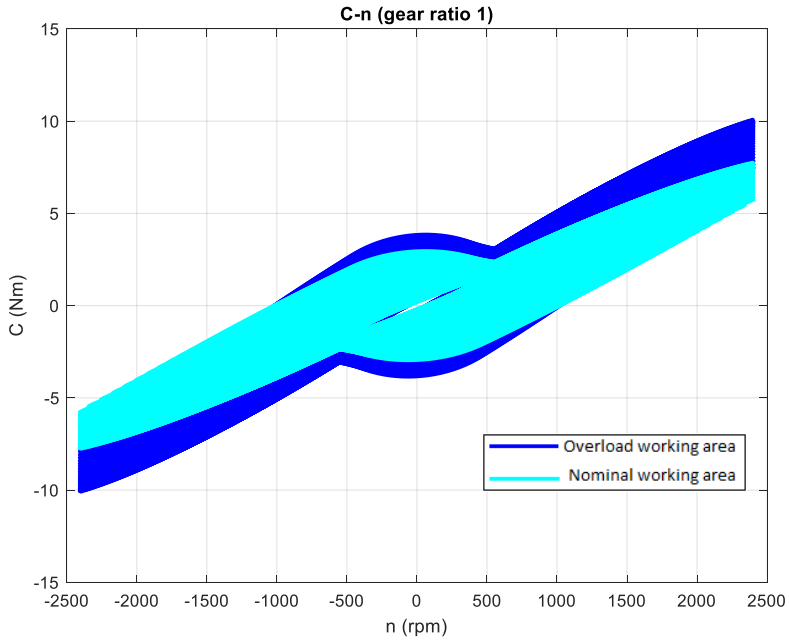

For completeness, we report also the motor angular velocity, the motor torque and power for the period in which there is the most intense cycle both for the overload and nominal condition. This period, after the new limit on the actuator velocity, passes from $T = 1.23\ s$ to $T = 1.55\ s$

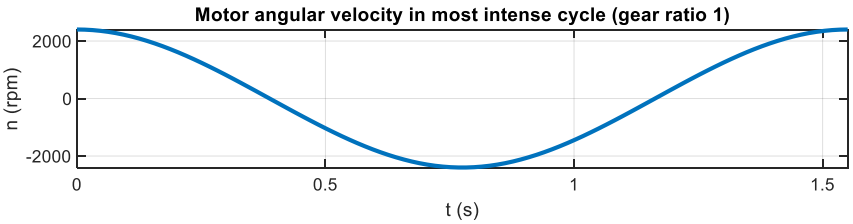
Motor angular velocity in most intense cycle (gear ratio 1)
n (rpm)
2000
0
-2000
0
0.5
1
1.5
t (s)

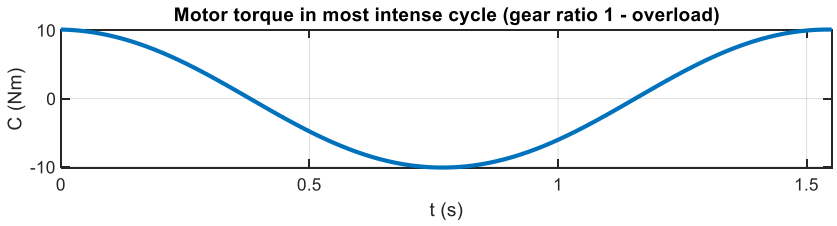
Motor torque in most intense cycle (gear ratio 1 - overload)
C (Nm)
10
0
-10
0
0.5
1
1.5
t (s)

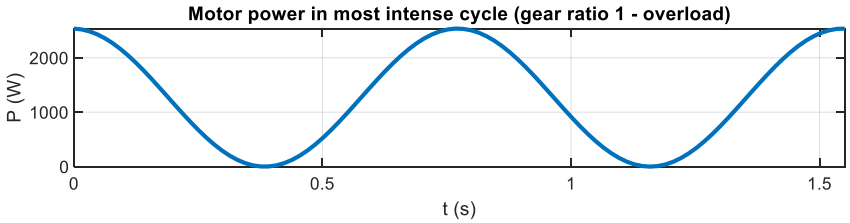
Motor power in most intense cycle (gear ratio 1 - overload)
P (W)
2000
1000
0
0
0.5
1
1.5
t (s)

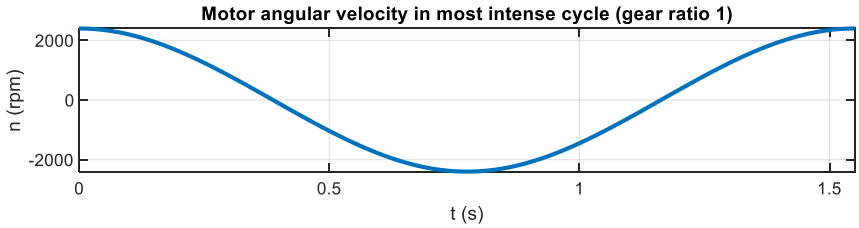
Motor angular velocity in most intense cycle (gear ratio 1)
n (rpm)
2000
0
-2000
0
0.5
1
1.5
t (s)

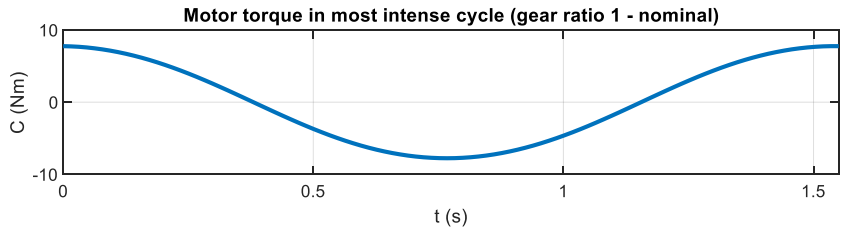
Motor torque in most intense cycle (gear ratio 1 - nominal)
C (Nm)
10
0
-10
0
0.5
1
1.5
t (s)

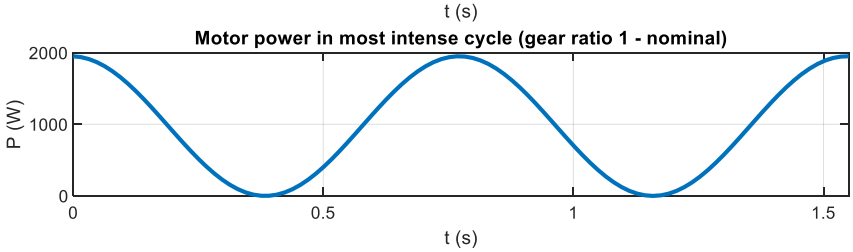
Motor power in most intense cycle (gear ratio 1 - nominal)
P (W)
2000
1000
0
0
0.5
1
1.5
t (s)

4.2.5.1 Analysis with gear ratio $i = 1$

The maximum value of torque imposes us a choice of a motor with a torque bigger then $10\ Nm$. Searching on catalogues, we selected the following three brushless motor

- ESTUN EMG 10
- LSIS XML-HE 15 A
- SVTM A 02-3.18-57

All of them appear, in first instances, to be suitable for our application; the best of the three it seems to be the ESTUN because its characteristic is closer to our maximum working area.

Here we report the characteristic C-n with gear ratio $i = 1$ with the other three characteristics of the suitable motors

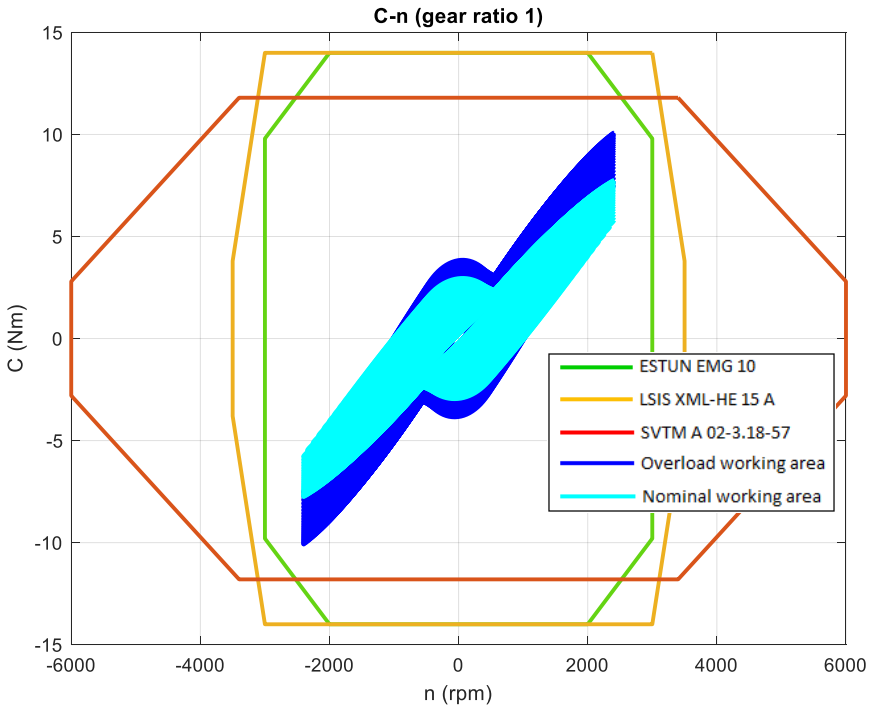

The use of a speed reducer, as already said above, gives us the possibility to use a motor with less torque and more velocity. This study will be done in the next paragraph.

4.2.5.2 Analysis with gear ratio $i = 2$

Pamoco provides a standard speed reducer, with gear ratio $i = 2$, for our electro cylinder; in particular, we focused on MSD - PNCE 63 - T1. This allows us to halve the torque and to double the angular velocity on the motor shaft.

The following is the new characteristic C-n that our motor has to be able to provide to drive the actuator when we use the above mentioned speed reducer

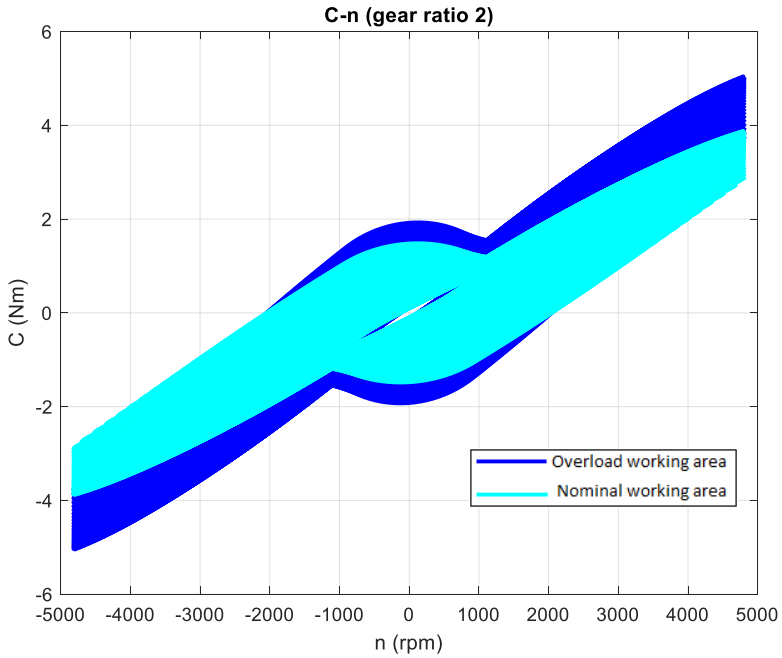

In which the cyan area represents the nominal working conditions while the blue one the overload working condition.

For completeness, we report also the motor angular velocity, the motor torque and power for the period in which there is the most intense cycle both for the overload and nominal condition. This period, after the new limit on the actuator velocity, passes from $T = 1.23\ s$ to $T = 1.55\ s$

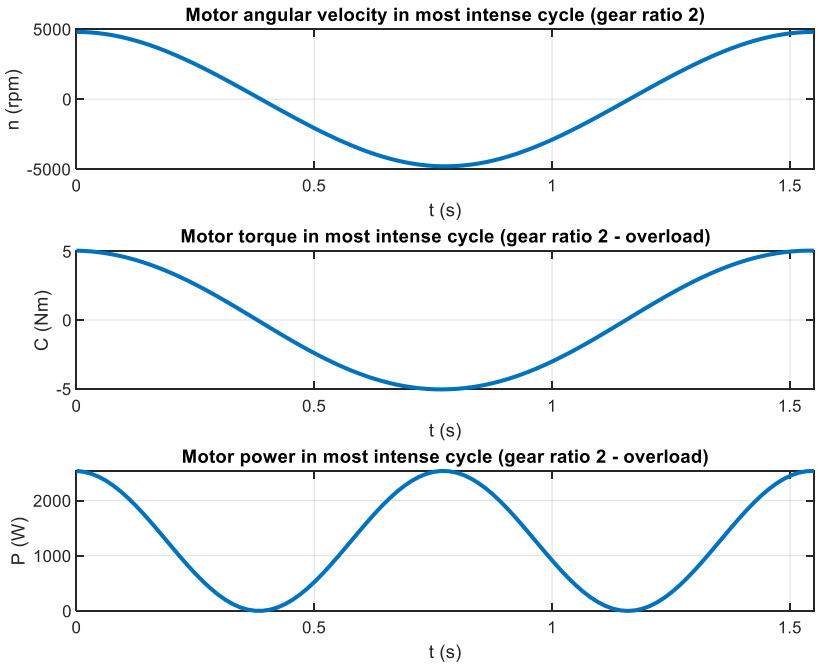

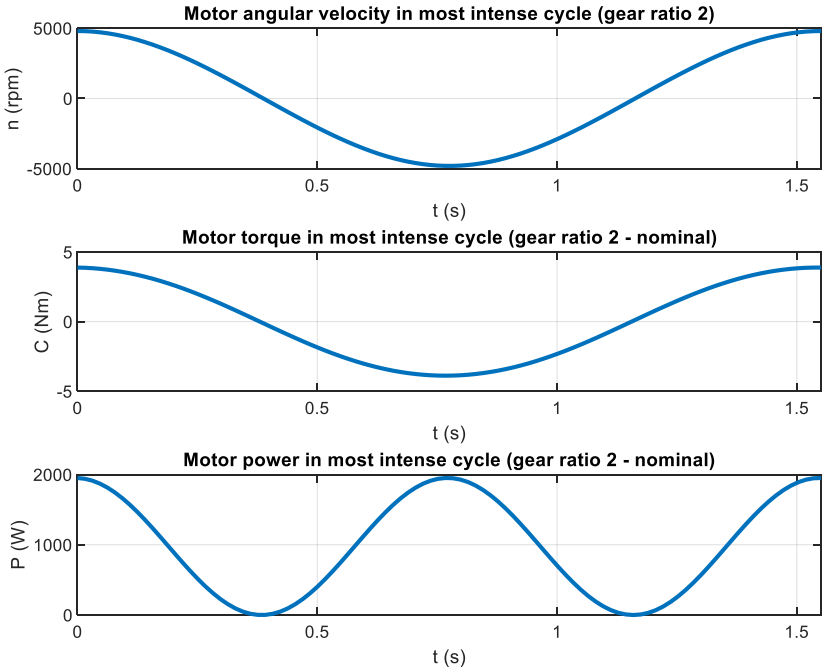

In this case, we have half of the previous torque and the double of the angular velocity; according to these values, we selected the following three brushless motors:

- LSIS XML-SC08A
- LSIS XML-FC10A
- LSIS XML-FEP09A

All of them appear, in first instances, to be suitable for our application; the best of the three it seems to be green because its characteristic is closer to our maximum working area.

Here we report the characteristic C-n with gear ratio $i = 2$ with the other three characteristics of the suitable motors

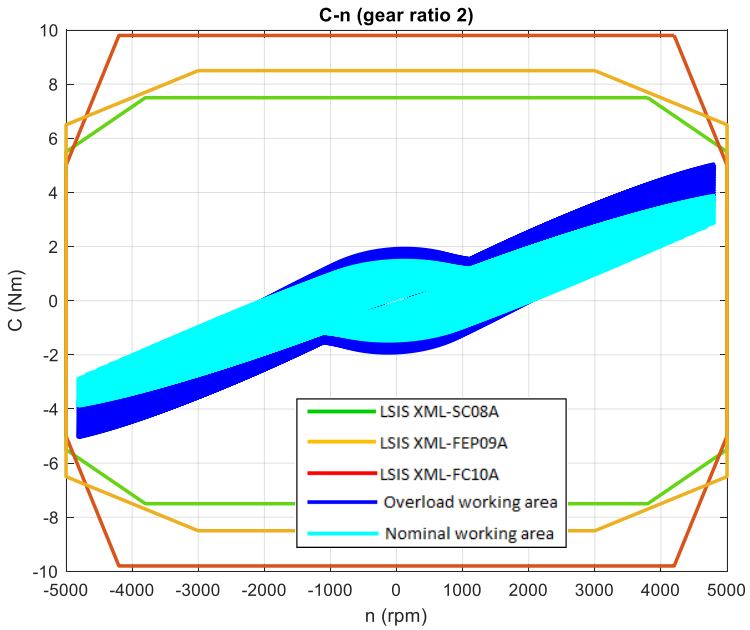

Summing up, once chosen the actuator we have evaluated the new F-v characteristic that is our input data for the motor choice. In fact, using equations found in the catalogue and the ones for the screw transmission, it is possible to generate the corresponding C-n characteristic for the motor. Then, we studied both the configuration without speed reducer and with gear ratio $i = 2$ obtaining for each case the corresponding C-n characteristic for the motor and the detail of the trend of angular velocity, overload torque and nominal torque for the period in which there is the most intense cycle. As usual, the use of the speed reducer helps us in the choice of the motor and it is the solution chosen.

Chapter 5

Conclusions and future works

In the following chapter it is summerized the work developed in this thesis and the main results obtained are pointed out. Then, we introduce the future possible works on this argument.

5.1 Conclusions

The goal of this thesis is the evaluation of the potentialities of the existing tank in terms of wave generation to test wave energy converter devices and a first dimensioning of the actuation system that has to generate waves. This two goals are achieved through the study of the linear water waves theory and researching then a first actuation system suitable for covering our working area.

To understand the problem, it was fundamental the study of the linear water waves theory made on the book *Water waves mechanics for engineers and scientists* (Dean Dalrymple - 1984); for the wavemaker theory, the main reference followed is *Physical models and laboratory techniques in coastal engineering* (Steven A. Hughes - 1993).

As already said, the first thing done is the analysis of the wave generation potentialities of the existing tank; for this part, our reference is [5]. Summing up, given the period range of interest, that is $T = 0.5\ s\ \div 2.5\ s$, we evaluated the maximum actuator stroke and the corresponding maximum wave height expected for each period; all these values are ideal since they do not take into account any limitation introduced by the actuation system. To complete the analysis, we reported for each period of the range the expected wave length and celerity.

To physically realize these waves, we have to make a first dimensioning of an actuation system. To do this we studied velocities, forces and the power requirement of the system; for this part, our reference is [6]. We first concentrate on the forces exerted by the water that are, as shown, the most important and we also done a first analysis of the power requirement; this first analysis was carried on both for water on one side and water on both sides. Then, practical reasons brought us to the configuration with water on both sides and then this case was studied in deep evaluating all the forces acting during a work cycle. The rotational equilibrium of the flap showed that in our case the most important force is the one given by the water confirming the approach of the linear wavemaker theory. Since we want to choose a linear actuator to move our flap, it is important to know the actuator stem velocity; this was obtained using motion composition.

For the first dimensioning of the actuator, we quite soon moved on the electro cylinder for the simplicity and flexibility. Then, we analyzed catalogues of several companies to find a good solution to our problem; at the end, the electro cylinders of Pamoco appears to be very interesting for our application since they introduce low reductions in wave generation and they have and IP 65 that allows these actuators to work in proximity of sloshing water. Even if this actuator represents a suitable choice, it introduces cuts in wave generation since it is not possible to reach the velocities required to generate the desired waves. In particular, this limit on the velocities yields to a limit on the strokes and then to consequences on the forces; for these reasons, it is

necessary to evaluate again the possible strokes for each period and all the quantities that depend from them. In particular, we evaluated again the forces exerted by the actuator to quantify the reduction that could be interesting for the motor choice; from this calculation it results the new F-v characteristic of the actuator. After the choice of the particular electro cylinder, we analyzed the mechanical transmission and several brushless motors that could be suitable for our application.

The new F-v characteristic is our input data for the motor choice. In fact, using equations found in the catalogue and the ones for the screw transmission, it is possible to generate the corresponding C-n characteristic for the motor. Then, we studied both the configuration without speed reducer and with gear ratio $i = 2$ obtaining for each case the corresponding C-n characteristic for the motor and the detail of the trend of angular velocity, overload torque and nominal torque for the period in which there is the most intense cycle. As usual, the use of the speed reducer helps us in the choice of the motor and it is finally the solution chosen.

In conclusion

- the wave generation capabilities of the existing tank, pointed out in this work, are considered interesting for testing hulls, marine structure and wave energy converter devices also with the reduction introduced by the chosen actuator;
- the first dimensioning of the actuation system represents a suitable starting point for a more detailed analysis that could be done with the technical office of Pamoco or in a future work. Clearly, it is also possible to enlarge the research to more providers.

5.2 Future works

This work could be the basis for several other thesis in different working area; in the following section, the main ideas are summarized.

First, since there is a strong interest in equipping our tank with a wavemaker, we have to study a suitable structure to hold this device. The idea is to have a structure independent from the tank which can be easy moved; for this reason, we surely need a base sufficient heavy to remain fixed to the bottom of the tank during the work cycles but also not too much heavy to not ruin the bottom of the tank. An iron steel structure will be fixed on the basis and will hold the actuator. Moreover, we need to think to a suitable configuration for the structure in iron steel that will hold the flap in Divinycell; then we have to study how to realize the link between this structure and the base and also studying in deep the resistance of the flap to the applied load to not have failure. Since there are cycling loads, a study to avoid fatigue failures in all the structure has to be made.

To use this device, it is also necessary to choose the brushless motor for the actuation system. This is strictly linked to the type of control we would like to realize. After this, it is necessary to implement the control architecture of the system to realize the motion described in the current work: it could be studied the position control and the force feedback control, analyzing advantages and disadvantages of them, and then physically implement them in our system.

As shown in the previous chapters, there are several other types of wavemaker. For our testing needs, we focused on the flap type wavemaker hinged to the bottom but it is possible to repeat

this analysis for the variable draft flap type wavemaker and studying advantages and disadvantages of them.

Finally, it is also possible to use this work as the basis for the creation of a numerical wave tank through CFD codes such as StarCCM+ to increase the testing potentialities and the possibility to deepen the design of the tested device.

Bibliography

[1] Dean R., Dalrymple R., *Water Wave Mechanics for Engineers and Scientists*, Singapore, Prentice Hall, 1984.

[2] Hughes S. A., *Physical models and laboratory techniques in coastal engineering,* Singapore, World Scientific Publishing, 1993.

[3] Biesel F., Suquet F. et un groupe d'ingénieurs au Laboratoire Dauphinois d' Hydraulique (Neyrpic, Grenoble), Les appareils générateurs de houle en laboratoire, in La Houille Blanche 1951.

[4] Pilch M., Biesel F., Suquet F. and a group of engineers at the Laboratoire Dauphinois d' Hydraulique (Neyrpic), *Laboratory wave generating apparatus*, University of Minnesota, Project Report No. 39, October 1953.

[5] De Barros Passos R., Fernandes A. C., *Design of a wave-maker facility through linear wave theory*, in Proceedings of the XXXVI Iberian Latin-American Congress on Computational Methods in Engineering Ney Augusto Dumont (Editor), ABMEC, Rio de Janeiro, RJ, Brazil, November 22-25, 2015.

[6] Liu Y., Cavalier G., Pastor J., Viera R. J., Guillory C., Judice K., Guiberteau K., Kozman T. A., *Design and construction of a wave generation system to model ocean conditions in the Gulf of Mexico*, in International Journal of Energy & Technology 4 (31) (2012) 1–7

[7] Krvavica N., Ružić I., Ožanić N, *New approach to flap-type wavemaker equation with wave breaking limit*, in Coastal Engineering Journal.

[8] Guillouzouic B., *Marinet D2.12 Collation of Wave Simulation Methods*.

[9] S. A. Sannasiraj, *Module II - Laboratory Wave Generation.*

[10] A. Mancini, Origini e sviluppo delle vasche navali, in Rivista Marittima Giugno 2000

[11] Chappell E. R., *Theory and Design of a wave generator for a short wave flume*, University of British Columbia, April 1969.

[12] H. E. Saunders, *Maneuvering and Seakeeping (MASK) Facility New Directional Wavemaker*.

[13] A. Mancini, Origini e sviluppo delle vasche navali, in Rivista Marittima Giugno 2000.

Websites

ITTC: https://ittc.info
MaRINET2: http://www.marinet2.eu
Edinburgh Design: http://www4.edesign.co.uk
Imperial War Museum: https://www.iwm.org.uk
Pamoco: https://www.pamoco.it
Wikipedia: https://it.wikipedia.org